# SUPERMASSIVE BLACK HOLES IN GALACTIC NUCLEI

Thesis by

Peter John Young

In Partial Fulfillment of the Requirements

for the Degree of

Doctor of Philosophy

California Institute of Technology

Pasadena, California

1979

(Submitted July 10, 1978)

ACKNOWLEDGEMENTS

To my adviser Wal Sargent, and to Peter Goldreich, Jerry Kristian and Jim Westphal I offer my most profuse thanks for more help, encouragement and hard cash than I really deserved. Without these people the work described here would have been quite impossible.

I also thank Alec Boksenberg (and his flying circus), Roger Blandford, Jim Gunn and Chris Wilson who provided invaluable aid in the form of wisdom and data.

A plenitude of fellow graduate students have contributed to my well-being during my sojourn at Caltech. Most particularly Kirk Borne, John Hoessel, Roger Linfield, Steve Kent, Russell Redman, Jon Romney, Don Schneider, Bill Sebok, Richard Wade and Howard Yee showed me the non-linear methods of convolution applicable to the USA. My especially warm thanks go to Doug Rabin who taught me that I did not exist merely to fulfil his own expectations.

Lastly I thank the late Ray Ballard, Lilo Hauck, Caltech and the Hale Observatories for allowing me to go gadding up and down mountains and for supporting my somewhat expensive late night activities in the computer centre and elsewhere.

"Mathematically, it was a sphere, or rather a negasphere; but the eye while it could see something, could not perceive it analytically. Nor could the mind envision it in three dimensions, for it was not essentially three-dimensional in nature. Light sank into the thing, whatever it was, and vanished. The peering eye could see nothing whatever of shape or of texture; the mind behind the eye reeled away before infinite vistas of nothingness.

Kinnison hurled his extra-sensory perception into it and jerked back, almost stunned. It was neither darkness nor blackness, he decided, after he recovered enough poise to think coherently. It was worse than that -- worse than anything imaginable -- an infinitely vast and yet non-existent realm of the total absence of everything whatever...

ABSOLUTE NEGATION!!!

(from "Grey Lensman", by E. E. "Doc" Smith)

ABSTRACT

The existence of supermassive black holes in galactic nuclei is investigated both theoretically and observationally. In addition the dynamics of flattened elliptical galaxies is examined observationally. Part I of the thesis deals with the theoretical distribution of a stellar population around a massive black hole in a galactic nucleus. Part II calculates the luminous energy output such a black hole could achieve by wreaking carnage among the stars in that nucleus. Part III is a photometric study of the radio galaxy M87 and concludes that this galaxy harbours some sort of massive object, if not a black hole. Part IV is a dynamical study of the same galaxy M87 via spectroscopic measurements of the velocity dispersion as a function of radius. It comes to the same conclusion as in Part III. Part V is a study of the dynamics of the E5 galaxy NGC 4473 which is found to exhibit scant rotation.

TABLE OF CONTENTS

Introduction Page 1

Part I: Stellar Density Cusp Around a Massive Black Hole Page 3

Part II: The Black Tide Model of QSOs. II: Carnage in an Isothermal Sphere Page 12

Part III: Evidence for a Supermassive Object in the Nucleus of the Galaxy M87 from SIT and CCD Area Photometry Page 29

Part IV: Dynamical Evidence for a Central Mass Concentration in the Galaxy M87 Page 39

Part V: Dynamics of the Flattened Elliptical Galaxy NGC 4473 Page 53

# INTRODUCTION

This thesis is an assemblage of five papers which have been published in the Astrophysical Journal. They are mostly concerned with various aspects, both theoretical and observational, of supermassive black holes in galactic nuclei as a possible power source for Quasars and consanguineous objects.

The first two parts of this thesis deal with theoretical results from stellar dynamics. We answer the following two questions:

(i) What is the distribution function of a stellar population around a black hole in a galactic nucleus?

(ii) At what rate could a massive black hole fuel itself and emit energy if it relies on the "surefire" sources from tidal disruption of stars and from high velocity collisions between stars?

Question (i) is answered analytically. Although I have performed numerical calculations including effects of angular momentum diffusion and also the self-gravity of the stars, I do not give the results here since they have never been published (the analytic solutions were found to be good approximations although numerical results were used to compare the theory with observation). Question (ii) is answered in the form of expected energy fluxes that a massive black hole could achieve. The results are

encouraging; Quasar luminosities can be attained in dense galactic nuclei.

Parts three and four are an observational hunt for massive black holes in galactic nuclei. Such an object was found in the nucleus of the radio galaxy M87 (although we could not definitely prove the object was a black hole). This project was made possible only by using various "wonder detectors" on large telescopes. We found a central steepening of the luminosity profile of M87 coupled with an increase in the velocity dispersion which exactly fitted the theoretical black hole models of galactic nuclei. A model independent analysis confirmed the presence of a large, "dark"central mass of $5 \times 10^9$ solar masses; a monster black hole if it be such.

Part five is an auxiliary titbit in galactic dynamics. We observed the E5 galaxy NGC 4473 and found, rather surprisingly, that it had very little rotation. The object is "pressure" supported with most of the kinetic energy in random motion. We also found evidence for a massive halo in the form of an increase in the mass to luminosity ratio of the stars with increasing radius.

THE ASTROPHYSICAL JOURNAL, 217:287–295, 1977 October 1


# STELLAR DENSITY CUSP AROUND A MASSIVE BLACK HOLE

PETER J YOUNG
Hale Observatories, California Institute of Technology and Carnegie Institution of Washington
*Received 1976 December 1; accepted 1977 March 30*

## ABSTRACT

This paper is concerned with the distribution of stars around a massive black hole in a dense star cluster. Spherical symmetry and isotropic distribution functions are assumed along with a power-law mass spectrum of stars to obtain a one-parameter family of equilibrium "zero-flow" solutions.

The analysis is performed using a Fokker-Planck equation to describe the stellar encounters in their Coulomb potentials in an imposed gravitational potential well of the form $\phi(r) = \phi_a(r_a/r)^{1/\alpha}$ ($\alpha = 1$ for a massive black hole). We find equilibrium solutions $f(E) = KE^p$, where $p = (3\alpha - 5/2)/2$, for the single-mass population case, in agreement with previous results, and for a power-law mass spectrum $f(E, m) = f_0 m^X \exp(-mE^{-Y})$, where $Y = 1/2(2X + 3)$ for $\alpha = 1$ and $X > -1$. This leads to the density scalings $\rho(r, m) \propto m^X \exp(-mr^Y) r^{-3/2}$ and $\rho(r) \propto r^{-3/2-z}$, where $Z = (X + 1)/2(2X + 3)$, which are close to that for a single-mass population. It is shown how this solution may be matched smoothly onto an isothermal sphere configuration with a similar power-law mass spectrum.

Assuming a stellar mass-luminosity relation $L \propto \mu^\gamma$, the luminous flux from the cusp scales as $L(r) \propto r^{-3/2-Z'}$ where $Z' = (X + \gamma)/2(2X + 3)$ (in the case $\alpha = 1$). In projection onto the sky this becomes $L_p(s) \propto s^{-1/2-Z'}$, which is steeper than that due to a single-mass population where $L_p(s) \propto s^{-3/4}$.

*Subject headings:* black holes — clusters: globular — stars: stellar dynamics

## I. INTRODUCTION

It has been suggested that X-ray sources associated with globular clusters are the result of gas accretion onto a massive black hole (Bahcall and Ostriker 1975; Silk and Arons 1975). The postulated mass of these objects is $\sim 10^3\ M_\odot$, which is sufficient to enable the black hole to gather around itself a number of stars trapped in bound orbits and forming a high-density cusp of stars in the cluster center which may be detectable by photometric techniques (Bahcall and Wolf 1976).

In application to this problem, and also to the problem of a black hole in a galactic nucleus (Lynden-Bell 1969), it is of interest to calculate the form of this density cusp and to compute the expected luminosity profile for comparison with observations. Preliminary observational work has resulted in the possible detection of an 800 $M_\odot$ black hole in the X-ray globular cluster M15 (Newell, DaCosta, and Norris 1976). Theoretical work on the form of the density cusp was pioneered by Peebles (1972) and extended by Bahcall and Wolf (1976), who sought an equilibrium "zero-flow" solution to the rate of orbital scattering in the region where the gravitational potential of the black hole is dominant ($\phi = -GM_H/r$), akin to the non-LTE solutions of stellar model atmospheres. The stellar distribution function for a single-mass population was of the form $f(E) = kE^{1.4}$, correcting the result of Peebles [$f(E) = kE^{3/4}$] who used a simple scaling argument. A conceptually simpler derivation using a Fokker-Planck equation has been provided by Lightman and Shapiro (1977), also for a single-mass population. Bahcall and Wolf (1977) have derived some elegant scaling relations for the density in the cusp when stars of more than one mass are involved, and have performed numerical integrations of density profiles mainly for the case of two masses. Stimulated by these results, the present work shows how the scaling relations found by Bahcall and Wolf (1977) can be used to separate the stellar distribution function for equilibrium "zero-flow" solutions into the form $f(E, m) = f_0(m) \exp[mK(E)]$, where $f_0(m)$ is a mass scaling function and $K(E)$ depends only on energy. The Maxwell-Boltzmann distribution (LTE) with $K(E) = -E$ is a special case of this form.

In order to obtain a self-similar power scaling law for the cusp with a mass spectrum present, the mass function $f_0(m) \propto m^X$ ($X > -1$) is used to obtain the stellar distribution function $f(E, m) = f_0 m^X \exp(-mE^{-Y})$; $Y = 1/2(2X + 3)$ for an equilibrium "zero-flow" solution. The resulting density profile in the cusp is a trifle less steep than that of a single-mass stellar population, but allowing for a realistic mass-luminosity relation, the luminosity profile is slightly steeper than would be expected from one-mass considerations. The limit of detectability of a central massive black hole in a globular cluster will be lowered as a result of the more massive stars in the cluster settling into the cusp and increasing its luminosity.

In the next section we present the details of the diffusion equations around the cusp, in § III the results are discussed, and lastly certain tedious derivations are banished to a pair of appendices.

## II. STELLAR DYNAMICS OF THE DENSITY CUSP

A Fokker-Planck equation is used to describe the small-angle diffusive encounters of stars in their Coulomb potentials, as in Lightman and Shapiro (1977). However, we employ diffusion coefficients for a general distribution of stellar velocities (Chandrasekhar 1942, 1943) to obtain the equation for the evolution of the stellar distribution function $f(E, m)$ as

$$\frac{\partial f}{\partial t} = -AE^{3\alpha-1/2}\frac{\partial}{\partial E}\left\{m\int_{-\infty}^{\infty} dE' f(E)\frac{\partial f(E')}{\partial E'}[\max(E, E')]^{3/2-3\alpha} - m_*\int_{-\infty}^{\infty} dE' f(E')\frac{\partial f(E)}{\partial E}[\max(E, E')]^{3/2-3\alpha}\right\}, \tag{II-1}$$

where $A = 16\pi^2 G^2 \ln\Lambda/(3\alpha - \frac{3}{2})$. The derivation may be found in Appendix A.

This is similar to the result of Bahcall and Wolf (1976) except that (i) it has been performed for stars in a power-law gravitational potential $\phi(r) = \phi_a(r_a/r)^{1/\alpha}$. For $\alpha = 1$ we recover their equation. (ii) $E$ is negative energy = binding energy to the cusp. This is as in Bahcall and Wolf (1976). Note that $E$ is on a per unit mass basis. (iii) Here $f$ = mass density in phase space rather than number density. We lose a factor $m_*^2$ in the coefficient $A$. (iv) Equation (II-1) applies to stars of mass $m$ diffusing against field stars of mass $m_*$ rather than the case $m = m_*$.

If we demand a "zero-flow" equilibrium solution, then the quantity in braces representing star flux through energy level $E$ must vanish. Then,

$$m\int_{-\infty}^{\infty} dE' f(E)\frac{\partial f(E')}{\partial E'}[\max(E, E')]^{3/2-3\alpha} = m_*\int_{-\infty}^{\infty} dE' f(E')\frac{\partial f(E)}{\partial E}[\max(E, E')]^{3/2-3\alpha}. \tag{II-2}$$

Integrating over the mass spectrum and displaying the dependence $f(E, m)$ explicitly,

$$mf(E, m)\int_0^{\infty} dm'\int_{-\infty}^{\infty} dE'\frac{\partial f(E', m')}{\partial E'}[\max(E, E')]^{3/2-3\alpha}$$

$$= \frac{\partial f(E, m)}{\partial E}\int_0^{\infty} m'dm'\int_{-\infty}^{\infty} dE' f(E', m')[\max(E, E')]^{3/2-3\alpha}. \tag{II-3}$$

From this we may deduce the mass-scaling relation of Bahcall and Wolf (1977). Defining a "local gradient" $p(E, m) = (E/f)/(\partial f/\partial E)$ [when $f = kE^p$, $p(E) = p$], we see from equation (II-3) that

$$p(E, m_1)/m_1 = p(E, m_2)/m_2, \tag{II-4}$$

where $m_1$ and $m_2$ are arbitrary masses. From this it may be deduced that

$$f(E, m) = f_0(m)\exp[mK(E)], \tag{II-5}$$

where $f_0(m)$ is an arbitrary mass scaling function and $K(E)$ is a function of energy only. Equations (II-4) and (II-5) do not rely on the assumed form of the potential $\phi(r)$ but hold in general for isotropic distribution functions in "zero-flow" equilibrium and are a necessary consequence of the fact that a Boltzmann distribution [$f(E, m) \propto e^{mE}$] satisfies the Fokker-Planck equation. Further discussion in terms of thermodynamic relations may be found in Appendix B. Inserting equation (II-5) into equation (II-3) leads to

$$\frac{\partial K}{\partial E}\int_{-\infty}^{\infty} dE'[\max(E, E')]^{3/2-3\alpha}\int_0^{\infty} dm'm'f_0(m')\exp[m'K(E')]$$

$$= \int_{-\infty}^{\infty} dE'\frac{\partial K}{\partial E'}[\max(E, E')]^{3/2-3\alpha}\int_0^{\infty} dm'm'f_0(m')\exp[m'K(E')], \tag{II-6}$$

which may be solved for $K(E)$ given the arbitrary function $f_0(m)$. We see that $K(E) = E$ is a trivial solution of equation (II-6), verifying that the Maxwell-Boltzmann distribution $f(E, m) = f_0(m)e^{mE}$ (noting that $E$ is negative energy) satisfies the problem for any mass scaling function $f_0(m)$ such that the integral $\int_0^{\infty} dm'm'f_0(m')e^{m'K}$ converges. However, this is not the physically realistic solution to the density cusp because it predicts high densities near the black hole where stars are destroyed by collisions among themselves, as was stressed by Peebles (1972). We shall instead look for power-law solutions with more modest rests of increase of stellar density near the black hole.

This may be done by demanding that

$$\int_0^{\infty} dm'm'f_0(m')\exp(m'K) \propto E^p \tag{II-7a}$$

and

$$\frac{\partial K}{\partial E} \propto E^{\beta}, \tag{II-7b}$$

whence we obtain from equation (II-6) that

$$\frac{1}{p+1}+\frac{1}{3\alpha-p-5/2}=\frac{1}{p+\beta+1}+\frac{1}{3\alpha-p-5/2-\beta}, \tag{II-8}$$

where all the terms must be positive for convergence of the integrals. The solution is

$$2p+\beta+7/2-3\alpha=0. \tag{II-9}$$

The solution for a single-mass population may be recovered by setting $f_0(m)=\delta(m-1)$. Then $\int_0^\infty dm'm'f_0(m')\exp(m'K)=e^K$, and we find $K=p\log(E)$, $dK/dE=p/E$. Thus, setting $\beta=-1$, the solution is $f(E)=kE^p$, where

$$p=(3\alpha-5/2)/2 \tag{II-10}$$

for $E>0$ and $f=0$ for $E<0$.

We need $0<p<(3\alpha-5/2)$ for convergence of the relevant integrals and for continuity of $f$ at $E=0$, so that "zero-flow" solutions exist only when $\alpha>5/6$. For the case of a massive black hole $\alpha=1$, and we find $p=1/4$ as found by Bahcall and Wolf (1976).

The two-mass stellar population may be investigated by setting

$$f_0(m)=c_1\delta(m-m_1)+c_2\delta(m-m_2), \tag{II-11}$$

when we find

$$\frac{\partial K}{\partial E}\int_{-\infty}^{\infty}dE'[\max(E,E')]^{3/2-3\alpha}[\exp(m_1K)+A\exp(m_2K)]$$

$$=\int_{-\infty}^{\infty}dE'\frac{\partial K}{\partial E'}[\max(E,E')]^{3/2-3\alpha}[\exp(m_1K)+A\exp(m_2K)], \tag{II-12}$$

with $A=c_2m_2/c_1m_1$. This may be solved approximately in the limits $E\to0$ and $E\to\infty$ when the lighter or heavier stars, respectively, dominate the cusp. Taking $m_2>m_1$ and setting $K(E)=p(E)\log(E)$, where $p(E)$ is assumed to vary only slowly with $E$, we find

$$0=\frac{(3\alpha-5/2-2pm_1)}{pm_1(3\alpha-3/2-pm_1)(pm_1+1)(3\alpha-5/2-pm_1)}+\frac{AE^{p(m_2-m_1)}(3\alpha-5/2-2pm_2)}{pm_2(3\alpha-3/2-pm_2)(pm_2+1)(3\alpha-5/2-pm_2)}. \tag{II-13}$$

The power-law exponents of the mass populations are $p_1=pm_1$ and $p_2=pm_2$ (satisfying eq. [II-4]). We see that as $E$ approaches infinity the heavier stars dominate in the deeper regions of the cusp, and so, setting $\mu=m_1/m_2$, $p_0=(3\alpha-5/2)/2$, we obtain

$$p_2\to p_0;\qquad p_1\to\mu p_0\quad(E\to\infty). \tag{II-14}$$

As $E$ approaches zero the lighter stars dominate (in the outer parts of the cusp) and, provided, $\mu\geq1/2$,

$$p_1\to p_0;\qquad p_2\to p_0/\mu\quad(E\to0;\mu\geq1/2). \tag{II-15}$$

If, however, $\mu<1/2$, the limiting solution (II-15) would demand that $p_2\to p_0/\mu>2p_0$, which the self-interactions of the massive stars will not permit. Instead we find

$$p_1\to2\mu p_0;\qquad p_2\to2p_0\quad(E\to0;\mu<1/2). \tag{II-16}$$

Since the characteristics of the power-law solution change rapidly near $p=2p_0$, with ever-increasing diffusion attempting to force stars out of the cusp, the closeness of $p_2$ to $2p_0$ is important. From equation (II-13) we find, approximately,

$$p_2\approx2p_0\left\{1-AE^{2p_0(1-\mu)}[2p_0(1-\mu)+1]\left[\frac{2\mu p_0+1}{2p_0+1}\right]\left[\frac{\mu(1-\mu)}{1-2\mu}\right]\right\}, \tag{II-17}$$

as $E$ approaches zero with $\mu<1/2$. This situation, with the pressure from the more massive stars supporting the lighter ones, would seem ripe for a two-mass instability, with the lighter stars collapsing until they are supported by their own pressure and the more massive ones being driven in even more rapidly by dynamical friction against these lighter stars.

The solution $p=$ constant is not possible for the two-mass case because of the different density gradients of the stars in the cusp, with lighter stars dominating at the outer edge and heavier ones in the center. The form of the asymptotic solutions (II-14), (II-15), (II-16) suggests that $p(E)$ is a monotonic decreasing function of $E$.

The transition region between the limiting solutions occurs where $AE^{p(m_2-m_1)} \approx 1$, where equation (II-12) must be solved numerically.

Turning now to the case of a mass spectrum, the possibility of obtaining a solution depends on choosing the function $f_0(m)$ suitably. A promising candidate might be $f_0(m) \propto m^X$ since this would allow self-similar scaling laws. Then,

$$\int_0^\infty dm' m'^{X+1} \exp(m'K) = (-K)^{-X-2}\Gamma(X+2) \propto E^p , \tag{II-18a}$$

and $(-K) \propto E^{-p/(X+2)}$, which yields

$$\beta = -p/(X+2) - 1 , \tag{II-18b}$$

which, combined with equation (II-9), gives

$$(-K) \propto E^{-Y} , \tag{II-19a}$$

where

$$Y = (3\alpha - 5/2)/(2X+3) . \tag{II-19b}$$

We need $\alpha > 5/6$ for $Y > 0$ (corresponding to a physically realistic solution), and we also need $X > -1$ to ensure that the integrals over mass converge. Then the stellar distribution function is

$$f(E, m) = f_0(m/m_*)^X \exp[-(m/m_*)(E_a/E)^Y] \quad (E \geq 0)$$
$$f(E, m) = 0 \qquad (E < 0) , \tag{II-20}$$

where $m_*$ and $E_a$ are convenient scaling parameters.

It may be noted that (i) $f \to 0$ (as $E \to 0$) for fixed $m > 0$; (ii) $f(\infty, m) = f_0(m/m_*)^X$. Upon integrating over mass we find a divergence at the upper end of the mass range (since $X > -1$). In practice the cusp has an inner edge at $E \approx E_c^*$ ("collision energy") (Frank and Rees 1976; Young 1977) where collisions destroy the stars. (iii) The mass spectrum has an exponential cutoff at a mass,

$$m_c/m_* = (E/E_a)^Y , \tag{II-21}$$

which progressively gets larger deep into the cusp. This is in line with intuitive ideas that the massive stars should settle further into the cusp than the lighter stars.

We may calculate the run of density in a cusp with distribution function (II-20) as

$$\rho(\phi, \mu) \propto \mu^X \phi^{3/2} \exp(-\mu\phi^{-Y}) \int_1^\infty x^{-(1+Y)/Y}(1 - x^{-1/Y}) \exp[-\mu\phi^{-Y}(x-1)]dx , \tag{II-22}$$

where $\phi$ is the gravitational potential in the cusp (normalized to unity at some reference radius $r_a$, which we shall take as the outer edge of the cusp, $r_a \approx GM_H/\sigma_v^2$; $\sigma_v$ = cluster velocity dispersion) and $\mu = m/m_*$. Then, approximately (for $\mu\phi^{-Y} \lesssim 1$ we neglect the integral in eq. [II-22]),

$$\rho(\phi, \mu) \approx \rho_a \mu^X \phi^{3/2} \exp(-\mu\phi^{-Y})/\Gamma(X+1) , \tag{II-23a}$$

$$\rho(\phi) \approx \rho_a \phi^{3/2+Z} ; \qquad Z = (3\alpha - 5/2)(X+1)/(2X+3) . \tag{II-23b}$$

We see that $Z \to (3\alpha - 5/2)/2$ as $X \to \infty$. This is reasonable because then the mass spectrum $\mu^X e^{-\mu}/\Gamma(X+1)$ approaches a single-mass population and we recover equation (II-10). For $-1 < X < \infty$ the density scaling law (II-23b) is a trifle less steep than that for a single-mass population.

If the mass-luminosity relation for the stars approximates $L(\mu) \propto \mu^\gamma$, then the luminosity flux from the cusp scales as

$$L(\mu) \propto \phi^{3/2+Z'} , \tag{II-24}$$

where $Z' = (3\alpha - 5/2)(X+\gamma)/(2X+3)$. For $\gamma > 3/2$ (a reasonable value might be $\gamma = 4$), we see that $Z' > (3\alpha - 5/2)/2$, and that the luminosity flux from the cusp scales more steeply with radius than for the one-mass case since the massive and more luminous stars settle more deeply into the cusp.

It is possible to match the cusp solution onto an isothermal sphere which satisfies the modified Lane-Emden equation,

$$\frac{1}{\xi^2}\frac{d}{d\xi}\left(\xi^2 \frac{d\psi}{d\xi}\right) = \int_0^\infty d\mu p(\mu) e^{-\mu\psi} , \tag{II-25}$$

where $p(\mu)$ is the mass scaling function such that $\int_0^\infty p(\mu)d\mu = 1$. The structural length of the isothermal sphere is

$$a^2 = \sigma_v^2/4\pi G\rho_0 , \tag{II-26}$$

where $\rho_0$ is the central density (due to stars of all masses). Taking $p(\mu) = \mu^X e^{-\mu}/\Gamma(X + 1)$ $(X > -1)$, we find

$$\frac{1}{\xi^2}\frac{d}{d\xi}\left(\xi^2 \frac{d\psi}{d\xi}\right) = (1 + \psi)^{-X-1}, \tag{II-27}$$

which has the asymptotic solutions,

$$\psi(\xi) \approx \left[\frac{(X + 2)^2}{2(4 + X)}\right]^{1/(2+x)} \xi^{2/(2+X)} \quad (\xi \to \infty)$$

$$\approx \frac{\xi^2}{6} - (1 + X)\frac{\xi^4}{120} + \cdots \quad (\xi \to 0), \tag{II-28}$$

and the density scalings are

$$\rho(\mu, \xi) = \rho_0 \mu^X e^{-\mu} e^{-\mu\psi(\xi)}/\Gamma(X + 1), \tag{II-29a}$$

$$\rho(\xi) = \rho_0/(1 + \psi)^{X+1}. \tag{II-29b}$$

These may be matched smoothly onto equation (II-23) by noting that $\psi = 0$ for the center of the isothermal sphere and $\phi = 1$ at the outer edge of the cusp. Then we set $\rho_a = \rho_0$, and the density within the cusp is then approximately

$$\rho(\mu, r) = \rho_0[\mu^X e^{-\mu}/\Gamma(X + 1)]\{1 + \phi^{3/2} \exp[-\mu(\phi^{-Y} - 1)]\}, \tag{II-30a}$$

$$\rho(r) = \rho_0(1 + \phi^{3/2+z}), \tag{II-30b}$$

which are similar in form to the distribution for the one-mass case, $\rho(\xi) = \rho_0(1 + \phi^{7/4})$ (Bahcall and Wolf 1976). The luminosity flux scaling is then

$$L(r) = L_0(1 + \phi^{3/2+z'}). \tag{II-31}$$

Equations (II-30) and (II-31) are of the form $[\rho_{\text{unperturbed}}(r) + \rho_{\text{cusp}}(r)]$, where the density at the edge of the cusp $r = r_a$ is taken to be $\rho_a = \rho_{\text{unperturbed}}(r_a)$ and the density $\rho_{\text{unperturbed}}(r)$ is that of the cluster without the black hole. This should be verified numerically since the problem is nonlinear; adding two solutions in this way is only a crude approximation, and it may turn out that $\rho_a$ is larger than is assumed here because of isothermal seepage of stars into the fringes of the potential well of the black hole.

If the luminosity of the cluster is dominated by red giant stars of mass $\mu_{\text{RG}}$, then equation (II-31) is inappropriate. The luminosity cusp will have the form of equation (II-23a) with $\rho_0$ replaced by $L_0$ and with $\mu = \mu_{\text{RG}}$. Near the edges of the cusp this will vary as $L_{\text{RG}}(\phi) \propto \phi^{3/2}$ if $\mu_{\text{RG}} \lesssim 1$ and somewhat more steeply if $\mu_{\text{RG}} \gtrsim 1$. In an aged globular cluster $\mu_{\text{RG}} \approx 0.8\ M_\odot$ would be a reasonable estimate of the red giant mass.

## III. DISCUSSION

We may note that the brief analysis in § II leaves undiscussed the following points which may be answerable only by numerical computation.

1. Stability. Numerical work by Bahcall and Wolf (1976, 1977) shows that the one- and two-mass cases are probably stable to radial perturbations. It is also easy to show that the distribution functions (II-10) and (II-20) considered here are stable to perturbations involving a change of slope or the superposition of a small rugosity.

2. The effect of an inner edge to the cusp at $E \approx E_c^*$. If this is sufficiently distant from the outer edge of the cusp at $E = E_a$, then the solutions may give a good approximation for $E_a < E < E_c^*$ with severe departures only near the boundaries. The numerical integrations of Bahcall and Wolf (1976, 1977) verify this for the one- and two-mass cases.

3. Perverse mass spectra. Suppose that the cusp is embedded in a stellar population whose mass spectrum is unlike that assumed for the cusp solution $(\mu^X e^{-\mu})$. Will the distribution function (II-20) still be a good approximation, and if so what value of $X$ will it decide to adopt?

4. Small number statistics. There will be problems with a discreteness of stars when the black hole mass $M_H$ is less than $10^3\ M_\odot$ in a globular cluster. The solutions of the Fokker-Planck equation may then only be true in an "ensemble-averaged" sense and liable to large statistical fluctuations, with $\sim 100$ stars in the cusp. One would feel much safer in an application to galactic nuclei when there may be $\sim 10^6$ stars trapped in the cusp of a $10^7\ M_\odot$ black hole.

Observations of the mass-scaling around a hypothetical massive black hole in a globular cluster are not feasible at present and are unlikely to be so for some time. Indeed, even the detectability of a density cusp in M15 (Newell, DaCosta, and Norris 1976) is a difficult task and at present yields only tentatively positive results. The importance of the density cusp is in the calculation of the rates at which stars may be destroyed by collisions between themselves (Young 1977) or by tidal disruption near the black hole (Hills 1975; Frank and Rees 1976; Lightman and Shapiro 1977), for such a black hole is best detected by the radiation emitted as the gaseous debris is consumed.

The mass scaling in the cusp manifests itself in the following ways: (i) In the presence of an inner edge to the cusp a gravitational diffusion flux (Bahcall and Wolf 1976) is generated. This will be larger for the more massive stars since they are more numerous and experience greater dynamical friction forces than the lighter stars, but suffer diffusion to the same degree. The composition of the gaseous debris will be biased toward the more massive stars. (ii) Although detection of the mass scaling of individual masses is not feasible, it may be possible to measure the integrated luminosity profile for the cusp. Then the mass scaling effects in raising the observed power of the power-law profile must be accounted for. In addition, the total luminosity from the cusp will be enhanced over that expected for the cluster core stellar population, leading to slightly lower thresholds of detection for the black hole.

I thank Roger Blandford, Peter Goldreich, Vincent Icke, Martin Rees, and Stuart Shapiro for discussions on this subject, and also John Bahcall for presentation and discussion of his own results prior to publication. I also thank the California Institute of Technology and Hale Observatories for supporting me while this work was performed.

## APPENDIX A

## DERIVATION OF THE STELLAR DIFFUSION EQUATION

The purpose of this appendix is to provide an abbreviated derivation of equation (II-1) from the Fokker-Planck equation using the method demonstrated by Lightman and Shapiro (1977), who derived the equation in $(E, J)$ space, particularized it to the case of an isotropic distribution function as is considered here, and obtained the solution $f(E) = KE^{1/4}$. We remove three approximations made by Lightman and Shapiro to derive a more generally applicable equation, those approximations being (i) the use of Maxwell diffusion coefficients, (ii) the evaluation of these coefficients at the rms stellar velocity at each point in the cusp, and (iii) the one-mass stellar population. Since we are concerned with the distribution of stars around the massive black hole, the assumption of an isotropic function $f(E)$ is adequate, but, as pointed out by Lightman and Shapiro, the removal of low-angular-momentum stars by the black hole induces a logarithmic anisotropy in the $J$ coordinate and the resulting "loss-cone" fluxes should be allowed for in computing the consumption rate by the hole.

It is gratifying that the resulting equation is that found by Bahcall and Wolf (1976), where the derivation was from first principles.

The Fokker-Planck equation is written in the form

$$\frac{\partial f}{\partial t} + \frac{\partial F_E}{\partial E} + \frac{1}{J}\frac{\partial}{\partial J}(JF_J) = 0\,, \tag{A1a}$$

$$F_E = f\langle \Delta E\rangle - \frac{1}{2}\frac{\partial}{\partial E}(f\langle \Delta E^2\rangle) - \frac{1}{2}\frac{\partial}{\partial J}(f\langle \Delta E \Delta J\rangle)\,, \tag{A1b}$$

$$F_J = f\langle \Delta J\rangle - \frac{1}{2}\frac{\partial}{\partial J}(f\langle \Delta J^2\rangle) - \frac{1}{2}\frac{\partial}{\partial E}(f\langle \Delta E \Delta J\rangle)\,, \tag{A1c}$$

which holds at each $(E, J, r, m)$ point in phase space. Using the divergence theorem, we may integrate over $J$, $r$ [if $f(E, J, m)$ is isotropic] to obtain,

$$\left[\frac{\partial f}{\partial t}\right] + \frac{\partial}{\partial E}\left(f[\kappa_1] + \frac{\partial f}{\partial E}[\kappa_2]\right) = 0 \tag{A2}$$

where square brackets indicate the integral over the $J$, $r$ coordinates in phase space,

$$[g] = 2\int_0^{r_*} dr r^2 v g\,, \tag{A3}$$

where $E = \phi(r_*)$ ($\phi$ = gravitational potential in cluster, $v$ = velocity of star = $[2(E - \phi)]^{1/2}$). The averaged diffusion coefficients are

$$[\kappa_1] = \left[\langle \Delta E\rangle - \frac{1}{2}\frac{\partial}{\partial E}\langle \Delta E^2\rangle - \frac{1}{2}\frac{\partial}{\partial J}\langle \Delta E \Delta J\rangle\right], \tag{A4a}$$

$$[\kappa_2] = [-\tfrac{1}{2}\langle \Delta E^2\rangle]\,, \tag{A4b}$$

$$\left[\frac{\partial f}{\partial t}\right] = \frac{\partial f}{\partial t}[1]\,. \tag{A4c}$$

Note that the $\langle \Delta E \Delta J \rangle$ contribution in equation (A4a) may not be neglected. From Lightman and Shapiro (1977),

$$\langle \Delta E \rangle = v \langle \Delta v_{\parallel} \rangle + \tfrac{1}{2}(\langle \Delta v_{\perp}^2 \rangle + \langle \Delta v_{\parallel}^2 \rangle), \tag{A5a}$$

$$\langle \Delta E^2 \rangle = v^2 \langle \Delta v_{\parallel}^2 \rangle, \tag{A5b}$$

$$\langle \Delta E \Delta J \rangle = J \langle \Delta v_{\parallel}^2 \rangle, \tag{A5c}$$

where the velocity diffusion coefficients (Chandrasekhar 1942, 1943) are

$$\langle \Delta v_{\parallel} \rangle = -\frac{k \rho m_*}{2v^2} \left(1 + \frac{m}{m_*}\right) \int_0^v N(v') dv', \tag{A6a}$$

$$\langle \Delta v_{\parallel}^2 \rangle = \frac{k \rho m_*}{3v} \left[\frac{1}{v^2} \int_0^v N(v') v'^2 dv' + v \int_0^\infty N(v') \frac{dv'}{v'}\right], \tag{A6b}$$

$$\langle \Delta v_{\perp}^2 \rangle = \frac{k \rho m_*}{3v} \left[\int_0^v \left(3 - \frac{v'^2}{v^2}\right) N(v') + \int_0^\infty \frac{2v}{v'} N(v') dv'\right], \tag{A6c}$$

$$k = 8\pi G^2 \ln \Lambda, \tag{A6d}$$

where $N(v)$ is the distribution of stellar velocities ($\int_0^\infty N(v) dv = 1$), and $\ln \Lambda$ is the ubiquitous Coulomb logarithm which allows for the long-range nature of the star-star interactions. After a modest amount of straightforward algebra,

$$\langle \Delta E \rangle - \frac{1}{2} \frac{\partial}{\partial E} \langle \Delta E^2 \rangle - \frac{1}{2} \frac{\partial}{\partial J} \langle \Delta E \Delta J \rangle = -\frac{k \rho m}{2v} \int_0^v N(v') dv', \tag{A7a}$$

$$-\frac{\langle \Delta E^2 \rangle}{2} = -\frac{k \rho m_*}{6} \left[\frac{1}{v^2} \int_0^v N(v') v'^2 dv' + v \int_0^\infty N(v') \frac{dv'}{v'}\right]. \tag{A7b}$$

Noting that $N(v')\rho(r) = 8\pi[E' - \phi(r)]f(E')$ (and $v'^2 = 2[E' - \phi(r)]$), we may evaluate the averaged coefficients,

$$[\kappa_1] = -4\pi(2^{1/2}) k m \int_0^{r_*} r^2 dr \int_{\phi(r)}^E dE' f(E')(E' - \phi(r))^{1/2}, \tag{A8a}$$

$$[\kappa_2] = -\frac{8\pi(2^{1/2})}{3} k m_* \int_0^{r_*} r^2 dr \left[\int_{\phi(r)}^E [E' - \phi(r)]^{3/2} + \int_E^\infty [E - \phi(r)]^{3/2}\right] f(E') dE', \tag{A8b}$$

$$[1] = 2(2^{1/2}) \int_0^{r_*} r^2 dr [E - \phi(r)]^{1/2}. \tag{A8c}$$

Now we assume an imposed gravitational potential $\phi(r) = -\phi_a (r_a/r)^{1/\alpha}$ (such that $\phi^\alpha$ is positive) and transform $E \to -E$ so that $E$ represents binding energy to the cusp. Then,

$$[\kappa_1] = -4\pi(2^{1/2}) k m r_a^{\,3\alpha} \phi_a^{\,3\alpha} B(\tfrac{3}{2}, 3\alpha - \tfrac{1}{2}) \int_E^\infty dE' f(E') E'^{1/2 - 3\alpha}, \tag{A9a}$$

which may be integrated by parts to yield

$$[\kappa_1] = -4\pi(2^{1/2}) k m r_a^{\,3\alpha} \phi_a^{\,3\alpha} \frac{B(\frac{3}{2}, 3\alpha - \frac{1}{2})}{3\alpha - 3/2} \left\{E^{3/2 - 3\alpha} \int_{-\infty}^E dE' \frac{\partial f}{\partial E'} + \int_E^\infty dE' E'^{3/2 - 3\alpha} \frac{\partial f}{\partial E'}\right\}, \tag{A9b}$$

where we require $f(E) \to 0$ ($E \to -\infty$). Similarly,

$$[\kappa_2] = -4\pi(2^{1/2}) k m_* r_a^{\,3\alpha} \phi_a^{\,3\alpha} \frac{B(\frac{3}{2}, 3\alpha - \frac{1}{2})}{3\alpha - 3/2} \left\{E^{3/2 - 3\alpha} \int_{-\infty}^E dE' f(E') + \int_E^\infty dE' f(E') E'^{3/2 - 3\alpha}\right\} \tag{A9c}$$

$$[1] = (8^{1/2}) r_a^{\,3\alpha} \phi_a^{\,3\alpha} B(\tfrac{3}{2}, 3\alpha - \tfrac{1}{2}) E^{1/2 - 3\alpha}. \tag{A9d}$$

Remembering to change the sign of $\partial/\partial E$ in equation (A2), we obtain

$$[1] \frac{\partial f}{\partial t} = \frac{\partial}{\partial E} \left\{f[\kappa_1] + \frac{\partial f}{\partial E} [\kappa_2]\right\}, \tag{A10}$$

which leads to equation (II-1) upon setting $k = 8\pi G^2 \ln \Lambda$ and replacing

$$E^{3/2-3\alpha}\int_{-\infty}^{E} dE' f(E') + \int_{E}^{\infty} E'^{3/2-3\alpha} dE' f(E')$$

by

$$\int_{-\infty}^{\infty} dE' f(E')[\max(E, E')]^{3/2-3\alpha}.$$

## APPENDIX B

## THERMODYNAMICS OF THE DENSITY CUSP

We shall consider the one-mass distribution function $f(E) = KE^p$, which leads to the following properties (where $E$ is negative or binding energy per unit mass and the gravitational potential satisfies $E = \phi - v^2/2$). The velocity dispersion is

$$\sigma_v^2 = [2/(5 + 2p)]\phi \quad (\mathrm{cm^2\ s^{-2}}), \tag{B1a}$$

leading to internal energy per unit mass

$$U = 3\sigma_v^2/2 \quad (\mathrm{ergs\ g^{-1}}). \tag{B1b}$$

If the density and gravitational potential are $\rho_a$ and $\phi_a$ at some fiducial radius, then

$$\rho/\rho_a = (\phi/\phi_a)^{p+3/2}, \tag{B2a}$$

and the "gas" pressure

$$p_g = \rho\sigma_v^2 \quad (\mathrm{dynes}). \tag{B2b}$$

Thus the stars in the cusp are packed in a polytropic sphere of index $n = p + 3/2$. For consistency we see that the equation of hydrostatic equilibrium $dp_g/d\phi = \rho$ is satisfied. The "temperature," defined although the distribution of velocities is not Maxwellian, is

$$T = m_*\sigma_v^2/k = [2/(2p + 5)]m_*\phi/k \quad (\mathrm{K}), \tag{B3}$$

where $m_*$ is the stellar mass and $k$ is Boltzmann's constant. Then the entropy per unit mass satisfies

$$\frac{\partial S}{\partial \phi} = \frac{1}{T}\left(\frac{\partial U}{\partial \phi} - \frac{p_g}{\rho^2}\frac{\partial \rho}{\partial \phi}\right) = -\frac{kp}{m_*\phi} \quad (\mathrm{K^{-1}}), \tag{B4a}$$

and thus

$$S - S_a = -\frac{kp}{m_*}\ln(\phi/\phi_a) \quad (\mathrm{ergs\ K^{-1}\ g^{-1}}), \tag{B4b}$$

which may be verified by calculating

$$S = -(k/m_*)\int f \ln f d^3\boldsymbol{v} \Big/ \int f d^3\boldsymbol{v} \quad (\mathrm{ergs\ K^{-1}\ g^{-1}}). \tag{B4c}$$

Lastly, the enthalpy is

$$H = U + p_g V = [5/(5 + 2p)]\phi \quad (\mathrm{ergs\ g^{-1}}). \tag{B5}$$

The star "gas" is isentropic in the cusp when $p = 0$ in accord with the polytropic index $n = 3/2$. When there is an inner edge to the cusp at $E = E_c{}^*$ (the outer edge being at $E_a$), then there is an exiguous "gravitational diffusion" flux $F_G(\mathrm{g\ s^{-1}})$ into the cusp, with a small anisotropy imposed on the distribution function to carry this flux. The energy balance as the stars descend may be expressed in terms of the relation familiar to engineers,

$$(\text{change in enthalpy}) = (\text{heating rate}) - (\text{work done}), \tag{B6a}$$

or

$$\delta H = \delta q - (-\delta\phi), \tag{B6b}$$

where $\delta q = T\delta S$. The rate at which the black hole consumes energy is

$$\dot{E} = -F_G E_c{}^* \quad (\mathrm{ergs\ s^{-1}}), \tag{B7a}$$

and the rate at which the black hole generates entropy in the cusp is

$$\dot{S} = (pk/m_*)F_G \ln (E_c^*/E_a) \quad (\text{ergs K}^{-1}\,\text{s}^{-1}) . \tag{B7b}$$

The energy generated by the consumption rate is $(M_{\text{cusp}}/t_R)E_a$, where the mass of the cusp is $M_{\text{cusp}}$ and the relaxation time at its outer edge is $t_R$. We must equate this rate to equation (B7a) to obtain (Shapiro and Lightman 1976)

$$F_G \approx (M_{\text{cusp}}/t_R)(E_a/E_c^*) \quad (\text{g}\,\text{s}^{-1}) , \tag{B8a}$$

in agreement with the numerical results of Bahcall and Wolf (1976). It has been pointed out (Shapiro and Lightman 1976) that the heat (eq. [B7a]) is transmitted through the cusp by conduction rather than convective transport by the descending stars. Indeed, from inspection of the above thermodynamic relations we see that a fraction $\sim(r_c^*/r_a)$ of the heat travels by convection. The exponent $p = 1/4$ may be derived via a dimensional argument (Shapiro and Lightman 1976) whereby a relation analogous to equation (B8a),

$$F_G(r) \approx [M_{\text{cusp}}(r)/t_R(r)][E(r)/E_c^*] \quad (\text{g}\,\text{s}^{-1}) , \tag{B8b}$$

is taken to hold for radii $r < r_a$ within the cusp. Then $F_G(r) = F_G(r_a) = F_G$ is demanded (conservation of the heat conducted out), and since $M_{\text{cusp}}(r) \approx \rho(r)r^3$, $t_R(r) \approx \sigma_v^3(r)/G^2 m_* \rho(r) \ln \Lambda$, and $E(r) \approx GM_H/r$, we find that $F_G(r)/F_G(r_a) = (r/r_a)^{1/2-2p}$, and consequently that $p = 1/4$.

Having considered the thermodynamics of the density cusp from the simpler viewpoint of the radial coordinate $r$, we shall now consider it in terms of the energy coordinate $E$ and generalize the treatment to the distribution function $f(E, m) = f_0(m) \exp [mK(E)]$ as was derived in § II for isotropic, zero-flow stellar populations.

The temperature of the stars at energy level $E$ is (Lynden-Bell 1975)

$$[kT(E, m)]^{-1} = -\partial/\partial\xi[\ln f(E, m)] , \tag{B9a}$$

where $\xi = mE$ is the energy of a star of mass $m$. This is exemplified by the Boltzmann distribution $f(E, m) = f_0(m) \exp (-mE/m_*\sigma_v^2)$, whence $T(E, m) = m_*\sigma_v^2/k$ independent of $m$ and $E$. Then, for the isotropic, zero-flow distribution function, we find

$$T(E, m) = -[kK'(E)]^{-1} \quad (\text{K}) , \tag{B9b}$$

which is independent of $m$. Pursuing this result, we may evaluate the entropy per unit mass $S(E, m)$ either from the relation $TdS = \delta Q = dE$ or directly from the formula

$$S(E, m) = -(k/m) \ln f(E, m) \quad (\text{ergs K}^{-1}\,\text{g}^{-1}) , \tag{B10a}$$

from which we find

$$\frac{\partial S}{\partial E}(E, m) = -kK'(E) \quad (\text{K}^{-1}) . \tag{B10b}$$

It is reasonable that $\partial S/\partial E$ should not depend on the stellar mass $m$; if it did, then the particles of different masses could cause a local increase in entropy by judicious fluxing. Equation (II-6) gives the condition for an isotropic, zero-flow distribution function as

$$\frac{\partial S}{\partial E}(E) = \left\langle \frac{\partial S}{\partial E'}(E') \right\rangle \tag{B11a}$$

or

$$1/T(E) = \langle 1/T(E') \rangle , \tag{B11b}$$

where expressions in angle brackets are the averages over $E'$, $m'$ weighted by $[\max (E, E')]^{-3/2} m' f(E', m')$ as defined in equation (II-6).

If collisions near the black hole remove stars with $E > E_c^*$, then a small "gravitational diffusion" flux $F_G(m)$ into the well of the black hole exists. Consideration of equation (II-1) suggests that this should scale as $F_G(m) \propto m\rho_m$, where $\rho_m$ is evaluated at $r_c^* \approx GM_H/E_c^*$ for the undisturbed "zero-flow" distribution.

## REFERENCES

Bahcall, J. N., and Ostriker, J. P. 1975, *Nature*, **256**, 23.
Bahcall, J. N., and Wolf, R. A. 1976, *Ap. J.*, **209**, 214.
———. 1977, *Ap. J.*, in press.
Chandrasekhar, S. 1942, *Principles of Stellar Dynamics* (Chicago: University of Chicago Press).
———. 1943, *Ap. J.*, **97**, 255.
Frank, J., and Rees, M. J. 1976, *M.N.R.A.S.*, **176**, 633.
Hills, J. G. 1975, *Nature*, **254**, 295.
Lightman, A. P., and Shapiro, S. L. 1977, *Ap. J.*, **211**, 244.
Lynden-Bell, D. 1969, *Nature*, **223**, 690.
———. 1975, *IAU Symposium No. 69, Dynamics of Stellar Systems*, ed. A. Hayli (Dordrecht: Reidel), p. 27.
Newell, B., DaCosta, G. S., and Norris, J. 1976, *Ap. J. (Letters)*, **208**, L55.
Peebles, P. J. E. 1972, *Ap. J.*, **178**, 371.
Shapiro, S. L., and Lightman, A. P. 1976, *Nature*, **262**, 743.
Silk, J., and Arons, J. 1975, *Ap. J. (Letters)*, **200**, L131.
Young, P. J. 1977, *Ap. J.*, **215**, 36.

PETER J YOUNG: Robinson Laboratory, 105-24, California Institute of Technology, Pasadena, CA 91125

THE ASTROPHYSICAL JOURNAL, 215:36–52, 1977 July 1


# THE BLACK TIDE MODEL OF QSOs. II. DESTRUCTION IN AN ISOTHERMAL SPHERE

PETER J YOUNG
Robinson Laboratory, California Institute of Technology, Pasadena
*Received 1976 November 5; revised 1977 January 3*

## ABSTRACT

The quasar models employing a black hole in a galactic nucleus are considered; it is shown that the black hole may be able to destroy the stellar population of the galactic nucleus in sufficient numbers to provide a power source for QSO, Seyfert nucleus, and radio galaxy phenomena.

The basic model is of a black hole embedded in an isothermal sphere. When the mass of the hole $M_H \lesssim 10^6\ M_\odot$ it grows mainly by tidally disrupting stars which stray within its Roche limit. This source of gaseous debris for the hole to accrete is cut off due to falling stellar densities outside the galactic nucleus coupled with insufficiently fast relaxation of the stellar population into low angular momentum orbits; luminosities above $10^9\ L_\odot$ are not possible. However, when $M_H \gtrsim 10^6\ M_\odot$ a high-density cusp of stars bound to the black hole generates gaseous debris from stellar collisions and gravitational diffusion processes and allows sufficient fuel to boost the power output of the black hole to $\gtrsim 10^{12}\ L_\odot$ in superdense galactic nuclei. This is cut off as the hole consumes the nucleus and lengthening relaxation times freeze the quasar into oblivion. This decay occurs only slowly with $L \propto t^{-1/2}$.

We consider a black hole growing in four selected galactic nuclei and demonstrate favorable energetics and a sufficient diversity of scenarios, from three free parameters, to enable active galactic nuclei phenomena to be understood in terms of this model.

In addition, the results are applied to the case of a massive black hole ($10^3\ M_\odot$) in a globular cluster, where it turns out that the tidal disruption processes are the most important as regards fueling the black hole. The seven known X-ray globular clusters are demonstrated to have high rates of encounter between stars and between the black hole and the stellar population when considering those stars in the nucleus not bound to the hole. It is demonstrated that a massive black hole could not have grown from a small ($10\ M_\odot$) precursor in one Hubble time.

*Subject headings:* black holes — clusters: globular — galaxies: nuclei — quasars

## I. INTRODUCTION

Following work by Lynden-Bell (1969) and Lynden-Bell and Rees (1971), it has been generally thought plausible that quasar activity may be associated with galactic nuclei. This feeling is strengthened by the visibility of galaxy-like nebulosity around some of the observed objects, and by the continuity between quasar activity and the nuclei of Seyfert galaxies (Rowan-Robinson 1976). In addition, many normal galaxies such as our own have relatively weak radio sources at their center, and even powerful radio galaxies are often observed to have compact radio sources centered on their nuclei. This great diversity of activity confined in each case to the small volume of a galactic nucleus may have a common cause, i.e., the presence of a black hole (Lynden-Bell 1969). Certainly, as regards quasar activity, unless quantities of matter comparable to a galactic mass are involved (in nuclear energy production, for example), the power output of $10^{11-13}\ L_\odot$ over a lifetime of $\sim 10^7$ yr (for example) may only be explained by the $0.3\ mc^2$ efficiency of conversion of matter to energy in an accretion disk around a Kerr black hole (with $J = 0.998\ M^2$). Then, since a mass of only $10^{7-8}\ M_\odot$ would be needed, this suggests that the energy liberated by a quasar may be explained if the black hole destroys a significant fraction of the stellar population in a galactic nucleus and subsequently accretes the matter.

Hills (1975) suggested that tidal disruption of stars which stray inside the Roche limit of the black hole could provide adequate fuel; a quasar would die when $M_H > 3 \times 10^8\ M_\odot$ as the Roche radius ($r_t \propto M^{1/3}$) was engulfed by the event horizon of the black hole ($r_g \propto M$). More recent work by Frank and Rees (1976) and Lightman and Shapiro (1977) using "loss-cone" theories has suggested that the fluxes are not as high as were estimated by Hills, since consumption of stars is limited by the rate at which stellar orbits diffuse into the "loss cone" where they are carried away to destruction at a peribarathron inside the Roche limit of the black hole. In addition, work by Bahcall and Wolf (1976), following Peebles (1972), on the form of a high-density cusp of stars around a black hole suggested that "gravitational diffusion" effects, whereby stars flow into the potential well of the hole, were less important to the development of the hole than tidal disruption processes.

Other work on the problem includes the question of the spin of the black hole (Young 1977), which can affect the power output by a factor of 5; details of the tidal disruption process around a Kerr hole, including the effects

of a red-giant population of stars (Young, Shields, and Wheeler 1977); and the effect of physical collisions between stars in the density cusp around the black hole.

The purposes of this paper are:

1. To calculate more precisely the rate at which a black hole in a galactic nucleus will tidally disrupt stars. We use an isothermal sphere to describe the galactic nucleus, in particular to allow the density falloff outside the nuclear regions to be taken into account.
2. To examine the possibility of quasar and Seyfert galaxy models relying on the tidal disruption models. We shall see that QSO luminosities of $10^{11-13}\,L_\odot$ may not be explained by this process, but that Seyfert nucleus luminosities may be.
3. To discuss the possibility of such models relying on other effects in a high-density cusp of stars around the black hole, viz., collisions and dynamical friction. These may well be capable of explaining quasar luminosity.
4. To examine the growth rate of a black hole placed in the nuclei of various types of galaxy; a "normal" spiral or elliptical galaxy, a compact E galaxy, a cD galaxy, and a superdense spiral or elliptical galaxy nucleus.
5. In an appendix the results obtained in this paper are applied to the somewhat similar case of a black hole in a globular cluster. Here it turns out that the gravitational diffusion and stellar collision effects are less important than the tidal disruption of stars from the loss-cone orbits.

## II. LOSS-CONE THEORY OF STELLAR DIFFUSION

Let us consider a spherically symmetric stellar population described by the distribution function

$$f(E, J)\, d^3\mathbf{r} d^3\mathbf{v}\,, \tag{II-1}$$

where $E$, $J$ are the stellar energy and angular momentum per unit mass, respectively. It is convenient to work in $(E, J)$ space, with

$$E = v_R^2/2 + v_T^2/2 + \phi(r)\,; \quad J = rv_T\,, \tag{II-2}$$

where $v_R$, $v_T$ are the stellar radial and transverse velocities, respectively, and $r$ is the radial coordinate from the cluster center.

Now,

$$d^3\mathbf{r} d^3\mathbf{v} = (4\pi r^2 dr)(2\pi v_T dv_T dv_R)\,, \tag{II-3a}$$

or,

$$d^3\mathbf{r} d^3\mathbf{v} = (4\pi r^2 dr)(2\pi J dJ dE/r^2 v_R)2\,, \tag{II-3b}$$

(as in Lightman and Shapiro 1977). The factor 2 in equation (II-3b) is to allow for the fact that $(v_R, v_T) \rightarrow (E, J)$ is a 2:1 mapping. Thus

$$d^3\mathbf{r} d^3\mathbf{v} = 16\pi^2 J dJ dE dr/v_R\,. \tag{II-4}$$

To integrate over the whole cluster, e.g., to find the total number of stars therein, we integrate over the following limits;

$$N = 16\pi^2 \int_0^\infty dE \int_0^{J_{\max}(E)} J dJ \int_{r_p}^{r_{ap}} dr/v_R\, f(E, J)\,, \tag{II-5}$$

where $J_{\max}(E)$ is the maximum angular momentum allowed for a star of energy $E$, and $r_p(E, J)$, $r_{ap}(E, J)$ are the periastron and apastron radii of a star $(E, J)$. The orbital period of such a star is

$$P(E, J) = 2 \int_{r_p}^{r_{ap}} dr/v_R\,. \tag{II-6}$$

In the example given in equation (II-5), since $f(E, J)$ is nearly constant around an orbital path (dynamical time scale $\ll$ relaxation time scale), the integral becomes

$$N = 8\pi^2 \int_0^\infty dE \int_0^{J_{\max}} J dJ f(E, J) P(E, J)\,. \tag{II-7}$$

The above results are taken from Lightman and Shapiro (1977).

Now suppose the black hole removes stars which stray into a loss cone in $(E, J)$ space, viz., the region $J < J_T = (2GM_H r_T)^{1/2}$, where $r_T$ is the Roche limit of the black hole of mass $M_H$. The diffusion of the stellar population in $J > J_T$ will slowly transport stars into the loss cone via relaxation processes in the star cluster, setting up a $J$-gradient in the distribution function to drive the diffusion into the loss cone. Two limiting cases of this process may

be considered (Frank and Rees 1976; Lightman and Shapiro 1977). If the root-mean-square diffusion in angular momentum of a star near the loss cone in one orbital period is $J_D$, then we may consider the following cases:

i) $J_D/J_T \ll 1$.—In this case a "diffusion" approximation is valid. The equation describing diffusion near the loss cone is

$$\left[\frac{\partial f(E, J, r, t)}{\partial t}\right]_{E,J,r} = \frac{\kappa(E, J, r, t)}{J}\left[\frac{\partial}{\partial J} J \frac{\partial f}{\partial J}(E, J, r, t)\right]_{E,r,t} \tag{II-8a}$$

where we show explicitly the dependence of $f$ on $(E, J)$ as in equation (II-1) and also on position in the orbit (radial coordinate $r$ in the spherically symmetric situation) and time $t$. As was mentioned above, the dependence of $f$ on $r$ is weak, but the dependence of $\kappa$ on $r$ is significant because of varying stellar density $\rho(r)$. Accordingly, we shall integrate equation (II-8a) over the radial coordinate $r$ to obtain the averaged equation

$$\left[\frac{\partial f(E, J, t)}{\partial t}\right]_{E,J} = \frac{J_D^2}{4P(E, J)} J^{-1}\left[\frac{\partial}{\partial J} J \frac{\partial f}{\partial J}(E, J, t)\right]_{E,t} \tag{II-8b}$$

where

$$J_D^2 = 4\int_{\text{orbit}} \kappa d\tau = 8\int_{r_p}^{r_{ap}} \kappa(dr/v_R)\,. \tag{II-8c}$$

We have set $f(E, J, r, t)$ equal to its average over one orbital path $f(E, J, t)$ and we have introduced $J_D^2$, which is the (two-dimensional) standard deviation of the angular momentum $J$ after diffusion of the stars around one orbital period $P(E, J)$. Equation (II-8b) should be applied to diffusion over an integer number of orbital paths; we shall consider diffusion around one orbital path since this is the interval between encounters of a star with the black hole. We shall assume steady-state conditions so that there is no dependence of the averaged value of $f$ on time $t$. Then we write $f(E, J)$ and solve equation (II-8b) with $\partial f/\partial t = 0$ to obtain the averaged distribution function

$$f(E, J) \approx f(E, J_{\max})\left[1 - \frac{\ln (J/J_{\max})}{\ln (J_T/J_{\max})}\right], \tag{II-9}$$

in order that $f(E, J_T) = 0$. Here we have assumed that $J_D^2$ is a function of $E$ only, and we have neglected convection terms of the form $\lambda \partial f/\partial J$. However, equation (II-9) will only be in error by a factor of order unity near the loss cone since $\lambda \to 0$ and $J \to 0$ (by symmetry). The flux of stars into the loss cone, $F$, is

$$F = 2\pi\int_{\text{orbit}} \kappa dt/(\ln \Lambda^*) = \pi J_D^2/(2 \ln \Lambda^*)\,, \tag{II-10}$$

where $\ln \Lambda^* = \ln (J_{\max}/J_T)$. The flux $F$ is per unit density of phase space $f(E, J_{\max})$, per orbital period $P$, per unit energy interval $dE = 1$, and per unit solid angle $\Omega(=4\pi)$ subtended by the cluster. Then the number of stars per unit time, per unit energy interval $dE = 1$ flowing into the loss cone, is $(4\pi Ff/P)P$, where the additional factor $P$ allows for the fact that the number of stars at a point in phase space is $N = fP$. The total flux in stars per unit time into the loss cone is then $\Phi = 4\pi \int dEfF$. Hopefully this will be made clearer below when an example is given using this formula.

To calculate $J_D^2$ we make use of the velocity diffusion coefficient perpendicular to the velocity vector (Spitzer 1962), which gives a two-dimensional standard deviation spread of $\langle \Delta v_\perp^2 \rangle$, whence

$$J_D^2 = 2\int_{r_p}^{r_{ap}} dr r^2 \langle \Delta v_\perp^2 \rangle / v_R\,, \tag{II-11a}$$

where

$$\langle \Delta v_\perp^2 \rangle = (8\pi G^2 m_* \rho \ln \Lambda / v)(\Phi - G)(x)\,, \tag{II-11b}$$

with $x = v/2^{1/2}\sigma_v$ and the $(\Phi - G)$ function (not to be confused with the tidal disruption rate $\Phi$ or the gravitation constant $G$) is given by Spitzer (1962). Since we are considering stars near the loss cone, we should evaluate $J_D^2$ for a star in a radial orbit with $J = 0$ when $r_p = 0$ and $r_{ap} = r_*$. Then $v_R = v$, and we find

$$J_D^2(E) = 8\pi G^2 m_* \ln \Lambda \int_0^{r_*} \rho(r) r^2 dr (\Phi - G)(x)/x^2 \sigma_v^2(r)\,, \tag{II-11c}$$

where

$$x = v/2^{1/2}\sigma_v(r) = [E - \phi(r)]^{1/2}/\sigma_v(r)\,, \tag{II-11d}$$

and $_*$ = mean stellar mass, ln $\Lambda$ = "Coulomb logarithm," $\rho(r)$ = stellar density, $\phi(r)$ = gravitational potential, and $\sigma_v(r)$ = one-dimensional velocity dispersion. The use of the value of $\langle \Delta v_\perp{}^2 \rangle$ for a Maxwellian velocity distribution in equation (II-11b) should be valid for any reasonable distribution of stellar velocities, departing only mildly from isotropy (viz., by the logarithmic dependence of $f$ in equation [II-9]).

ii) $J_D/J_T \gg 1$.—Then stars may scatter in and out of the loss cone in one orbital period, and sufficient mixing near the loss cone results in only a very slightly anisotropic distribution function. Thus the flux in one orbital period is

$$F = \pi J_T{}^2 . \tag{II-12}$$

Accordingly we shall take

$$F = \pi J_D{}^2/2 \ln \Lambda^* \quad [J_D/J_T < (2 \ln \Lambda^*)^{1/2}] , \tag{II-13}$$

$$= \pi J_T{}^2 \quad [J_D/J_T > (2 \ln \Lambda^*)^{1/2}] .$$

Writing $f(E, J_{\max}) \equiv f(E)$, we obtain for the total flux rate into the loss cone

$$\Phi = 4\pi \int_0^\infty dE f(E) F(J_D, J_T) \quad (\text{stars s}^{-1}) \tag{II-14a}$$

(the factor $4\pi$ is to allow for the total solid angle subtended by the stellar population). When $J_D/J_T \gg 1$ everywhere in the cluster, $F(J_D, J_T) = \pi J_T{}^2$ and

$$\Phi = 4\pi^2 J_T{}^2 \int_0^\infty dE f(E) . \tag{II-14b}$$

Since

$$4\pi \int_0^\infty dE f(E) = 4\pi \int_0^\infty v dv f(v^2/2) = n_0 \langle v^{-1} \rangle ,$$

where $n_0$ is the central density of the cluster (stars pc$^{-3}$), and $\langle v^{-1} \rangle$ the mean inverse velocity,

$$\Phi = \pi J_T{}^2 n_0 \langle v^{-1} \rangle \quad (\text{stars s}^{-1}) , \tag{II-15}$$

which is in agreement with a simple $\langle n \sigma v \rangle$ argument.

## III. DIFFUSION IN AN ISOTHERMAL SPHERE

The isothermal sphere may be described (Chandrasekhar 1939) by

$$\frac{1}{\xi^2} \frac{d}{d\xi} \left( \xi^2 \frac{d\psi}{d\xi} \right) = e^{-\psi(\xi)} ; \qquad \psi = \frac{d\psi}{d\xi} = 0 (\xi = 0) , \tag{III-1}$$

where the density is $\rho = \rho_0 e^{-\psi(\xi)}$ ($\rho_0$ = central density) and the radial coordinate is $r = a\xi$. The structural length, $a$, is given by

$$a^2 = \sigma_v{}^2/4\pi G \rho_0 . \tag{III-2}$$

We note that

$$\psi(\xi) \approx \xi^2/6 - \xi^4/120 + \xi^6/1890 \quad (\xi \to 0) , \tag{III-3a}$$

$$\rho(\xi)/\rho_0 \approx 1 - \xi^2/6 \quad (\xi \to 0) , \tag{III-3b}$$

$$\rho(\xi)/\rho_0 \approx 2\xi^{-2} \quad (\xi \to \infty) . \tag{III-3c}$$

The gravitational potential is $\phi(r) = \sigma_v{}^2 \psi(\xi)$, with constant velocity dispersion $\sigma_v$. The stellar distribution function is

$$f(E) = n_0 \exp(-E/\sigma_v{}^2)/[\sigma_v (2\pi)^{1/2}]^3 , \tag{III-4}$$

where the stellar number density is $n_0 = \rho_0/m_*$. This gives rise to a Maxwellian distribution of velocities at every point in the cluster. If $J_D/J_T \gg 1$ everywhere in the cluster, then the consumption rate of a central black hole is as calculated by Hills (1975):

$$\Phi = \pi J_T{}^2 \langle v^{-1} \rangle n_0 = J_T{}^2 (2\pi)^{1/2} \sigma_v{}^{-1} n_0 , \tag{III-5}$$

where $\langle v^{-1} \rangle_{\text{Maxwell}} = \sigma_v{}^{-1} (2/\pi)^{1/2}$.

The diffusion in angular momentum in an isothermal sphere (from eq. [II-11c]) is

$$J_D{}^2(E) = 8\pi G^2 m_* \ln \Lambda a^3 \rho_0 \sigma_v{}^{-2} \int_0^{\xi^*} \xi^2 d\xi e^{-\psi} (\Phi - G)(x)/x^2 , \tag{III-6}$$

$$x^2 = \epsilon - \psi(\xi) ; \qquad \epsilon = E/\sigma_v{}^2 ; \qquad \psi(\xi^*) = \epsilon .$$

Thus

$$J_D^2(\epsilon) = 2Gm_* a \ln \Lambda \kappa(\epsilon) , \tag{III-7a}$$

where we have used equation (III-2) and where $\kappa(\epsilon)$ is the integral in equation (III-6). We shall calculate $\kappa(\epsilon)$ in the limiting cases when $\epsilon \ll 1$ and $\epsilon \gg 1$.

i) $\epsilon \ll 1$.—From equation (III-3a), with $\psi(\xi) \approx \xi^2/6$,

$$\epsilon = \psi(\xi^*) \approx \xi^{*2}/6 ,$$

$$\kappa(\epsilon) \approx \int_0^{\xi^*} \xi^2 d\xi (\Phi - G)(x)/x^2 , \tag{III-7b}$$

where

$$x^2 = (\xi^{*2} - \xi^2)/6 .$$

We have set $\exp[-\psi(\xi)] \approx 1$. Making the approximation

$$(\Phi - G)(x) \approx (4/(3\sqrt{\pi}))x \quad (x \to 0) , \tag{III-7c}$$

we find

$$\kappa(\epsilon) \approx [4(2/3\pi)^{1/2}] \int_0^{\xi^*} \xi^2 d\xi/(\xi^{*2} - \xi^2)^{1/2} = 2(6\pi)^{1/2}\epsilon . \tag{III-8}$$

ii) $\epsilon \gg 1$.—Here we approximate using equation (III-3c): $e^{-\psi(\xi)} \approx 2\xi^{-2}$, and then

$$\kappa(\epsilon) \approx \int_0^{\xi^*} 2 d\xi (\Phi - G)(x)/x^2 , \tag{III-9}$$

with

$$x^2 = \epsilon - \psi(\xi) .$$

The major contribution to the integral (III-9) is when $\xi \approx \xi^*$; the lever action of radius $\xi^*$ acting on the velocity diffusion to give the angular momentum diffusion compensates for the lower density outside the core of the cluster. Thus we take $(\Phi - G)$ as in equation (III-7c) to obtain

$$\kappa(\epsilon) \approx (8/3)e^{-\epsilon/2} \operatorname{erf}\{(\epsilon/2)^{1/2}\} . \tag{III-10}$$

Suppose that the critical energy for which $J_D(\epsilon)/J_T = \{2 \ln \Lambda\}^{1/2}$ is $\epsilon = \epsilon_{\text{crit}} = E_{\text{crit}}/\sigma_v^2$, which may be calculated using equations (III-8) or (III-10) above, and by using $J_T^2 = 2GM_H r_T$. Then we divide the flux into the loss cone into two portions,

$$\Phi = \Phi_1|_{\epsilon < \epsilon_{\text{crit}}} + \Phi_2|_{\epsilon > \epsilon_{\text{crit}}} . \tag{III-11}$$

The cluster parts with $\epsilon < \epsilon_{\text{crit}}$ suffer from depleted loss cones, whereas those parts with $\epsilon > \epsilon_{\text{crit}}$ have full loss cones.

From equation (II-14a),

$$\Phi_2 = 4\pi \int_{\epsilon_{\text{crit}}}^{\infty} dE f(E) \pi J_T^2 = \Phi \exp(-\epsilon_{\text{crit}}) , \tag{III-12}$$

where $\Phi$ is given by equation (III-5). Similarly,

$$\Phi_1 = 4\pi \int_{\infty}^{\epsilon_{\text{crit}}} dE f(E)[\pi J_D^2(\epsilon)/2 \ln \Lambda^*] . \tag{III-13a}$$

Thus

$$\Phi_1 = \Phi G m_* a J_T^{-2} \ln \Lambda / \ln \Lambda^* \int_0^{\epsilon_{\text{crit}}} d\epsilon e^{-\epsilon} \kappa(\epsilon) . \tag{III-13b}$$

In the limit $\epsilon_{\text{crit}} \ll 1$, the expression for $\Phi_1$ becomes (using eq. [III-8])

$$\Phi_1 = \Phi[1 - \exp(-\epsilon_{\text{crit}})(1 + \epsilon_{\text{crit}})]/\epsilon_{\text{crit}} \approx \Phi \epsilon_{\text{crit}}/2 . \tag{III-14}$$

Then

$$\Phi_1 + \Phi_2 \approx \Phi(1 - \epsilon_{\text{crit}}/2 + \cdots) . \tag{III-15}$$

A star in radial motion with energy $\epsilon$ can attain a radius $\xi = (6\epsilon)^{1/2}$ for $\xi \leqslant \sqrt{2}$. Thus the cutoff in the flux $\Phi$, starting when $\epsilon_{\rm crit} \approx 1$, occurs when the depleted loss cones are pushed out to a distance $\xi \approx 2$. This is caused by the sharp drop in stellar density for $\xi > \sqrt{2}$. In the limit $\epsilon_{\rm crit} \gg 1$ we find (using eq. [III-10]),

$$\int_0^{\epsilon_{\rm crit}} d\epsilon e^{-\epsilon} \kappa(\epsilon) \to \frac{8\sqrt{2}}{3} \quad (\epsilon_{\rm crit} \to \infty) . \tag{III-16a}$$

Then

$$\Phi_2 \to 0 ; \qquad \Phi_1 \to \Phi G m_* a J_T^{-2} \left(\frac{8\sqrt{2}}{3}\right) \ln \Lambda / \ln \Lambda^* . \tag{III-16b}$$

Thus the constant flux attained as $\epsilon_{\rm crit} \to \infty$ is

$$\Phi_\infty = \left(\frac{16\sqrt{\pi}}{3}\right)(G m_* a n_0/\sigma_v)(\ln \Lambda / \ln \Lambda^*) \quad (star\ s^{-1}) . \tag{III-16c}$$

No contribution to luminosity will be made for $M_H \gtrsim 3 \times 10^8\ M_\odot$ by tidal disruption since after this point the Roche limit is engulfed by the event horizon. As will be seen in § V, the cutoff (eq. [III-15]) and attainment of the limiting flux (eq. [III-16c]) will occur for $M_H \ll 3 \times 10^8\ M_\odot$ in most circumstances.

As will also be shown in § V, for the cases of interest $\epsilon_{\rm crit}$ corresponds to a radius well outside the radius of influence of the black hole in a galactic nucleus. Consequently, the high-density cusp around the black hole has depleted loss cones and makes little contribution to the tidally disrupted flux, the unfortunate stars being removed from the population of the cluster not bound to the black hole.

## IV. DIFFUSION IN A DENSITY CUSP

The loss-cone theory of § II may also be used to obtain the tidal disruption rate of stars held bound to the black hole in the high-density cusp around it. This has relevance to globular clusters (Appendix A), and the calculations may be compared with those of Frank and Rees (1976) and Lightman and Shapiro (1977).

We shall take the stellar distribution function to be (Peebles 1972)

$$f(E) = KE^p ,$$

$$K = \rho_a/(2^{5/2}\pi m_*)(r_a/GM_H)^{p+3/2}[1/B(\tfrac{3}{2}, p+1)] \tag{IV-1a}$$

(where $E$ is negative energy = binding energy to the cusp). Then

$$\rho(r) = \rho_a(r_a/r)^{p+3/2} , \tag{IV-1b}$$

$$\sigma_v(r) = [2/(5+2p)](GM_H/r) , \tag{IV-1c}$$

$$\langle E \rangle(r) = [(2+2p)/(5+2p)](GM_H/r) , \tag{IV-1d}$$

where $r_a$ is the accretion radius of the black hole = "radius of influence"

$$r_a \approx 2GM_H/3\sigma_v^2 . \tag{IV-2}$$

This assumes the gravitational potential of the black hole $\phi = -GM_H/r$ dominates that of the cluster for $r < r_a$. The cusp solution breaks down at a radius

$$r_c^* \approx (Gm_*/r_*)(\ln \Lambda)^{-1/2} , \tag{IV-3}$$

at which radius the cross section for physical collisions between stars equals the diffusion cross section, resulting in the destruction by collisions of stars interior to this radius. Thus the cusp runs from $r_c^* < r < r_a$ in radius or $E_a < E < E_c^*$ in binding energy, where $E_a = GM_H/r_a$; $E_c^* = GM_H/r_c^*$.

In the limit that $J_D \gg J_T$ everywhere in the cusp, then the tidal disruption flux, from equation (II-14b) is,

$$\Phi = 4\pi^2 J_T^2 K \int_{E_a}^{E_c} E^p dE . \tag{IV-4}$$

The truncation at $E = E_c^*$ is necessary to avoid the divergence of the integral as a result of the infinite central density given by equation (IV-1b). Then

$$\Phi_{\rm cusp} = \frac{\pi}{(\sqrt{3})(p+1)B(\frac{3}{2}, p+1)} \frac{\rho_a}{m_*} \frac{J_T^2}{\sigma_v} \left(\frac{E_c^*}{E_a}\right)^{p+1} \left[1 - \left(\frac{E_a}{E_c^*}\right)^{p+1}\right] , \tag{IV-5}$$

so that the enhancement over the basic $\langle n\sigma v\rangle$ flux [eq. (III-5)] is

$$\frac{\Phi_{\rm cusp}}{\Phi} = \frac{1}{2}\left(\frac{2\pi}{3}\right)^{1/2}[(p+1)B(\tfrac{3}{2},p+1)]^{-1}\frac{\rho_a}{\rho_0}\left(\frac{E_c^*}{E_a}\right)^{p+1}\left[1-\left(\frac{E_a}{E_c^*}\right)^{p+1}\right]. \tag{IV-6}$$

If $J_D \ll J_T$ in the cusp, to evaluate the flux it is necessary to have knowledge of the diffusion in angular momentum $J_D(E)$. This may be found from equation (II-11c); we set $\Phi = -GM_H/r$; $\sigma_v^2 = [2/(5+2p)]GM_H/r$ and $X^2 = 1 - rE/GM_H$ to obtain

$$J_D^2(E) = 16\pi I(p)\ln\Lambda(Gm_*\rho_a r_a^4/M_H)\left(\frac{E}{E_a}\right)^{p-5/2}, \tag{IV-7}$$

where

$$I(p) = \int_0^1 (dX/X)(1-X^2)^{-p+3/2}(\Phi - G)\{X[(5+2p)/2]^{1/2}\} \approx 3/4\,. \tag{IV-8}$$

The critical energy $E_{\rm crit}$ such that $J_D^2(E_{\rm crit})/J_T^2 = 2\ln\Lambda^*$ is given by

$$\left(\frac{E_{\rm crit}}{E_a}\right)^{5/2-p} = 4\pi I(p)\frac{\ln\Lambda}{\ln\Lambda^*}\left(\frac{\rho_a r_a^3}{M_H}\right)\left(\frac{m_*}{M_H}\right)\left(\frac{r_a}{r_T}\right) \tag{IV-9}$$

and the flux into the loss cones, assuming $J_D \ll J_T$ everywhere in the cusp (i.e., $E_{\rm crit} < E_a$), by

$$\Phi_{\rm cusp} = \frac{2\pi}{(\sqrt{3})(3-4p)B(\frac{3}{2},p+1)}\left[1-\left(\frac{E_a}{E_c^*}\right)^{3/2-2p}\right]\left(\frac{\rho_a}{m_*}\right)\left(\frac{J_T^2}{\sigma_v}\right)\left(\frac{E_{\rm crit}}{E_a}\right)^{5/2-p}. \tag{IV-10}$$

Thus the depletion in flux due to empty loss cones is

$$\frac{\Phi_{\rm cusp}^*}{\Phi_{\rm cusp}} = \frac{2(p+1)}{3-4p}\frac{[1-(E_a/E_c^*)^{3/2-2p}]}{[1-(E_a/E_c^*)^{p+1}]}\left(\frac{E_a}{E_c^*}\right)^{p+1}\left(\frac{E_{\rm crit}}{E_a}\right)^{5/2-p} \tag{IV-11}$$

and the ratio to the basic $\langle n\sigma v\rangle$ flux is

$$\frac{\Phi_{\rm cusp}^*}{\Phi} = \frac{(p+1)}{3-4p}\left(\frac{2\pi}{3}\right)^{1/2}[(p+1)B(\tfrac{3}{2},p+1)]^{-1}\left[1-\left(\frac{E_a}{E_c^*}\right)^{(3/2)-2p}\right]\left(\frac{\rho_a}{\rho_0}\right)\left(\frac{E_{\rm crit}}{E_a}\right)^{5/2-p}. \tag{IV-12}$$

For typical cases $p \approx 1/4$; $E_c^*/E_a = 10$ (galaxy) or $10^3$ (globular cluster), and $\rho_a/\rho_0 \approx \exp(3/2)$. Then from equation (IV-6) we see that when the loss cones in the cusp are filled (i.e., $J_D \gg J_T$ or $E_{\rm crit} > E_c^*$), then $\Phi_{\rm cusp}/\Phi \gg 1$, as might be expected. If they are depleted throughout the cusp (i.e., $J_T \gg J_D$ or $E_{\rm crit} < E_a$), then (from eq. [IV-10a]) we see $\Phi_{\rm cusp}^*/\Phi_{\rm cusp} \ll 1$, and in fact the rate drops below even the $\langle n\sigma v\rangle$ rate, $\Phi_{\rm cusp}^*/\Phi \ll 1$.

It turns out that the full loss-cone case is applicable to globular clusters (Appendix A) and the depleted case to galaxies (§ V). If $E_a < E_{\rm crit} < E_c^*$, the intermediate case between completely full and totally depleted loss cones is then

$$\frac{\tilde\Phi_{\rm cusp}}{\Phi} = \frac{1}{2}\left(\frac{2\pi}{3}\right)^{1/2}[(p+1)B(\tfrac{3}{2},p+1)]^{-1}\left(\frac{\rho_a}{\rho_0}\right)\left(\frac{E_{\rm crit}}{E_a}\right)^{p+1}\left\{\left[1-\left(\frac{E_a}{E_{\rm crit}}\right)^{p+1}\right]+\frac{2(p+1)}{3-4p}\left[1-\left(\frac{E_{\rm crit}}{E_c^*}\right)^{3/2-2p}\right]\right\}. \tag{IV-13}$$

If $E_c^* \gg E_a$ then we have approximately

$$\Phi_{\rm cusp} \approx (\rho_a/\rho_0)(E_c^*/E_a)^{p+1}\Phi \propto M_H^{4/3} \tag{IV-14a}$$

when loss cones are full throughout the cusp (i.e., $E_{\rm crit} \gg E_c^*$), and

$$\tilde\Phi_{\rm cusp} \approx (\rho_a/\rho_0)(E_{\rm crit}/E_a)^{p+1}\Phi \propto M_H^{q} \tag{IV-14b}$$

when $E_a \ll E_{\rm crit} \ll E_c^*$. The exponent is $q = (4/3) + (5/3)(p+1)/(5/2-p) = 61/27$ (when $p = 1/4$); the value of $(E_{\rm crit}/E_a)$ is from equation (IV-9).

Lastly,

$$\Phi_{\rm cusp}^* \approx (\rho_a/\rho_0)(E_{\rm crit}/E_a)^{5/2-p}\Phi \propto M_H^3 \tag{IV-14c}$$

when $E_{\rm crit} \ll E_a$ and loss cones are depleted throughout the cusp.

## V. NUMERICAL EXAMPLES

In this section we shall compute the loss-cone tidal disruption rates in a galactic nucleus, and for that purpose it is convenient to work in terms of the central density $\rho_6(\rho_0$ in units of $10^6\ M\ \mathrm{pc}^{-3})$ and $v_{200}(\sigma_v$ in units of $200\ \mathrm{km\ s}^{-1})$ which define the structure of the isothermal sphere to be used as an approximation. The black-hole mass will be measured in Megasols, $M_6 = M_H/10^6\ M_\odot$. Then we find,

$$a = 0.86 v_{200} \rho_6^{1/2} \quad \text{(pc)}, \tag{V-1a}$$

$$r_a = 0.072\ M_6 v_{200}^{-2} \quad \text{(pc)}, \tag{V-1b}$$

$$r_T = 2.1 \times 10^{-6}\ M_6^{1/3} \quad \text{(pc)}, \tag{V-1c}$$

where $r_T$ is the mean value of the Roche peribarathron for main-sequence stars weighted for a realistic mass spectrum and including the effects of partial disruption (Young, Shields, and Wheeler 1977) but not "tidal capture" (Frank and Rees 1976). We shall take a mean stellar mass $m_* = 0.5\ M_\odot$ to convert the fluxes calculated in §§ III and IV from (stars $\mathrm{s}^{-1}$) to $(M_\odot\ \mathrm{yr}^{-1})$. Then the basic $\langle n\sigma v\rangle$ flux is

$$\Phi = 2 \times 10^{-4}\ M_6^{4/3} \rho_6 v_{200}^{-1} \quad (M_\odot\ \mathrm{yr}^{-1}). \tag{V-2}$$

First we shall determine the point at which the drop-off in density outside the nucleus truncates this basic flux. This occurs when (§ III) $\epsilon_{\mathrm{crit}} = 1$. We obtain $\epsilon_{\mathrm{crit}}$ from equation (III-8) and the condition $J_D(\epsilon_{\mathrm{crit}})/J_T = [2 \ln \Lambda]^{1/2}$, when we find

$$\epsilon_{\mathrm{crit}} = (\ln \Lambda^*/\ln \Lambda)(\pi/6)^{1/2}(M_H/m_*)(r_T/a) = 3.4\ M_6^{4/3} \rho_6^{1/2}\ v_{200}^{-1}. \tag{V-3}$$

The "cutoff" mass such that $\epsilon_{\mathrm{crit}} = 1$ is therefore

$$M_6^* = 0.4 \rho_6^{-3/8} v_{200}^{3/4}. \tag{V-4}$$

The limiting flux as $\epsilon_{\mathrm{crit}} \to \infty$ is (from eq. [III-16c])

$$\Phi_\infty = 9 \times 10^{-5} \rho_6^{1/2} \quad (M_\odot\ \mathrm{yr}^{-1}) \tag{V-5}$$

to which the tidal flux monotonically rises as $M_H$ increases.

The tidal growth time scale based on the $\langle n\sigma v\rangle$ flux (eq. [V-2]) is defined as the time required for the black hole to grow from a given mass $M_6$ to infinite mass,

$$\tau_{\mathrm{tide}} = 1 \times 10^{10}\ M_6^{-1/3} \rho_6^{-1} v_{200} \quad \text{(yr)}, \tag{V-6}$$

and the time to grow from $M_6$ to $M_6'$ is then

$$\tau = \tau_{\mathrm{tide}}[1 - (M_6/M_6')^{1/3}] \quad \text{(yr)}. \tag{V-7}$$

We shall now verify that the loss cones in the density cusp around the black hole are depleted and that the cusp contributes little to the tidal disruption rate. From equation (IV-9),

$$(E_{\mathrm{crit}}/E_a)^{-p+5/2} = 6 \times 10^{-5}\ M_6^{5/3} \rho_6 v_{200}^{-8}. \tag{V-8}$$

The flux, from equation (IV-12), is then

$$\Phi_{\mathrm{cusp}}^*/\Phi \approx (\rho_a/\rho_0)(E_{\mathrm{crit}}/E_a)^{-p+5/2} \approx 10^{-4}\ M_6^{5/3} \rho_6 v_{200}^{-8}, \tag{V-9}$$

which, in the cases to be considered, is usually negligible. It may not be in the case of a compact $E$ galaxy with low central velocity dispersion $v_{200} \approx 0.5$. Then $(E_{\mathrm{crit}}/E_a) = 1$ when $M_6 \approx 10$. Since, however, for the compact $E$ system $M_6^* \approx 0.1$, this effect is never important.

For red-giant stars we must modify the effective Roche radius to

$$r_T^{\mathrm{RG}} \approx 4 r_T, \tag{V-10a}$$

and the red-giant density is

$$\rho_{\mathrm{RG}} \approx 0.02\ \rho \tag{V-10b}$$

(these results being from the detailed calculations of Young, Shields, and Wheeler 1977). Thus

$$\Phi_{\mathrm{RG}} \approx 0.08\ \Phi, \tag{V-11a}$$

$$\Phi_{\infty,\mathrm{RG}} \approx 0.02\ \Phi_\infty, \tag{V-11b}$$

are the basic $\langle n\sigma v\rangle$ and limiting rates, respectively. The flux cutoff occurs earlier, at $M_6{}^*{}_{,\mathrm{RG}} \approx M_6{}^*/4$. Thus the red-giant flux can never be very important until the expansion of the event horizon fills the main-sequence Roche limit, leaving only the red-giant flux contributing to the luminosity (the main-sequence flux becomes "dark"; it plunges directly into the hole). Details of this cutoff for a Kerr hole are given in Young, Shields, and Wheeler 1977. The effect of the massive stars (i.e., the red giants) settling into the nucleus has not been included. This would increase $\rho_{\mathrm{RG}}$ and decrease $\sigma_{v,\mathrm{RG}}$, but the effect is not likely to be important.

We see, from the fluxes given by equations (V-2) and (V-5), noting that $1\ M_\odot\ \mathrm{yr}^{-1} = 4.5 \times 10^{12}\ L_\odot$ (at $\eta = 0.3\ mc^2$ efficiency), that tidal disruption fluxes are not able to provide the power of a QSO ($10^{11-13}\ L_\odot$), although they may reach Seyfert galaxy nucleus power ($10^{9-11}\ L_\odot$) in a dense galactic nucleus. However, other effects to be discussed in § VI will be more important. The question of the relevance of the tidal flux relative to these other processes in various types of galactic nuclei will be returned to in § VII.

We may now comment that we have assumed that the black hole is at the exact center of a spherically symmetric cluster, and further that we have neglected large-angle scatterings between the stars. We note the following:

1. The tidal disruption rate of stars will only be affected by the motion of the black hole in the cluster when (*a*) it is large enough to have depleted loss cones and (*b*) the "square dance" executed by the black hole is sufficient to smear out the loss cones. The radial excursions of the hole are roughly (Bahcall and Wolf 1976)

$$\langle r^2\rangle^{1/2} = 3a(m_*/M_H)^{1/2}\,. \tag{V-12a}$$

The tidal impact parameter is given by

$$b_T = J_T/3^{1/2}\sigma_v\,, \tag{V-12b}$$

and so

$$(\langle r^2\rangle/b_T{}^2) \approx 54\pi(m_*/M_H)(\rho_0 a^3/M_H)(a/r_T)\,. \tag{V-12c}$$

Trouble may result when (*a*) $\epsilon_{\mathrm{crit}} > 1$ and (*b*) $\langle r^2\rangle/b_T{}^2 \gg 1$. For a globular cluster this problem does not occur, but in a galactic nucleus we find, for $\epsilon_{\mathrm{crit}} = 1$, that $\langle r^2\rangle/b_T{}^2 \approx 100$ and that serious smearing occurs. This may be allowed for by considering the loss cone to be of size $J_s \approx J_T(\langle r^2\rangle/b_T{}^2)^{1/2}$. In the diffusion approximation we would consider diffusion over $J_s{}^2/J_T{}^2$ orbital periods rather than one orbital period, since the star will expect to orbit this many times within the loss cone before being destroyed, and we find that we must change $\ln \Lambda^*$ to $\ln(J_{\max}/J_s)$, which does not alter the flux rates drastically.

2. The oscillating potential of the black hole acting upon stars in the cluster may stir up the stars in the nucleus somewhat more rapidly than star-star encounters and increase the relaxation rate into the loss cones. We have not allowed for the possibility of this effect.

3. In the case of a rotating (axisymmetric) galaxy we note that in the region where the potential of the black hole is dominant the gravitational potential is spherically symmetric, $J$ is still conserved around an orbital path of a star (without collisions), and the concept of a loss cone $J < J_T$ is still valid. However, in the cluster at large, in general only the azimuthal component $J_z$ of the angular momentum $\boldsymbol{J}$ is conserved; $J_x$ and $J_y$ are changed by motion through the potential so that the concept of a loss cone becomes less simple. If the angular velocity of the galactic nucleus is $\Omega$, then the resulting centrifugal potential is $(\Omega^2 r^2 \cos^2\theta)/2$. Since

$$dJ_x/dt \approx -\partial\psi/\partial\theta \approx \Omega^2 r^2 \cos\theta \sin\theta\,,$$

we would expect $J_x$ to change significantly on time scales (at $r \approx r_{\mathrm{crit}}$)

$$\Delta t \approx J_{\max}/\Omega^2 r^2{}_{\mathrm{crit}} \approx (4\pi G\rho_0/\Omega^2)(a/r_{\mathrm{crit}})$$

in an isothermal sphere; i.e., in $(\Omega^2\xi_{\mathrm{crit}})^{-1}$ dynamical time scales. This may be important if $\xi_{\mathrm{crit}}$ and $\Omega^2$ are large enough that $(t_R/t_D) > (\Omega^2\xi_{\mathrm{crit}})^{-1}$. If $(t_R/t_D) \approx 10^6$ and $\xi_{\mathrm{crit}} \approx 1$, then $\Omega \gtrsim 10^{-3}$ will suffice. We leave the investigation of the importance of this for later work. (I thank Richard Wolf for pointing out this effect.)

4. Large-angle scatterings occur at a rate $1/(8\ln\Lambda)$ of the rate at which small-angle, diffusive scatterings occur (Spitzer 1962). Since the large-angle scattering is largely unaffected by the presence of a depleted loss cone, we may crudely set

$$\Phi_{\mathrm{ls}} \approx \Phi_{<n\sigma v>}/(8\ln\Lambda)\,. \tag{V-13}$$

This is never an important source of flux because the "luminous flux" cuts off when $M_H \approx 3 \times 10^8\ M_\odot$ as the Roche tidal limit is engulfed by the event horizon of the black hole. It should be noted that the large-angle scattering does not suffer from the cutoff due to depleted loss cones and may therefore be an important factor in the growth of a large black hole via a "dark" plunge flux.

## VI. STELLAR COLLISIONS

The rate at which stars collide in an isothermal sphere, and also in a density cusp around a black hole, can be calculated with the following results:

$$C_{\rm cusp} \approx 8\pi^2\left(\frac{\rho_a}{m_*}\right)^2 r_a{}^3\left[\frac{Gq_c(m+m_*)}{\sigma_v}\alpha_1 + 2q_c{}^2\sigma_v\alpha_2\right], \tag{VI-1a}$$

$$\alpha_1 \approx (2p-\tfrac{1}{2})^{-1}[(E_c{}^*/E_a)^{2p-1/2}-1] \approx \ln(E_c{}^*/E_a), \tag{VI-1b}$$

$$\alpha_2 \approx (2p+\tfrac{1}{2})^{-1}[(E_c{}^*/E_a)^{2p+1/2}-1] \approx (E_c{}^*/E_a), \tag{VI-1c}$$

where $q_c$ is the collision periastron. For stars $m = m_* \approx 0.5\ M_\odot$, $r_* \approx 0.5\ R_\odot$, $q_c \approx 1\ R_\odot$. The collision rate in an isothermal sphere is

$$C_{\rm cluster} \sim 20\pi^{3/2}\left(\frac{\rho_0}{m_*}\right)^2 a^3\left[\frac{G(m+m_*)q_c}{\sigma_v} + 4q_c{}^2\sigma_v\right]. \tag{VI-2}$$

The ratio of the collision rates

$$C_{\rm cusp}/C_{\rm cluster} \approx \frac{2\sqrt{\pi}}{5}\left(\frac{\rho_a}{\rho_0}\right)^2\left(\frac{r_a}{a}\right)^3, \tag{VI-3a}$$

and this ratio reaches a maximum when $r_a = 2^{1/2}a$; and taking $\rho_a \approx \rho_0 \exp(3/2)$ (see below),

$$C_{\rm cusp}/C_{\rm cluster}|_{\rm max} \approx 40. \tag{VI-3b}$$

Approximating the run of density in an isothermal sphere by

$$\rho(\xi) = \rho_0(\xi < 2^{1/2}); \qquad \rho(\xi) = 2\rho_0\xi^{-2} \quad (\xi > 2^{1/2}), \tag{VI-4}$$

we see that we may write the collision rates in a cusp as

$$C = C_{\rm crit}\begin{cases}(M/M_{\rm crit})^3 & (M < M_{\rm crit})\\ (M_{\rm crit}/M) & (M > M_{\rm crit}),\end{cases} \tag{VI-5}$$

where $M_{\rm crit}$ is the mass of the black hole such that $r_a = 2^{1/2}a$. We take $\rho_a \approx \rho(r_a)\exp(3/2)$ to allow for the isothermal seepage of stars into the fringes of the potential well of the hole according to a Boltzmann distribution. We may compute

$$M_{\rm crit,6} = 17\rho_6{}^{-1/2}v_{200}{}^3. \tag{VI-6}$$

The collision energy

$$E_c{}^{*1/2} \approx 625\ {\rm km\ s^{-1}} \tag{VI-7a}$$

[with $E_c{}^* \approx (Gm_*/q_c)(\ln\Lambda)^{1/2}$; $m_* = 0.5\ M_\odot$; $q_c = 1\ R_\odot$, $\ln\Lambda \approx 17$]. Thus

$$E_c{}^*/E_a \approx 6v_{200}{}^{-2}. \tag{VI-7b}$$

For a typical galactic nucleus the cusp only extends a short distance in logarithmic radius. In a cD galaxy with high central velocity dispersion, $v_{200} \approx 2.5$; $E_c{}^* \approx E_a$, and the cusp does not form properly.

It is important to separate the effects of low-velocity collisions (resulting in stellar fusion) and high-velocity (disruptive) collisions given by the first and second terms of equation (VI-1), respectively. We find

$$C_{\rm cusp}{}^{\rm hv} = (2\times10^{-6})\,M_6{}^3\rho_6{}^2v_{200}{}^{-7} \quad (M_\odot\ {\rm yr^{-1}}), \tag{VI-8a}$$

$$C_{\rm crit}{}^{\rm hv} = (10^{-2})\rho_6{}^{1/2}v_{200}{}^2 \quad (M_\odot\ {\rm yr^{-1}}), \tag{VI-8b}$$

for the fluxes due to high-velocity collisions only. We have set $p = 1/4$ (Bahcall and Wolf 1976). The low-velocity collisions do not generate gaseous flux, but the rate is

$$C_{\rm cusp}{}^{\rm lv} = (5\times10^{-7})\,M_6{}^3\rho_6{}^2v_{200}{}^{-7}\ln(6v_{200}{}^{-2}), \quad (M_\odot\ {\rm yr^{-1}}), \tag{VI-8c}$$

or

$$C_{\rm cusp}{}^{\rm lv} = C_{\rm cusp}{}^{\rm hv}[\ln(6v_{200}{}^{-2})/4] \quad (M_\odot\ {\rm yr^{-1}}). \tag{VI-8d}$$

For a galactic nucleus $C_{\rm cusp}{}^{\rm lv} \approx C_{\rm cusp}{}^{\rm hv}/2$.

Most of the high-velocity collisions occur near the inner edge of the cusp at relative velocities $\gtrsim 1200\ {\rm km\ s^{-1}}$. The binding energy per unit mass of a typical main-sequence star is $\sim(300\ {\rm km\ s^{-1}})^2$ and the collision energy per

unit mass is $\sim(600 \text{ km s}^{-1})^2$, so there is adequate energy to entirely disrupt both stars. The debris from collisions in the cusp is bound to the black hole and is likely to be accreted; that from collisions in the unbound stellar population has an uncertain fate.

Another process which operates in the cusp is "gravitational diffusion" (Bahcall and Wolf 1976) in which the presence of an inner edge to the cusp destroys the steady-state nature of the solution $f(E) = KE^p$ (with $p = 1/4$). From numerical integration the rate found by Bahcall and Wolf was

$$D_{\text{cusp}} \approx (32/9)[M_{\text{cusp}}/t_R(r = r_a)](E_a/E_c^*) . \tag{VI-9}$$

The mass of the cusp is

$$M_{\text{cusp}} = 1.7 \times 10^4 M_6^3 v_{200}^{-6} \rho_6 \quad (M_\odot) \tag{VI-10a}$$

and the relaxation time at $r = r_a$ is

$$t_R = (7 \times 10^{10}/\ln \Lambda) v_{200}^3 \rho_6^{-1} = (4 \times 10^9) v_{200}^3 \rho_6^{-1} \quad (\text{yr}) . \tag{VI-10b}$$

Then

$$D_{\text{cusp}} = 2 \times 10^{-6} M_6^3 v_{200}^{-7} \rho_6^2 \quad (M_\odot \text{ yr}^{-1}) , \tag{VI-11a}$$

$$D_{\text{crit}} = 10^{-2} \rho_6^{1/2} v_{200}^2 \quad (M_\odot \text{ yr}^{-1}) , \tag{VI-11b}$$

where the scaling is as in equation (VI-5).

A point to note is that the rates $C_{\text{cusp}}$, $D_{\text{cusp}}$ have been calculated using a solution for the cusp in which $M_H > M_{\text{cusp}}$. In actual fact, when $M_H \gtrsim M_{\text{crit}}$ we have $(M_{\text{cusp}}/M_H) \approx 5$ (its maximum value). This will add the mass of the cusp to that of the black hole, enlarging the "accretion radius" $r_a$ and increasing the effective size of the cusp, which may raise the rates $C_{\text{cusp}}$, $D_{\text{cusp}}$ somewhat above the values quoted here, but we shall continue to use equations (VI-8) and (VI-11) for illustrative purposes.

The growth time scales ($M_6$ to infinite mass) are

$$\tau_C = 2 \times 10^{11} M_6^{-2} \rho_6^{-2} v_{200}^{6+4p} \quad (\text{yr}) , \tag{VI-12a}$$

$$\tau_D = 2 \times 10^{11} M_6^{-2} \rho_6^{-2} v_{200}^7 \quad (\text{yr}) , \tag{VI-12b}$$

to be multiplied by $[1 - (M_6/M_6')^2]$ when the growth time from $M_6$ to $M_6'$ is required. The fluxes $C_{\text{cusp}}$, $D_{\text{cusp}}$ are of the same order of magnitude and may each be capable of explaining QSO luminosities in the denser galactic nuclei ($\rho_6 = 10^{1-2}$) or Seyfert nucleus luminosities in the more modest galaxies ($\rho_6 \lesssim 10$). This will be discussed in more detail in the next section.

## VII. DISCUSSION

The conditions in galactic nuclei are, at the present time, largely unknown, with only a handful of velocity dispersion measures and estimates of central density. Because of this we shall select values of $\rho_6$ and $v_{200}$ that are compatible with these estimates (de Vaucouleurs 1974) and also with the galactic structure as described by the $r^{1/4}$ law in the measurable regions (Young 1976).

We shall calculate the flux rates generated by the black hole for the various processes described in §§ II–VI, but we will not concern ourselves with speculations about how much of the debris the black hole finally accretes or with what efficiency, but will assume that it is all eaten at $\eta = 0.3\, mc^2$ (for a Kerr hole with $J = 0.998\, M^2$), although the hole may be Schwarzschild (and $\eta = 0.06\, mc^2$) when it is fed only by the tidal disruption flux (Young 1977). It should be noted, however, that the tidal disruption flux generates debris with angular momentum for a Keplerian orbit around the hole at $r = r_T$, but that collisions and gravitational diffusion yield debris orbiting at $r = r_c^* \gg r_T$. The binding energies are similar, and the tidal flux ends up as gas clouds moving in highly elliptical orbits between $r_T$ and $r_c^*$, whereas the collision/gravitational diffusion flux, which dominates when the hole is large, is initially in circular orbit at $r_c^*$. We may therefore expect differences in kind as well as degree in the power output of the hole, depending upon which flux is dominant.

In Table 1 we give the parameters and flux rates of a black hole embedded in four selected galactic nuclei, these scenarios also being displayed in Figures 1*a*–1*d*. The Eddington flux and luminosity are given by

$$L_{\text{Edd}} = 3 \times 10^{10} M_6 \quad (L_\odot) ,$$

$$F_{\text{Edd}} = 7.5 \times 10^{-3} (0.3/\eta) M_6 \quad (M_\odot \text{ yr}^{-1}) ,$$

$$\tau_{\text{Edd}} = 1.3 \times 10^8 (\eta/0.3) \quad (\text{yr}) ,$$

TABLE 1

GROWTH OF A BLACK HOLE IN A GALACTIC NUCLEUS

| Quantity | "Normal" Galaxy | Compact E | cD | Superdense Nucleus |
|---|---|---|---|---|
| $\rho_6$ | 1 | 10 | 0.5 | 50 |
| $v_{200}$ | 1 | 0.5 | 2.5 | 1.5 |
| $a$ (pc) | 0.86 | 0.14 | 3.0 | 0.18 |
| $r_T$ (pc) | $2.1 \times 10^{-6} M_6^{1/3}$ | $2.1 \times 10^{-6} M_6^{1/3}$ | $2.1 \times 10^{-6} M_6^{1/3}$ | $2.1 \times 10^{-6} M_6^{1/3}$ |
| $\epsilon_{crit}$ | $3.4 M_6^{4/3}$ | $21 M_6^{4/3}$ | $0.96 M_6^{4/3}$ | $16 M_6^{4/3}$ |
| $M_6$* | 0.4 | 0.1 | 1.0 | 0.13 |
| $\Phi$ ($M_\odot$ yr$^{-1}$) | $2 \times 10^{-4} M_6^{4/3}$ | $4 \times 10^{-3} M_6^{4/3}$ | $4 \times 10^{-5} M_6^{4/3}$ | $7 \times 10^{-3} M_6^{4/3}$ |
| $\Phi_\infty$ ($M_\odot$ yr$^{-1}$) | $9 \times 10^{-5}$ | $3 \times 10^{-4}$ | $6 \times 10^{-5}$ | $6 \times 10^{-4}$ |
| $L_\infty$ ($L_\odot$) | $4 \times 10^8$ | $10^9$ | $3 \times 10^8$ | $3 \times 10^9$ |
| $\tau_{tide}$ (yr) | $10^{10} M_6^{-1/3}$ | $7 \times 10^8 M_6^{-1/3}$ | $7 \times 10^{10} M_6^{-1/3}$ | $4 \times 10^8 M_6^{-1/3}$ |
| $r_a$ (pc) | $0.072 M_6$ | $0.29 M_6$ | $0.012 M_6$ | $0.032 M_6$ |
| $M_{crit,6}$ | 17 | 0.67 | 380 | 8.1 |
| $C_{cusp}^{hv}$ ($M_\odot$ yr$^{-1}$) | $2 \times 10^{-6} M_6^3$ | $3 \times 10^{-2} M_6^3$ | $8 \times 10^{-10} M_6^3$ | $3 \times 10^{-4} M_6^3$ |
| $C_{crit}^{hv}$ ($M_\odot$ yr$^{-1}$) | $10^{-2}$ | $8 \times 10^{-3}$ | $4 \times 10^{-2}$ | $2 \times 10^{-1}$ |
| $L_{crit}$ ($L_\odot$) | $5 \times 10^{10}$ | $4 \times 10^{10}$ | $2 \times 10^{11}$ | $7 \times 10^{11}$ |
| $\tau_C$ (yr) | $2 \times 10^{11} M_6^{-2}$ | $2 \times 10^7 M_6^{-2}$ | $6 \times 10^{14} M_6^{-2}$ | $2 \times 10^9 M_6^{-2}$ |
| $D_{cusp}$ ($M_\odot$ yr$^{-1}$) | $2 \times 10^{-6} M_6^3$ | $3 \times 10^{-2} M_6^3$ | $8 \times 10^{-10} M_6^3$ | $3 \times 10^{-4} M_6^3$ |
| $D_{crit}$ ($M_\odot$ yr$^{-1}$) | $10^{-2}$ | $8 \times 10^{-3}$ | $4 \times 10^{-2}$ | $2 \times 10^{-1}$ |
| $L_{crit}$ ($L_\odot$) | $4 \times 10^{10}$ | $4 \times 10^{10}$ | $2 \times 10^{11}$ | $8 \times 10^{11}$ |
| $\tau_D$ (yr) | $2 \times 10^{11} M_6^{-2}$ | $2 \times 10^7 M_6^{-2}$ | $5 \times 10^{14} M_6^{-2}$ | $2 \times 10^9 M_6^{-2}$ |

where $\tau_{Edd}$ is the $e$-folding time of the black hole. If at any stage the flux rates are greater than $F_{Edd}$, then material may either be blown out of the nucleus or stored in an accretion disk for later consumption. We comment on the effects of a black hole in the four selected nuclei as follows:

*a) "Normal" Galaxy; $\rho_6 = 1$; $v_{200} = 1$ (Fig. 1a)*

We may consider initial black-hole masses of between 10 $M_\odot$ (from stellar evolution [Wheeler and Shields 1976]) and $10^4$ $M_\odot$ (from collapse of a supermassive star, for example). In that case the growth time scale to $\sim 10^6$ $M_\odot$, where the cusp effects around the black hole create a "runaway" to high luminosity (see Fig. 1), is $\gtrsim 5 \times 10^{10}$ yr, so that the hole cannot have grown much above $10^5$ $M_\odot$. In that case it will be fed by tidal disruption of unbound stars and can output energy at $\sim 10^7$ $L_\odot$ (for estimates of the strength of Sag A see Lynden-Bell and Rees 1971). Thus black holes which were created too small or in an insufficiently dense galactic nucleus will have failed to mature into fully fledged QSO or Seyfert phenomena and may explain "weak" active nuclei such as to be found in our own Galaxy.

*b) Compact E Galaxy; $\rho_6 = 10$; $v_{200} = 0.5$ (Fig. 1b)*

This nucleus is a splendid place to cultivate a black hole. It may grow from 10 $M_\odot$ to $10^6$ $M_\odot$ in only $3 \times 10^{10}$ yr, when a cusp will form and the hole will wreak havoc in the nucleus and attain a power output of $10^{11}$ $L_\odot$. Despite the fact that the high density and low velocity dispersions in the nuclei of these compact E systems allow the hole to impose its will on the nucleus and grow rapidly, such galaxies are not observed to be active. This is curious since one might expect at least a few black holes of 10 $M_\odot$ to form from stellar evolution. It suggests that "glut" problems (Young, Shields, and Wheeler 1977) may not allow a small black hole $M_H \lesssim 10^4$ $M_\odot$ to grow. Alternatively, rare events of this type may occur and may manifest themselves as weak "quasars" with no traces of surrounding nebulosity.

*c) cD Galaxy; $\rho_6 = 0.5$, $v_{200} = 2.5$ (Fig. 1c)*

Since these galaxies have large effective radii, the nuclear density is probably quite low. The central velocity dispersion for M87 has been measured at 500 km s$^{-1}$ (de Vaucouleurs 1974). These two properties make life difficult for a black hole in the nucleus; it can spend $10^{10}$ yr growing from 1–2 $\times$ $10^5$ $M_\odot$. We would expect a black hole in such a nucleus to be "stillborn," never developing into a QSO—at least not by the processes discussed here. If $M_H \approx 10^5$ $M_\odot$ it could output power at $10^7$ $L_\odot$ for an essentially indefinite period from tidal disruption of unbound stars (the power of the peculiar cD galaxy N5128 = Cen A is $10^{7-8}$ $L_\odot$; Kellerman *et al.* 1975).

The cD galaxy could develop into a powerful ($\gtrsim 10^{10}$ $L_\odot$) object only if the galaxy condensed around a seed black hole of $\gtrsim 10^7$ $M_\odot$, allowing a cusp to form immediately. It has been suggested that a galaxy may form around a primordial black hole of this mass (Ryan 1972).

*d) Superdense Nucleus; $\rho_6 = 50$, $v_{200} = 1.5$ (Fig. 1d)*

In this example a peak luminosity of $\sim 10^{12}$ $L_\odot$ may be attained, with growth from $10^4$ $M_\odot$ taking only $2 \times 10^9$ yr. Quasars should occur in those relatively rare galaxies which enjoy both a high central density and the benefit

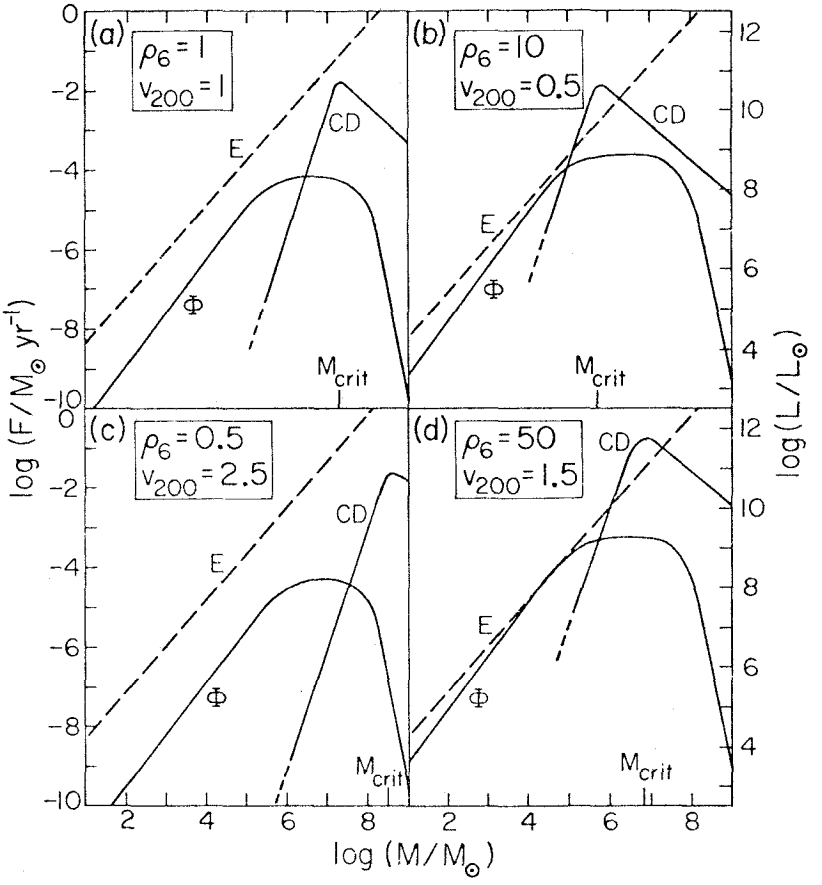


FIG. 1.—Growth of a black hole in various galactic nuclei. E is the Eddington limiting flux, Φ the tidal disruption rate, and CD the stellar collision plus gravitational diffusion fluxes from the density cusp. Conversion of $M_\odot\ \mathrm{yr}^{-1}$ to $L_\odot$ is via an efficiency of $0.3\ mc^2$.

of an initial massive black hole. Seyfert nuclei may be explained by lowering the central density to $\rho_6 \approx 5$ when luminosities $\lesssim 10^{11}\ L_\odot$ may be attained after $10^{10}$ yr. On this hypothesis quasars peaking after $2 \times 10^9$ yr at $10^{12}\ L_\odot$ should be noisy diers, since after $10^{10}$ yr the luminosity would still be $10^{10}\ L_\odot$ and decaying slowly as $t^{-1/2}$. The lifetime at peak luminosity would be $\sim 10^7$ yr, after which the quasar could expect a long lifetime as a slowly decaying radio galaxy (perhaps).

In conclusion, it seems as if the black hole residing in a galactic nucleus may indeed be able to extract the energy to become a quasar by destroying the stars of the nucleus with tidal disruption and by star-star collisions in a high-density cusp around the hole. We may explain QSO luminosities of up to $\sim 10^{12}\ L_\odot$ by this type of model but we cannot explain the superluminous objects emitting $\gtrsim 10^{13}\ L_\odot$ in a time-averaged sense without invoking absurdly high densities in galactic nuclei. However, the total energy output of a QSO ($\gtrsim 10^{61}$ ergs) may be explained with ease, and the many scenarios available by varying the parameters $\rho_6$, $v_{200}$, and $M_H(t = 0)$ make it possible to explain a variety of activity in galactic nuclei by the model of a black hole wreaking carnage in an isothermal sphere.

I thank Peter Goldreich, Gregory Shields, Craig Wheeler, and Richard Wolf for valuable assistance and helpful suggestions. I also thank the University of Texas at Austin and the California Institute of Technology for providing cash for my support while this work was performed.

## APPENDIX

## GROWTH OF A BLACK HOLE IN A GLOBULAR CLUSTER

There has been much speculation concerning the presence of a massive black hole ($M_H \approx 10^3\ M_\odot$) in certain globular clusters (Bahcall and Ostriker 1975; Silk and Arons 1975) to explain X-ray emission from 7 of these

objects [N1851, N6440, N6441, N6624, N7078 (M15), N6712, and MXB 1730–335; (Giacconi *et al.* 1974; Clark, Markert, and Li 1975; Canizares and Neighbours 1975; Cominsky *et al.* 1977), and X-ray bursts from two (N6624; N1851, [Grindlay *et al.* 1976; Forman and Jones 1976]). Certain other objects are suspected emitters [e.g., N5904 (M5)]. In addition, a luminosity excess in the central regions of M15 has been interpreted as evidence for a central massive object, $M = 800 \approx 300\ M_\odot$ (Newell, DaCosta, and Norris 1976). Papers by Frank and Rees (1976), Lightman and Shapiro (1977), and Hills (1976) concerned themselves with the rate at which such a black hole would destroy stars in the cluster by tidal disruption of the stellar population held bound to the black hole in a "density cusp" around it. Here we shall comprehensively analyze the fluxes obtainable from tidal disruption of both bound and unbound stars, the rate of stellar collisions in the cusp and in the cluster at large (see also Hills and Day 1976), and the rate of gravitational diffusion into the potential well of the black hole (Bahcall and Wolf 1976).

We shall again approximate the cluster as an isothermal sphere, and we will scale the nucleus parameters to $\rho_4$ (central density in $10^4\ M_\odot\ \mathrm{pc}^{-3}$) and $v_{10}$ (one-dimensional velocity dispersion in units of 10 km s$^{-1}$). The black-hole mass will be rated in Kilosols ($M_3 = 10^3\ M_\odot$). Then

$$a = 0.43 v_{10} \rho_4^{-1/2} \quad \text{(pc)}, \tag{A-1a}$$

$$r_a = 0.029\ M_3 v_{10}^{-2} \quad \text{(pc)}, \tag{A-1b}$$

$$r_T = 4.5 \times 10^{-7}\ M_3^{1/3} \quad \text{(pc)}. \tag{A-1c}$$

Again using $m_* = 0.5\ M_\odot$, the basic $\langle n\sigma v\rangle$ flux for tidal disruption of unbound stars is

$$\Phi = 4 \times 10^{-9}\ M_3^{4/3} \rho_4 v_{10}^{-1} \quad (M_\odot\ \mathrm{yr}^{-1}). \tag{A-2}$$

For the mass of black hole considered, $M_3 \approx 1 \ll M_3^*$, and the limiting flux is

$$\Phi_\infty = 9 \times 10^{-6} \rho_4^{1/2} \quad (M_\odot\ \mathrm{yr}^{-1}), \tag{A-3a}$$

with

$$M_3^* = 230 \rho_4^{-3/8} v_{10}^{3/4}, \tag{A-3b}$$

$$\epsilon_{\mathrm{crit}} = 7 \times 10^{-4}\ M_3^{4/3} \rho_4^{1/2} v_{10}^{-1}. \tag{A-3c}$$

For the flux due to tidal disruption from the density cusp we need to evaluate the quantity $E_{\mathrm{crit}}$ in order to determine whether the loss cones in the cusp are filled or depleted. From equation (IV-9)

$$\left(\frac{E_{\mathrm{crit}}}{E_a}\right)^{5/2-p} = 0.66\ M_3^{5/3} \rho_4 v_{10}^{-8}, \tag{A-4}$$

where we have taken $(\rho_a/\rho_0) \approx \exp(3/2)$, $\ln \Lambda^* = \ln (J_{\max}/J_T) \approx 5$; and $\ln \Lambda \approx \ln (N/2) \approx 10$. It is thus marginal whether the cusp has full or depleted loss cones. From equation (VI-7b) we find

$$E_c^*/E_a \approx 2400 v_{10}^{-2}, \tag{A-5}$$

so that the cusp extends over a healthy range of $\log r$. In that case (unless $v_{10}$ is small), $E_{\mathrm{crit}} \approx E_a$ rather than $E_{\mathrm{crit}} \approx E_c^*$. Then from equations (IV-13) and (IV-12) the tidal flux from the cusp is

$$\frac{\Phi_{\mathrm{cusp}}}{\Phi} = \begin{cases} 1.5(E_{\mathrm{crit}}/E_a)^{p+1} & (E_{\mathrm{crit}}/E_a > 1) \\ 1.5(E_{\mathrm{crit}}/E_a)^{5/2-p} & (E_{\mathrm{crit}}/E_a < 1) \end{cases}, \tag{A-6a}$$

or,

$$\frac{\Phi_{\mathrm{cusp}}}{\Phi} = \begin{cases} 1.5[0.66\ M_3^{5/3} \rho_4 v_{10}^{-8}]^{(p+1)/(5/2-p)} & (E_{\mathrm{crit}}/E_a > 1) \\ M_3^{5/3} \rho_4 v_{10}^{-8} & (E_{\mathrm{crit}}/E_a < 1) \end{cases}. \tag{A-6b}$$

Thus for $E_{\mathrm{crit}}/E_a \gtrless 1$, $\Phi_{\mathrm{cusp}}/\Phi \gtrless 1.5$, and $\Phi_{\mathrm{cusp}}$ only begins to surpass $\Phi$ when the loss cones in the cusp begin to fill up.

The numerical values are

$$\Phi_{\mathrm{cusp}} = \begin{cases} (5 \times 10^{-9})\ M_3^{61/27} \rho_4^{14/9} v_{10}^{-49/9} & (E_{\mathrm{crit}}/E_a < 1) \\ (4 \times 10^{-9})\ M_3^3 \rho_4^2 v_{10}^{-9} & (E_{\mathrm{crit}}/E_a > 1) \end{cases},$$

(setting $p = 1/4$).

For the black-hole masses considered, $M_3 \approx 1$, there is no complication concerning the interaction of the cusp loss cones with the drop in density outside the nucleus of the globular cluster. Furthermore, $\Phi_{\mathrm{cusp}}$ does not exceed $\Phi$ by more than a small factor.

Next we shall calculate the rate of collision in the unbound stellar population from equation (VI-2). We note that in a globular cluster the gravitationally focused collisions outweigh the geometric cross section collisions; thus

$$C_{\text{cluster}} = 10^{-8}\rho_4^{1/2}v_{10}^2 \quad (M_\odot\ \text{yr}^{-1}) \tag{A-7}$$

(taking $q_c = 1\ R_\odot$, $m_* = 0.5\ M_\odot$, and noting that two stars are involved in each collision). These collisions in the cluster at large are more likely to result in stellar fusion than destruction, since the collision velocities are low, $\sim 10$ km s$^{-1}$. In $1.2 \times 10^{10}$ yr we would expect

$$N_c = 4 \times 10^2\rho_4^{1/2}v_{10}^2 \quad \text{(collisions)}, \tag{A-8}$$

which may be compared with the results of Hills and Day (1976).

The collision rate in the cusp, from equation (VI-8), is

$$C_{\text{cusp}}^{\text{hv}} = (2 \times 10^{-10})\, M_3^3\rho_4^2 v_{10}^{-7} \quad (M_\odot\ \text{yr}^{-1}), \tag{A-9a}$$

$$C_{\text{crit}}^{\text{hv}} = (2 \times 10^{-6})\rho_4^{1/2}v_{10}^2 \quad (M_\odot\ \text{yr}^{-1}), \tag{A-9b}$$

$$C_{\text{cusp}}^{\text{lv}} = 2C_{\text{cusp}}^{\text{hv}}, \tag{A-9c}$$

$$C_{\text{cusp}} = C_{\text{cusp}}^{\text{lv}} + C_{\text{cusp}}^{\text{hv}} \approx (6 \times 10^{-10})\, M_3^3\rho_4^2 v_{10}^{-7}. \tag{A-9d}$$

We see that low-velocity collisions tend to dominate in the cusp, mostly occurring near the outer edge. The mass of the black hole for which the collision fluxes peak is

$$M_{\text{crit},3} = 21\rho_4^{1/2}v_{10}^3 \gg 1. \tag{A-10}$$

Last we shall calculate the gravitational diffusion fluxes from equation (VI-9), with

$$M_{\text{cusp}} = 11\, M_3^3 v_{10}^{-6}\rho_4 \quad (M_\odot), \tag{A-11a}$$

$$t_R = (9 \times 10^8/\ln\Lambda)v_{10}^3\rho_4^{-1} = 9 \times 10^7 v_{10}^3\rho_4^{-1} \quad \text{(yr)}, \tag{A-11b}$$

taking $\ln\Lambda \approx 10$, $\rho_a/\rho_0 \approx \exp(3/2)$. Then

$$D_{\text{cusp}} = 2 \times 10^{-10}\, M_3^3 v_{10}^{-7}\rho_4^2 \quad (M_\odot\ \text{yr}^{-1}), \tag{A-11c}$$

$$D_{\text{crit}} = 2 \times 10^{-6}\rho_4^{1/2}v_{10}^2 \quad (M_\odot\ \text{yr}^{-1}). \tag{A-11d}$$

The cusp cannot really be said to exist until $M_{\text{cusp}} \gtrsim 10$, which occurs when

$$M_3 \gtrsim v_{10}^2\rho_4^{-1/2}.$$

If the cusp has not formed, then the only contribution is from the tidal disruption of unbound stars. When the cusp does form, this is soon surpassed by tidal disruption, collision, and gravitational diffusion effects from the cusp, in that order of importance. The growth time scale for the tidal disruption of unbound stars is

$$\tau_{\text{tide}} = 7 \times 10^{11}\, M_3^{-1/3}\rho_4^{-1}v_{10} \quad \text{(yr)}. \tag{A-12}$$

We see, then, that a black hole could not have grown from 10 $M_\odot$ to $10^3$ $M_\odot$ in one Hubble time ($1.2 \times 10^{10}$ yr); a massive black hole would have had to be formed as such, possibly from runaway gravothermal collapse (Spitzer 1975; Aarseth and Lecar 1975).

Table 2 shows flux rates for the 30 major globular clusters selected by Frank and Rees (1976) (with $\rho_4 > 0.5$) from the data of Peterson and King (1975), Bahcall and Hausman (1976), and references therein. The data for the X-ray globular N6440 is uncertain; values consistent with the known constraints are given for $\rho_4$ and $a$. Six of the X-ray globulars are marked by an asterisk, the suspect M5 by an asterisk in parentheses: (*). Discounting the suspect M5, the other X-ray globular clusters tend to high $\rho_4$ and $v_{10}$, and low '$a$' (N6712 is an exception). This has the result that both the unbound stellar $\langle n\sigma v\rangle$ and the unbound stellar collision $C_{\text{cluster}}$ rates for these globulars are high, whereas the $\Phi_{\text{cusp}}$, $C_{\text{cusp}}$, $D_{\text{cusp}}$ rates are not especially high or different from those of other globulars. This may be suggestive of a swarm of small black holes, or binary system mechanisms (Hills 1976), rather than cusp processes around a massive black hole. The enigmatic globular M80 has exceptionally high $\Phi$ and $C_{\text{cluster}}$ rates (Hills and Day 1976) but has not been seen to be active as regards X-rays.

Figure 2 displays the $\Phi$ and $C_{\text{cluster}}$ values for the globular clusters of Table 2, and all others from the data of Table 4 of Peterson and King for which ($\Phi$, $C$) are both greater than $5 \times 10^{-10}$ $M_\odot$ yr$^{-1}$. Last, Figure 3 shows the flux rates for a black hole from 10 $M_\odot$ to $3 \times 10^4$ $M_\odot$ in the globular M15 to display the relative importance of these quantities and their scalings with the hole mass.

TABLE 2

FLUX RATES ONTO A BLACK HOLE ($10^3\ M_\odot$) IN A CLUSTER GLOBULAR

| NGC | Other Name | $\rho_4$ ($10^4\ M_\odot$ pc$^{-2}$) | $V_{10}$ (10 km s$^{-1}$) | $a$ (pc) | $\Phi$ ($10^{-8}\ M_\odot$ yr$^{-1}$) | $\left[\frac{E_{crit}}{E_a}\right]^{5/2-p}$ | $\Phi_{cusp}$ ($10^{-8}\ M_\odot$ yr$^{-1}$) | $M_{cusp}$ ($M_\odot$) | $C_{cluster}$ ($10^{-8}\ M_\odot$ yr$^{-1}$) | $C_{cusp}$ ($10^{-8}\ M_\odot$ yr$^{-1}$) | $D_{cusp}$ ($10^{-8}\ M_\odot$ yr$^{-1}$) | $\tau_{tide}$ ($10^{10}$ yr) | $M_3$* ($10^3\ M_\odot$) | $M_{crit,3}$ ($10^3\ M_\odot$) |
|---|---|---|---|---|---|---|---|---|---|---|---|---|---|---|
| 104 | 47 Tuc | 4.2 | 1.05 | 0.22 | 1.8 | 1.9 | 3.9 | 34 | 7.9 | 0.7 | 0.24 | 17.0 | 140 | 12.0 |
| 362 | | 3.7 | 0.93 | 0.21 | 1.8 | 4.4 | 6.6 | 63 | 1.8 | 1.2 | 0.43 | 17.0 | 133 | 8.8 |
| 1851* | | 10.0 | 0.91 | 0.12 | 4.8 | 14.0 | 35.0 | 194 | 9.2 | 10.0 | 3.7 | 6.4 | 90 | 5.0 |
| 2808 | | 6.1 | 1.30 | 0.23 | 2.1 | 0.49 | 1.6 | 14 | 14.0 | 0.31 | 0.11 | 15.0 | 142 | 18.0 |
| 5824 | | 9.3 | 0.78 | 0.11 | 5.2 | 45.0 | 76.0 | 454 | 6.5 | 26.0 | 9.4 | 5.9 | 83 | 3.3 |
| 5904(*) | M5 | 0.59 | 0.68 | 0.38 | 0.38 | 8.5 | 2.1 | 66 | 1.2 | 0.28 | 0.098 | 81.0 | 210 | 8.6 |
| 6093 | M80 | 33.0 | 0.84 | 0.063 | 17.0 | 88.0 | 370.0 | 1030 | 14.0 | 196.0 | 70.0 | 1.8 | 54 | 2.2 |
| 6266 | M62 | 3.2 | 0.88 | 0.21 | 1.6 | 5.9 | 7.0 | 76 | 4.8 | 1.3 | 0.48 | 19.0 | 135 | 8.0 |
| 6273 | M19 | 1.4 | 0.56 | 0.20 | 1.1 | 96.0 | 25.0 | 499 | 1.3 | 6.0 | 2.2 | 28.0 | 131 | 3.1 |
| 6284 | | 5.5 | 0.65 | 0.12 | 3.7 | 114.0 | 95.0 | 802 | 3.5 | 33.0 | 12.0 | 8.3 | 88 | 2.5 |
| 6293 | | 5.8 | 0.54 | 0.096 | 4.7 | 529.0 | 304.0 | 2570 | 2.5 | 170.0 | 48.0 | 6.5 | 75 | 1.4 |
| 6304 | | 0.66 | 0.54 | 0.29 | 0.54 | 60.0 | 9.5 | 293 | 0.83 | 1.7 | 0.62 | 57.0 | 169 | 4.1 |
| 6333 | M9 | 1.1 | 0.63 | 0.26 | 0.77 | 29.0 | 8.8 | 194 | 1.5 | 1.6 | 0.58 | 40.0 | 157 | 5.0 |
| 6341 | M92 | 2.2 | 0.75 | 0.22 | 1.3 | 14.0 | 9.7 | 136 | 2.9 | 1.9 | 0.69 | 24.0 | 138 | 6.0 |
| 6356 | | 0.72 | 0.84 | 0.43 | 0.38 | 1.9 | 0.84 | 23 | 2.1 | 0.09 | 0.033 | 81.0 | 228 | 15.0 |
| 6440†* | | 30.0 | 1.3 | 0.1 | 10.0 | 2.4 | 26.0 | 68 | 32.0 | 8.0 | 2.7 | 3.1 | 78 | 8.4 |
| 6441* | | 12.0 | 1.10 | 0.14 | 4.8 | 3.7 | 16.0 | 75 | 15.0 | 4.0 | 1.4 | 6.4 | 97 | 8.1 |
| 6522 | | 12.0 | 0.70 | 0.087 | 7.5 | 137.0 | 216.0 | 1120 | 5.9 | 93.0 | 33.0 | 4.1 | 69 | 2.1 |
| 6528 | | 3.2 | 0.61 | 0.15 | 2.3 | 110.0 | 58.0 | 683 | 2.3 | 17.0 | 6.2 | 13.0 | 103 | 2.7 |
| 6541 | | 2.6 | 0.71 | 0.19 | 1.6 | 27.0 | 17.0 | 223 | 2.8 | 4.0 | 1.4 | 19.0 | 124 | 4.7 |
| 6624* | | 5.0 | 0.69 | 0.13 | 3.2 | 64.0 | 58.0 | 510 | 3.7 | 18.0 | 6.4 | 9.6 | 95 | 3.1 |
| 6626 | M28 | 5.2 | 0.78 | 0.15 | 2.9 | 25.0 | 30.0 | 254 | 4.9 | 8.3 | 2.9 | 11.0 | 103 | 4.4 |
| 6637 | M69 | 0.60 | 0.63 | 0.35 | 0.42 | 16.0 | 3.3 | 106 | 1.1 | 0.5 | 0.17 | 73.0 | 197 | 6.8 |
| 6712* | | 0.14 | 0.46 | 0.54 | 0.12 | 41.0 | 7.4 | 150 | 0.29 | 0.24 | 0.08 | 230.0 | 270 | 5.7 |
| 6715 | M54 | 4.5 | 1.01 | 0.20 | 2.0 | 2.7 | 5.5 | 47 | 7.6 | 1.0 | 0.36 | 15.0 | 132 | 10.0 |
| 6752 | | 1.2 | 0.63 | 0.25 | 0.84 | 32.0 | 10.0 | 211 | 1.5 | 1.9 | 0.69 | 36.0 | 152 | 4.8 |
| 6760 | | 1.1 | 0.60 | 0.25 | 0.81 | 43.0 | 12.0 | 259 | 1.3 | 2.3 | 0.82 | 38.0 | 151 | 4.3 |
| 6864 | M75 | 2.0 | 0.94 | 0.29 | 0.94 | 2.2 | 2.2 | 32 | 4.4 | 0.33 | 0.12 | 33.0 | 169 | 12.0 |
| 7078* | M15 | 3.9 | 1.03 | 0.22 | 1.7 | 2.0 | 3.9 | 36 | 7.3 | 0.67 | 0.23 | 18.0 | 141 | 12.0 |
| 7089 | M2 | 0.70 | 0.92 | 0.47 | 0.33 | 0.9 | 0.45 | 13 | 2.5 | 0.04 | 0.017 | 93.0 | 247 | 20.0 |
| 7099 | M30 | 8.1 | 0.60 | 0.091 | 5.9 | 318.0 | 281.0 | 1910 | 3.6 | 125.0 | 45.0 | 5.2 | 72 | 1.6 |

* X-ray globulars.

(*) Suspected X-ray globular.

† Data uncertain, taken to be consistent with known limits.

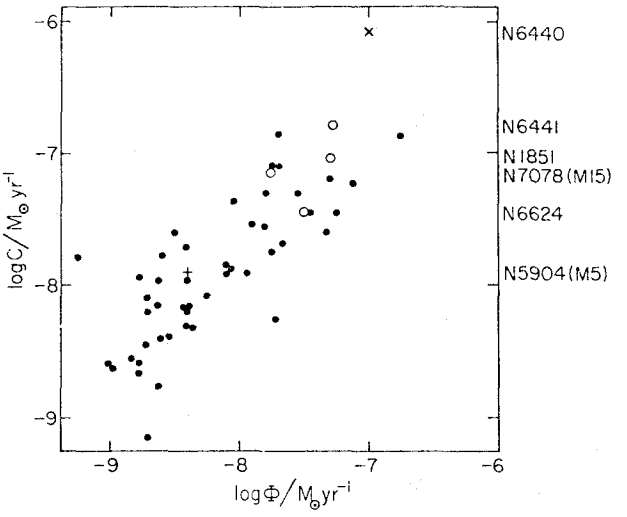


FIG. 2

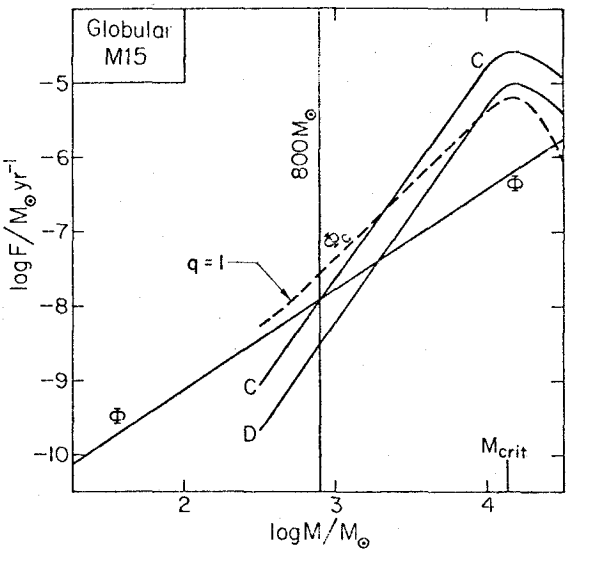


FIG. 3

FIG. 2.—Stellar collision rate $C$ and tidal disruption rate $\Phi$ of stars not bound to a black hole in a globular cluster, in units of $M_\odot$ yr$^{-1}$. The X-ray globulars are marked by open circles but the position of N6440 (*cross*) is uncertain. That of the suspected X-ray globular N5904 is marked by a plus. Dots are non–X-ray globulars.

FIG. 3.—Flux rates in the globular cluster M15. The unbound tidal flux is $\Phi$, the tidal flux from the cusp is $\Phi_{cusp}$, the collision and gravitational diffusion rates in the cusp are $C$ and $D$, respectively. The arrow marking $q = 1$ denotes the point at which loss cones in the cusp cease to be depleted. $C$ includes both the high- and low-velocity collision rates; the rate of the high-velocity disruptive collisions $C^{hv}$ alone is equal to the gravitational diffusion rate $D$.

## REFERENCES

Aarseth, S. J., and Lecar, M. 1975, *Ann. Rev. Astr. Ap.*, **13**, 1.
Bahcall, J. N., and Ostriker, J. P. 1975, *Nature*, **256**, 23.
Bahcall, J. N., and Wolf, R. A. 1976, *Ap. J.*, **209**, 214.
Bahcall, N. A., and Hausman, M. A. 1976, *Ap. J. (Letters)*, **207**, L181.
Canizares, C. R., and Neighbours, J. E. 1975, *Ap. J. (Letters)*, **199**, L97.
Chandrasekhar, S. 1939, *An Introduction to the Study of Stellar Structure* (New York: Dover).
Clark, G. W., Markert, T. H., and Li, F. K. 1975, *Ap. J. (Letters)*, **199**, L93.
Cominsky, L., Forman, W., Jones, C., and Tananbaum, H. 1977, *Ap. J. (Letters)*, **211**, L9.
de Vaucouleurs, G. 1974, in *Formation and Dynamics of Galaxies, IAU Symposium No. 58*, ed. J. R. Shakeshaft (Dordrecht: Reidel).
Forman, W., and Jones, C. 1976, *Ap. J. (Letters)*, **207**, L177.
Frank, J., and Rees, M. J. 1976, *M.N.R.A.S.*, **176**, 633.
Giacconi, R., Murray, S., Gursky, H., Kellogg, E., Schreier, E., Matilsky, T., Koch, D., and Tananbaum, H. 1974, *Ap. J. Suppl.*, **27**, 37.
Grindlay, J., Schreier, E., Schnopper, H., Gursky, H., Parsignault, D., and Heise, J. 1976, *Ap. J. (Letters)*, **205**, L127.
Hills, J. G. 1975, *Nature*, **254**, 295.
———. 1976, *Ap. Letters*, **17**, 95.
Hills, J. G., and Day, C. A. 1976, *Ap. Letters*, **17**, 87.
Kellerman, K. I., Clark, B. G., Niell, A. E., and Shaffer, D. B. 1975, *Ap. J. (Letters)*, **197**, L113.
Lightman, A. P., and Shapiro, S. L. 1977, *Ap. J.*, **211**, 244.
Lynden-Bell, D. 1969, *Nature*, **223**, 690.
Lynden-Bell, D., and Rees, M. J. 1971, *M.N.R.A.S.*, **152**, 461.
Newell, B., DaCosta, G. S., and Norris, J. 1976, *Ap. J. (Letters)*, **208**, L55.
Peebles, P. J. E. 1972, *Ap. J.*, **178**, 371.
Peterson, C. J., and King, I. R. 1975, *A.J.*, **80**, 427.
Rowan-Robinson, M. 1976, *Nature*, **262**, 97.
Ryan, M. P. 1972, *Ap. J. (Letters)*, **177**, L79.
Silk, J., and Arons, J. 1975, *Ap. J. (Letters)*, **200**, L131.
Spitzer, L. 1962, *Physics of Fully Ionized Gases* (New York: Interscience).
———. 1975, in *IAU Symposium No. 69, Dynamics of Stellar Systems*, ed. A. Hayli (Dordrecht: Reidel).
Wheeler, J. C., and Shields, G. A. 1976, *Nature*, **259**, 642.
Young, P. J. 1976, *A.J.*, **81**, 807.
———. 1977, *Ap. J.*, **212**, 227.
Young, P. J., Shields, G. A., and Wheeler, J. C. 1977, *Ap. J.*, **212**, 367.

PETER J YOUNG: Robinson Laboratory of Astrophysics, California Institute of Technology, Pasadena, CA 91109

THE ASTROPHYSICAL JOURNAL, 221:721–730, 1978 May 1


# EVIDENCE FOR A SUPERMASSIVE OBJECT IN THE NUCLEUS OF THE GALAXY M87 FROM SIT AND CCD AREA PHOTOMETRY

PETER J YOUNG, JAMES A. WESTPHAL, JEROME KRISTIAN, AND CHRISTOPHER P. WILSON
Hale Observatories, California Institute of Technology, Carnegie Institution of Washington
AND
FREDERICK P. LANDAUER
Space Photography Section, Jet Propulsion Laboratory
*Received 1977 June 10; accepted 1977 October 7*

## ABSTRACT

Two-dimensional SIT and CCD detectors have been used to measure the surface brightness of the peculiar elliptical radio galaxy M87. Measurements were made in three broad-band colors (*B*, *V*, and *R*) to a distance of 80″ from the nucleus, with 1″ spatial resolution and photometric accuracy of the order of 1%.

The data are given in some detail and are compared with earlier photographic results. The most obvious feature of the data is a bright, barely resolved central luminosity spike, which is not seen in similar data on other nearby normal ellipticals. Also, attempts to fit isothermal or King models away from the nuclear spike show additional excess luminosity in the central regions of the galaxy ($r < 10''$), which cannot be fitted by such a model.

A model-independent dynamical analysis, using the photometric data combined with spectrographic results by Sargent *et al.*, shows that the nucleus of M87 contains a compact mass of low luminosity, with $M = 5 \times 10^9\ M_\odot$, $r < 100$ pc, and $M/\mathscr{L} > 60$. All of the existing data is well fitted by a King model containing a central black hole of mass $M = 3 \times 10^9\ M_\odot$ and a point luminosity source. While such a model is not uniquely required by the data, it is perhaps the most plausible of several possible models considered. At present, M87 is probably the best case for a hypothetical massive black hole in a galaxy nucleus.

*Subject headings:* galaxies: individual — galaxies: nuclei — galaxies: photometry — galaxies: structure

## I. INTRODUCTION

Theoretical attempts to understand quasars, radio galaxies, and active galaxy nuclei have demonstrated the attractiveness of a gravitational source of energy, such as a black hole (e.g., Lynden-Bell 1969). The mass of the central object is thought to be at least $10^8\ M_\odot$, which is the mass equivalent of the total energy output of a quasar or radio galaxy, and might be much higher if the processes that convert mass to energy are inefficient. An object with this mass would have observable effects on the dynamics of the galactic nucleus in which it is embedded. These effects may be probed with optical observations of luminosity profiles and absorption-line widths to detect a bright central "cusp" of stars bound to the massive object and to observe an increased stellar velocity dispersion within this cusp.

The peculiar E0 galaxy M87 (=NGC 4486 = Arp 152 = 3C 274 = Virgo A) appears to be a particularly promising candidate for a black hole or supermassive object quest. It is relatively close, it is known to be an active (core-halo) radio source with compact central components (Cohen *et al.* 1969; Kellermann *et al.* 1973), and there is evidence for ejection of mass from the nucleus in the form of the optical jets (Felten 1968; Felten, Arp, and Lynds 1970). The total anomalous radiation output from the galaxy is $\sim 2 \times 10^{42}$ ergs s$^{-1}$ (Moffet 1975), which places it among the weaker of the supergiant elliptical galaxy radio sources.

In this paper and another (Sargent *et al.* 1978), photometric and spectroscopic observations of M87 are presented that have been successful in detecting a supermassive object in the nucleus of this galaxy. The mass of the object is $\sim 5 \times 10^9\ M_\odot$, which causes large and easily observable effects on the dynamics of the nucleus of M87.

Here we present the photometric data obtained with digital SIT and CCD systems on the Palomar 60 inch and 200 inch telescopes. In § II we discuss the observations and the reduction procedures for the digital data; in § III we present the photometric profile of M87; in § IV we fit theoretical models to the luminosity profile and give the model-independent argument for a central supermassive object; and in § V we present a discussion.

## II. OBSERVATIONS AND REDUCTION PROCEDURES

The two-dimensional SIT detector system has been described in Westphal, Kristian, and Sandage (1975). The raster scan on the silicon target yields 256 × 256

pixels, each 47 $\mu$m square. Photometry with the SIT has demonstrated an accuracy of 0.03 mag. The CCD was made by Texas Instruments for JPL under NASA contract 7-100. The array contains 400 × 400 pixels, each 23 $\mu$m square, and is used in a direct mode with no gain. This is made possible by the very low readout-noise characteristics of the device. Unpublished photometry by Kristian and Westphal over a 12 mag range has shown no departure from linearity, and agreement with a photoelectric sequence by Sandage to within 2%. Laboratory tests of the CCD and internal deviations on the standard stars suggest that the CCD itself has a photometric accuracy of 1% or better.

The results for M87 presented here are based on three separate observing runs with a total of 20 exposures in three broad-band colors (*B*, *V*, and *R*). A journal of observations and additional information pertinent to the telescopes and detectors are given in Table 1. The SIT observations were made with a variety of exposure times including unsaturated frames of the central regions of M87 and frames in which the center was heavily saturated in order that high signal-to-noise ratio be obtained in the regions of the galaxy at the edge of the frame (at $r = 80''$). The seeing profile and sky brightness were monitored by interlacing the galaxy observations with exposures of similar length on a field 30′ south of M87. The large dynamic range of the CCD enabled one exposure in each color to yield the desired signal-to-noise ratio over the whole frame without saturation of the central regions. The seeing profiles for the CCD frames were found by using faint stars in the same frame as the galaxy; this was permitted again because of the large dynamic range of the CCD. By choosing blue objects, we ensured that none of the "seeing stars" was one of the coterie of globular clusters encircling M87. The CCD observations in seeing with FWHM = 1″ and pixel size 0″.25 provided the best-quality data for the nuclear regions of M87.

The CCD photometer system directly images onto the target diode array which has an extremely uniform pixel spacing because of the manufacturing procedure. The only image distortions in this system are due to the Ross corrector lens at the 200 inch prime focus, which amount to less than 0.2% across the detector for near-axis positions. The image scale was determined by directly measuring the diode separation as 22.875 $\mu$m and using the known image scale of 11″.06 mm$^{-1}$ to give 0″.2530 ± 0″.0003 per pixel. As a check we also measured the length of the M87 jet and compared this with the astrometry of de Vaucouleurs, Angione, and Fraser (1968). From this we found 0″.254 ± 0″.001 per pixel.

The SIT system uses an electrostatically focused intensifier stage which has pincushion distortion. In addition, inequality of the horizontal and vertical readout deflections gives different image scales in the $x$ and $y$ directions. To remove these distortions we compared the positions of 54 stars in a field near the globular cluster M92 as measured on the SIT and on a prime focus direct photograph. This procedure removed the 6% quadratic pincushion terms and the 9% difference in the $x$ and $y$ scales of the SIT to an accuracy of 5 $\mu$m (=0″.05). The SIT frames of M92 used for this analysis were coeval with the M87 data taken in 1975.

The sky brightness level was determined and subtracted from all exposures. Typical sky brightness levels were found to be $\mu_R = 20.53 \pm 0.02$ mag arcsec$^{-2}$, $\mu_V = 21.34 \pm 0.01$, and $\mu_B = 22.28 \pm 0.02$ for the 1975 SIT data. Mean absorption coefficients for Palomar were used to remove atmospheric extinction.

The data were tied to the Johnson-Morgan system by observation of the *B*, *V*, *R* standards of Sandage (1973). Residuals were ~0.04 mag for the SIT and ~0.02 mag for the CCD.

The SIT photometry was found to be unreliable near heavily saturated regions, probably because of charge migration effects and bending of the electron readout beam. This border effect extended for ~20 pixels around the very heavily saturated areas on the long exposures, with the intensity levels perturbed below the true values. The existence of this effect was evident on checking against shorter exposures, and the afflicted data were excised from the analysis. A second check was available from comparison with the

TABLE 1

OBSERVATIONS OF M87

| | Data Set 1 (1975 Mar 14) | Data Set 2 (1977 Feb 25) | Data Set 3 (1977 May 22) |
|---|---|---|---|
| Telescope | 200 in. | 60 in. | 200 in. |
| Detector | SIT | SIT | CCD |
| Pixel Format | 256 × 256 | 256 × 256 | 400 × 400 |
| Pixel Size (arcsec) | 0.52 | 0.73 | 0.26 |
| Image Scale (arcsec mm$^{-1}$) | 11.06* | 15.32 | 11.06* |
| Seeing Disk (FWHM) (arcsec) | 1.7 | 2.0 | 1.0 |
| No. of Exposures on M87 | 14 | 3 | 3 |
| Focus and f-ratio | Prime focus* f3.67 | Cassegrain f8.83 | Prime focus* f3.67 |

* With Ross corrector lens.

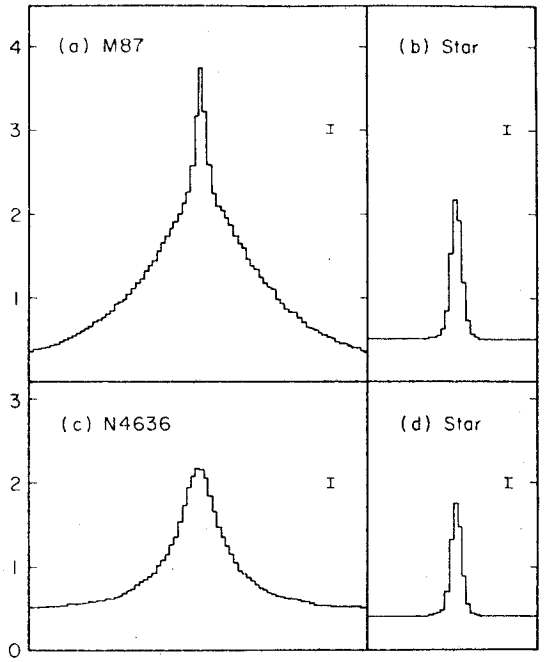


FIG. 1.—$V$ band photometric profiles depicting a 1 × 80 pixel slice from the SIT data for (*a*) M87, showing the abnormal central luminosity spike; (*b*) a star profile for the M87 data with $\sigma_* = 0''.67$; (*c*) NGC 4636, a typical elliptical galaxy profile; (*d*) star profile for NGC 4636. Each pixel is 0".5 wide and the intensity scale is linear. Error bars of length 2 $\sigma$ are given.

CCD data, which were nowhere saturated; these agreed well with the short-exposure unsaturated SIT frames.

## III. LUMINOSITY PROFILE OF M87

### *a) The Luminosity Cusp in M87*

The center of M87 has long been known to contain a small, abnormally bright "nucleus" superposed on the core of the galaxy. This is well shown on the deconvolved IIIa-J plates of Arp and Lorre (1976). Of the other 30 nearby elliptical galaxies for which we have photometric data, none shows a similar feature. To illustrate the bright central cusp in M87, we have plotted a 1 × 80 pixel slice across the center in the EW direction from a short exposure SIT frame in the $V$ band. This is shown in Figure 1 together with a similar slice across the galaxy NGC 4636. These galaxies are both classified as type E0 with similar diameters ($A_e$ = 3'.2 for M87 and $A_e$ = 2'.2 for NGC 4636; de Vaucouleurs, de Vaucouleurs, and Corwin 1976) and are at similar distances [M87 is a principal member of the Virgo I(E) group at $\Delta$ = 13.6 Mpc; NGC 4636 is in the Virgo X(G26) group at $\Delta$ = 14.3 Mpc; de Vaucouleurs 1975]. The profile of NGC 4636 was entirely typical of the other 30 galaxies in the survey, with a smooth well-resolved core region. It may be seen in Figure 1, however, that M87 has a bright central luminosity spike scarcely larger than the seeing disk. As we shall see in § IV*a*, the anomaly in the luminosity profile of M87 is not confined to the central arcsecond but extends out to $r = 20''$.

### *b) Radial Luminosity Profile of M87*

i) The central regions of M87 were inspected on the distortion-free CCD data frames and were found to have no detectable ellipticity ($\epsilon < 0.02$) for $r < 30''$.

ii) The nuclear luminosity spike was found to be centered to within 0".02 (= 1.5 pc) of the center of M87 as defined by the isophotes for $5'' < r < 30''$ (with due allowance for the effects of the optical jet).

Consequently we formed a mean luminosity profile by summing the data in narrow annuli ($\sim\frac{1}{2}$ pixel wide) concentric with the central cusp but avoiding the region of the optical jet. A composite profile was then created by using the CCD data for the inner regions, short-exposure SIT data for the intermediate regions, and long-exposure SIT data for the outer regions near the edge of the frame.

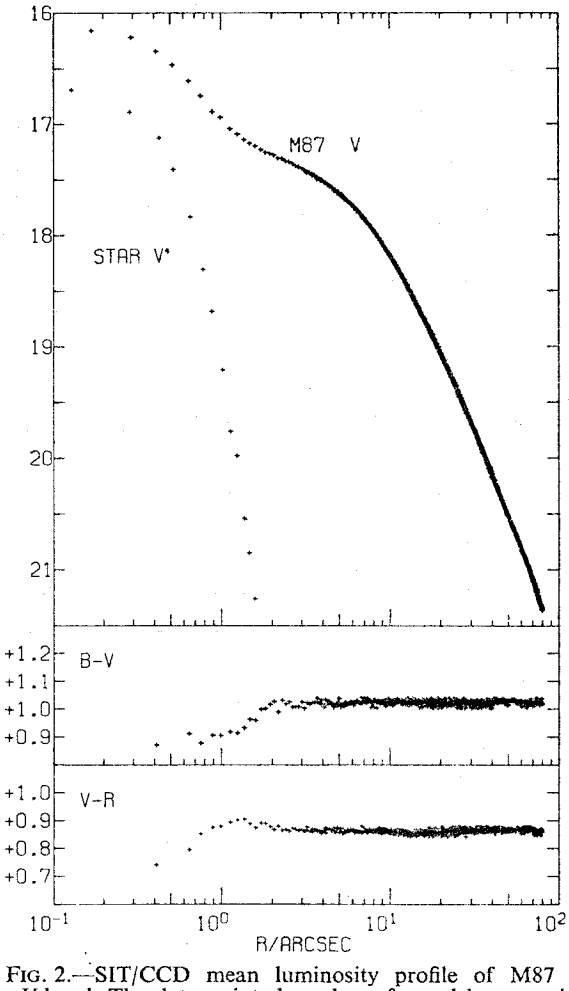


FIG. 2.—SIT/CCD mean luminosity profile of M87 in the $V$ band. The data points have been formed by summing pixels in narrow annuli concentric with the nuclear luminosity spike, and the intensity scale is $\mu_V$ = mag arcsec$^{-2}$. The instrumental plus seeing profile is represented by the star image extracted from the CCD frame of M87 in the $V$ band. Values of the colors ($B - V$) and ($V - R$) inside a simulated 1" diameter aperture together with the mean annular values outside this aperture are given below the luminosity profile.

TABLE 2

PHOTOMETRIC DATA FOR M87

| $r''$ (1) | $\log r''$ (2) | $\mu_V$* (3) | $B-V$† (4) | $V-R$† (5) | $V_p$ (6) | $\nu_V$ (7) | $V_s$ (8) |
|---|---|---|---|---|---|---|---|
| 0.17 | −0.771 | 16.158 | ... | ... | ... | ... | ... |
| 0.29 | −0.533 | 16.265 | ... | ... | ... | ... | ... |
| 0.41 | −0.385 | 16.347 | ... | ... | ... | ... | ... |
| 0.52 | −0.288 | 16.470 | 0.87‡ | 0.74‡ | 16.50‡ | ... | ... |
| 0.65 | −0.189 | 16.616 | 0.91 | 0.80 | 16.09 | ... | ... |
| 0.76 | −0.119 | 16.750 | 0.88 | 0.85 | 15.80 | ... | ... |
| 0.89 | −0.052 | 16.895 | 0.91 | 0.88 | 15.55 | ... | ... |
| 1.00 | −0.002 | 16.946 | 0.90 | 0.88 | 15.36 | ... | ... |
| 1.19 | +0.075 | 17.072 | 0.91 | 0.90 | 15.08 | ... | ... |
| 1.42 | +0.153 | 17.163 | 0.94 | 0.89 | 14.80 | 19.66 | 15.79 |
| 1.66 | +0.219 | 17.220 | 0.98 | 0.88 | 14.56 | 19.83 | 15.60 |
| 1.89 | +0.277 | 17.265 | 1.01 | 0.88 | 14.34 | 19.97 | 15.43 |
| 2.12 | +0.326 | 17.297 | 1.01 | 0.88 | 14.15 | 20.08 | 15.26 |
| 2.36 | +0.372 | 17.325 | 1.02 | 0.87 | 13.97 | 20.18 | 15.09 |
| 2.59 | +0.413 | 17.352 | 1.02 | 0.87 | 13.81 | 20.27 | 14.93 |
| 2.83 | +0.452 | 17.385 | 1.01 | 0.86 | 13.65 | 20.35 | 14.77 |
| 3.07 | +0.487 | 17.409 | 1.01 | 0.86 | 13.51 | 20.43 | 14.62 |
| 3.30 | +0.518 | 17.432 | 1.02 | 0.86 | 13.38 | 20.56 | 14.34 |
| 3.70 | +0.568 | 17.477 | 1.03 | 0.86 | 13.18 | 20.61 | 14.26 |
| 4.30 | +0.633 | 17.544 | 1.02 | 0.86 | 12.95 | 20.75 | 13.95 |
| 4.88 | +0.688 | 17.608 | 1.01 | 0.86 | 12.73 | 20.88 | 13.69 |
| 5.47 | +0.738 | 16.672 | 1.02 | 0.86 | 12.52 | 21.01 | 13.44 |
| 6.05 | +0.782 | 17.737 | 1.02 | 0.86 | 12.34 | 21.13 | 13.23 |
| 6.65 | +0.823 | 17.805 | 1.03 | 0.86 | 12.18 | 21.25 | 13.03 |
| 7.23 | +0.859 | 17.875 | 1.03 | 0.86 | 12.05 | 21.36 | 12.86 |
| 7.83 | +0.894 | 17.944 | 1.02 | 0.86 | 11.91 | 21.47 | 12.70 |
| 8.41 | +0.925 | 18.010 | 1.02 | 0.86 | 11.79 | 21.58 | 12.55 |
| 8.99 | +0.954 | 18.076 | 1.02 | 0.86 | 11.69 | 21.68 | 12.42 |
| 9.64 | +0.984 | 18.146 | 1.02 | 0.86 | 11.58 | 21.79 | 12.29 |
| 10.6 | +1.024 | 18.249 | 1.02 | 0.86 | 11.45 | 21.95 | 12.11 |
| 11.9 | +1.075 | 18.381 | 1.02 | 0.86 | 11.28 | 22.17 | 11.90 |
| 13.3 | +1.125 | 18.528 | 1.03 | 0.86 | 11.12 | 22.40 | 11.70 |
| 15.0 | +1.176 | 18.678 | 1.02 | 0.86 | 10.96 | 22.65 | 11.51 |
| 16.8 | +1.226 | 18.829 | 1.02 | 0.86 | 10.81 | 22.90 | 11.33 |
| 18.8 | +1.275 | 18.987 | 1.02 | 0.86 | 10.68 | 23.17 | 11.16 |
| 21.1 | +1.325 | 19.149 | 1.02 | 0.86 | 10.55 | 23.45 | 11.00 |
| 23.7 | +1.375 | 19.320 | 1.02 | 0.87 | 10.42 | 23.73 | 10.86 |
| 26.1 | +1.416 | 19.471 | 1.02 | 0.86 | 10.32 | 23.97 | 10.73 |
| 28.3 | +1.452 | 19.584 | 1.02 | 0.86 | 10.24 | 24.19 | 10.64 |
| 31.6 | +1.500 | 19.767 | 1.03 | 0.86 | 10.13 | 24.48 | 10.51 |
| 34.4 | +1.537 | 19.906 | 1.03 | 0.87 | 10.05 | 24.71 | 10.42 |
| 37.1 | +1.569 | 20.017 | 1.03 | 0.87 | 9.99 | 24.89 | 10.34 |
| 39.9 | +1.601 | 20.139 | 1.02 | 0.86 | 9.92 | 25.09 | 10.27 |
| 42.9 | +1.632 | 20.265 | 1.03 | 0.87 | 9.86 | 25.28 | 10.19 |
| 46.3 | +1.666 | 20.401 | 1.03 | 0.86 | 9.79 | 25.48 | 10.12 |
| 50.2 | +1.701 | 20.536 | 1.02 | 0.87 | 9.73 | 25.70 | 10.04 |
| 56.2 | +1.750 | 20.711 | 1.02 | 0.87 | 9.64 | 26.00 | 9.94 |
| 63.1 | +1.800 | 20.903 | 1.02 | 0.86 | 9.54 | 26.30 | 9.84 |
| 71.0 | +1.851 | 21.113 | 1.02 | 0.86 | 9.46 | 26.61 | 9.73 |
| 79.1 | +1.898 | 21.349 | 1.02 | 0.86 | 9.38 | 26.90 | 9.64 |

* Formal error is ±0.005 (1 $\sigma$ value).

† Formal error is ±0.01.

‡ Values for centered 1″ diameter aperture.

NOTE.—$\mu_V$ = surface brightness in the $V$ band (mag arcsec$^{-2}$) at radius $r$ from the center of M87; $(B-V)$, $(V-R)$ = surface colors at radius $r$; $V_p$ = magnitude enclosed by simulated aperture of radius $r$; $\nu_V$ = spatial luminosity density in mag arcsec$^{-3}$; $V_s$ = magnitude enclosed by sphere of radius $r$.

Continuity among the various segments of data was good to 0.01 mag.

The resulting 1995 data points are displayed in Figure 2 and are collected into 144 mean points given in Table 2. Also shown in Figure 2 is a star profile for the CCD data in the $V$ band as derived from a faint star on the $V$ exposure for M87. The Gaussian core, $I = I_0 \exp(-r^2/2\sigma_*^2)$, for the star image has a standard deviation $\sigma_* = 0''.46 \pm 0''.01$ or an FWHM = $1''.08 \pm 0''.02$.

Additional data given in Table 2 are the $V$ magnitudes in simulated circular apertures, the spatial luminosity density, and the magnitude contained within variously sized spheres centered on M87. In

finding the latter two quantities, we have assumed spherical symmetry for the inversion of the Abel integrals created by fitting analytic functions to the data. We do not give values inside 1".42 where seeing effects start to perturb the profile. All quantities in Table 2 are uncorrected for the seeing profile, since deconvolution procedures merely act as noise magnifiers; seeing effects will be allowed for in subsequent sections by appropriate convolution of theoretical models.

### c) *Comparison with Previous Photometry*

The CCD/SIT photometry may be compared with the photographic photometry of Oemler (1976) in the $V$ band and Kormendy (1977) in the $G$ band, and with a photoelectric profile in the $B$ band by de Vaucouleurs and Nieto (1977). Color corrections $(B - V) = +1.02$ and $(G - V) = +0.36$ were used to transform all magnitudes into the $V$ system, and no zero-point corrections were applied. We have plotted the discrepancies $\Delta\mu_V = \mu_V - \mu_V{}^*$, where $\mu_V{}^*$ is the SIT/CCD value, in Figure 3.

The following points may be noted after inspection of Figure 3.

i) The CCD/SIT profile agrees with the photographic photometry of Oemler (1976) for $5'' < r < 80''$. The discrepancies are of the order 0.1 mag, which is the expected accuracy of the photographic data. A discontinuity of 0.1 mag may be seen in the Oemler data at $r = 36''$.

ii) The CCD/SIT profile also agrees with the photoelectric data of de Vaucouleurs and Nieto (1977) for $15'' < r < 80''$ except for a zero-point discrepancy of $\sim$0.1 mag.

iii) The data of Kormendy (1977) show systematic discrepancies of up to $\sim$0.4 mag. While deviations inside $r = 1''$ may be expected owing to differing seeing profiles and the inability of a photographic plate to cope with strong luminosity gradients, the systematic deviation for $3'' < r < 80''$ must cause concern. It cannot be due to an effect of changing color, since it was determined that the $(B - V)$ and $(V - R)$ colors in M87 are constant in this radial range.

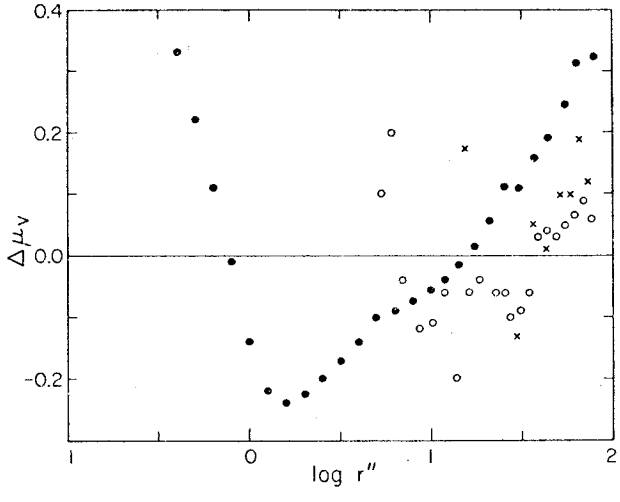


FIG. 3.—Comparison of the SIT/CCD photometry to the photographic of Oemler (○) and Kormendy (●), and the photoelectric data of de Vaucouleurs and Nieto (×). We have plotted the residuals $\Delta\mu_V = \mu_V - \mu_V|_{\text{SIT/CCD}}$ with all photometry transformed into the $V$ band and no zero-point corrections applied.

A comparison of the SIT and the CCD profiles showed agreement to within 0.01 mag at all points except inside the central arcsecond, where the higher resolution CCD data rose slightly above the SIT data. In Figure 2 the individual SIT and CCD data points are plotted, and the difference between them is scarcely visible at the 1% level.

### d) *Discussion of the SIT/CCD Results*

The following points may be noted after scrutiny of Figure 2.

i) The colors of M87, $(B - V) = 1.02 \pm 0.01$ and $(V - R) = 0.86 \pm 0.01$, are constant for $1''.7 < r < 80''$ with $\Delta(B - V) < 0.01$ and $\Delta(V - R) < 0.01$.

ii) The bright nucleus is slightly bluer than the rest of the galaxy with $(B - V) = +0.87$ and $(V - R) = +0.74$ for a simulated 1" diameter aperture centered on the "cusp."

iii) The star profile has dropped to 1% of its central intensity at $r = 1''.7$. Because of this, and also because of the constancy of the colors for $r > 1''.7$, we shall fit theoretical models of the luminosity profile in the range $r > 1''.7$. This will avoid any possible contamination by a possible blue, nonthermal point source in the center. In addition there is no evidence of dust absorption in excess of $A_v = 0.05$ mag, and the emission lines of [O II] λ3737, [N II] λ6548, 6593, [S II] λ6724 cannot perturb the photometric profile to a significant degree. Since the galaxian colors are constant for $r > 1''.7$, we shall assume, for the purpose of model fitting, that the stellar population has a constant mass-luminosity ratio.

## IV. COMPARISON WITH THEORETICAL MODELS

### a) *Isothermal and King Models*

The modified isothermal sphere models of King (1966) have met with great success in fitting the luminosity profiles of normal elliptical galaxies (King 1975). In the case of M87, however, the deviations from a King model are large and easily observable, since the disagreement extends out to $r = 20''$. Beyond this radius the King model with a ratio of tidal radius $r_T$ to core radius $r_c$ $\log r_T/r_c = 2.10$ is a reasonable fit to the luminosity profile of M87. This is shown in Figure 4, where we have fitted such a model to the photographic photometry of Oemler (1976) for $5'' < r < 4'.5$. Outside $r = 4'.5$ there is a faint extended corona (de Vaucouleurs and Nieto 1977). The failure of the King model to fit the CCD/SIT photometry in the central regions is shown in Figure 5, where discrepancies of up to 0.25 mag are present for $1''.7 < r < 10''$. It is evident that the observed profile does not curve sharply enough as it rises into the core regions, and then refuses to flatten off as $r \to 0$, but continues

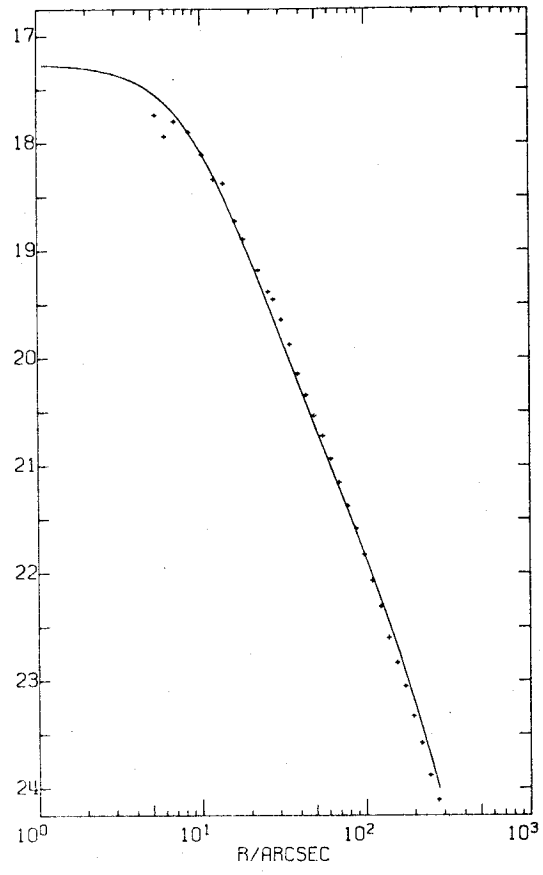


FIG. 4.—The $V$ band photographic data of Oemler (1976) have been fitted with a King model. The core radius is $r_c$ = 9.″6 and the "tidal" radius is $r_T$ = 20.′1 (log $r_T/r_c$ = 2.10). The intensity scale is $\mu_V \equiv$ mag arcsec$^{-2}$.

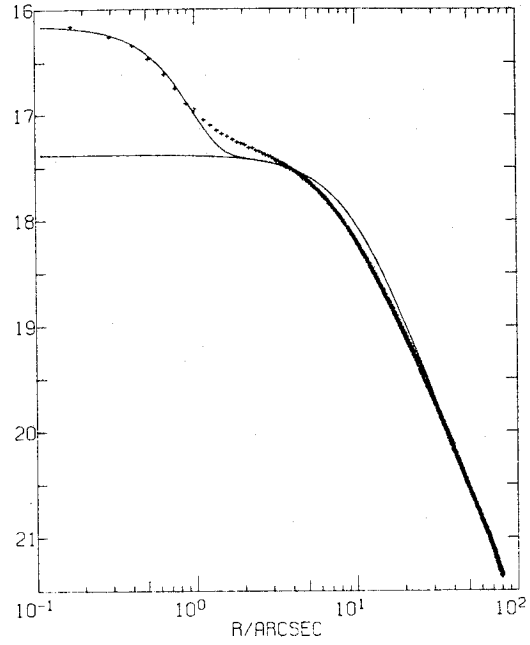


FIG. 5.—An attempt to fit a King model (with log $r_T/r_c$ = 2.10) to the SIT/CCD $V$ band profile of M87. This is the best fit we could obtain by varying the three parameters of the model. Adding a central point luminosity source improves the fit for $r < 1''$ but leaves residuals of 0.2 mag for $1'' < r < 20''$. The intensity scale is $\mu_V \equiv$ mag arcsec$^{-2}$.

to rise even at $r = 1.''7$ where the central luminosity spike begins to be noticeable. The fit cannot be improved by adding a central point luminosity source (see Fig. 5 again), since this cannot affect matters outside $r = 1.''7$.

We may justify the use of single mass King models after the work of Lynden-Bell (1967), who showed that the expected distribution function after galactic collapse has the same velocity dispersion for all stellar masses. Exploratory attempts to fit the luminosity profile of M87 with two mass King models met with limited success. A reasonable fit was obtained by loading the core of the model with a second population of massive stars concentrated inside $r = 2''$. The total mass required to perturb the profile sufficiently was $\sim 5 \times 10^9\ M_\odot$. We shall not pursue this type of model any further because it fails to fit the velocity dispersion data of Sargent *et al.* (1978); the model predicts a constant velocity dispersion $\sigma_v$ for the visible stars across the core of the galaxy, whereas $\sigma_v$ is observed to increase sharply as $r \to 0$.

### *b) Models with a Large Central Mass*

A stellar dynamics code (VAMPIRE) was written to determine the equilibrium distribution of a stellar population around a massive black hole[1] in a galactic nucleus. This is done by solution of a Fokker-Planck equation in $(E, J)$ space for a multimass stellar population simultaneously with Poisson's equation to determine the relaxed configuration. A minor adaptation allowed the effects of a black hole growing adiabatically in a collisionless stellar population to be studied. These two cases do not differ drastically and result in density profiles $\rho(r) \propto r^{-7/4}$ near the black hole for the relaxed models and $\rho(r) \propto r^{-3/2}$ for the adiabatic models. We shall not discuss the details of the VAMPIRE models further, since they are described in Young (1977).

A satisfactory fit between the observed profile of M87 and a black hole model is shown in Figure 6. This results in a determination of certain parameters.

i) The core radius of the galaxy,

$$r_c = 9.''6 \pm 0.''5 = (698 \pm 36)\delta_{15}\ \mathrm{pc}\,,$$

where $\delta_{15} = \Delta/15$ Mpc is the distance to M87. Estimates of this distance vary from $\Delta = 13.6$ Mpc (de Vaucouleurs 1975) to $\Delta = 19.5$ Mpc (Sandage and Tammann 1974), and we shall include the parameter $\delta_{15}$ where relevant without introducing its uncertainty in the formal error estimates.

[1] A "black hole" in the present context is a nonluminous mass which is pointlike (i.e., which has a size smaller than the seeing disk and the relevant physical length scales). It includes, but does not necessarily imply, the case of a mass which lies within its own Schwarzschild radius.

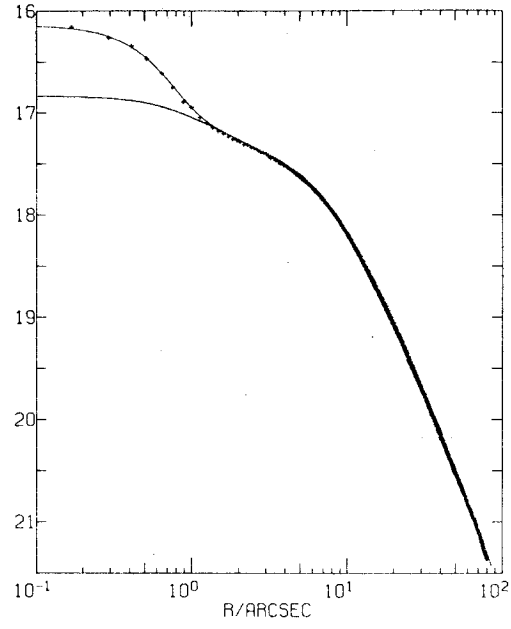


FIG. 6.—The luminosity profile of M87 fitted with a black hole model. An additional point luminosity profile is necessary to fit the data inside $r = 1''.5$. The deviation of the model from the data is $\lesssim 0.02$ mag, giving a black hole mass of $\sim 3 \times 10^9$ $M_\odot$. The intensity scale is $\mu_V \equiv$ mag arcsec$^{-2}$.

ii) The tidal radius is given by

$$\log r_T/r_c = 2.10 \pm 0.02 ,$$

as was determined previously from the data of Oemler (1976). It is by no means clear that the $r_T$ represents a true tidal cutoff rather than just a convenient way to truncate the stellar distribution function. However, this parameter has a negligible effect on the profile for $r < 10''$, wherein lies the action.

iii) Core surface brightness

$$\mu_V = 17.20 \pm 0.02 \text{ mag arcsec}^{-2} .$$

With an absorption $A_V = 0.14$ due to our own Galaxy, we deduce the core surface luminosity to be

$$L_c = (5.5 \pm 0.1) \times 10^3 L_\odot \text{ pc}^{-2} .$$

The relation between core surface luminosity $L_c$ and core spatial luminosity $L_0$ is

$$L_c = 2L_0 r_c ,$$

and so we find

$$L_0 = (4.0 \pm 0.2)\delta_{15}^{-1} L_\odot \text{ pc}^{-3}$$

Since the central luminosity profile is perturbed away from an isothermal sphere by the central black hole, the above parameters are those that would pertain if the black hole were absent.

iv) Mass of black hole

$$\mu_H = M_H/4\pi\rho_0(r_c/3)^3 = 0.6 \pm 0.1$$

(where $\rho_0$ = core mass density). Thus we find

$$M_H = (4.0 \pm 0.8) \times 10^8 (M/\mathscr{L})\delta_{15}^2 M_\odot ,$$

where $M/\mathscr{L}$ is the mass-luminosity ratio of the stellar population. The "cusp radius" where the kinetic energy of a typical core star is equal to the potential energy in the gravitational well of the black hole is

$$r_a = \mu_H r_c = 5''.8 \pm 1''.0 = (422 \pm 73)\delta_{15} \text{ pc} .$$

We see that both the core and the central cusp of M87 are well resolved, being 20 and 12 times the seeing disk, respectively. The effects of seeing have been allowed for by appropriate convolution of the model for the fit shown in Figure 6.

v) The observed profile of M87 rises above that predicted by the black hole model inside $r = 1''.7$. This may be allowed for by adding a point luminosity source to the center with the following magnitude and colors

$$V_s = 16.69 \pm 0.05 ,$$

$$(B - V)_s = +0.73 \pm 0.03 ,$$

$$(V - R)_s = +0.59 \pm 0.03 .$$

We assume that the colors of the underlying galaxy remain at their values $(B - V) = +1.02$ and $(V - R) = +0.86$ for $r > 1''.7$. The total luminosity of this point source (in the $V$ band) is

$$L_s = (4.7 \pm 0.2) \times 10^7 \delta_{15}^2 L_\odot .$$

vi) The spectroscopic data of Sargent *et al.* (1978) give a core velocity dispersion of $\sigma_v = 278 \pm 11$ km s$^{-1}$. From the relation $\sigma_v^2 = 4\pi G\rho_0(r_c/3)^2$, we find the core mass density to be

$$\rho_0 = (26 \pm 3)\delta_{15}^{-2} M_\odot \text{ pc}^{-3} ,$$

and the mass-luminosity ratio of the stellar population is

$$M/\mathscr{L} = (6.5 \pm 0.6)\delta_{15}^{-1} .$$

The mass of the black hole then becomes

$$M_H = (2.6 \pm 0.5) \times 10^9 M_\odot .$$

Our value for $M/\mathscr{L}$ is much lower than previous estimates ($M/\mathscr{L} \sim 50$), which were based on (1) spuriously high velocity dispersion measurements of $\sigma_v \sim 500$ km s$^{-1}$ (Minkowski 1962; Brandt and Roosen 1969), and (2) use of the virial theorem applied to the whole galaxy when only the central velocity dispersion was known.

### c) *Considerations of the Large Nuclear Mass*

A model-independent demonstration of the large nuclear mass in M87 is given in Sargent *et al.* (1978), along with a general and practical method for determining the mass-luminosity ratio as a function of

radius given both photometric and velocity dispersion data. Denoting $M(r)$ as the mass enclosed within a sphere of radius $r$, and $\mathscr{L}(r)$ the luminosity similarly enclosed, considerations of the innermost points for which dynamical data exists gave a mass enclosed within 1".5 as

$$M(1''.5) = (6.5 \pm 1.5) \times 10^9 \delta_{15}\, M_\odot .$$

For a 1".5 radius aperture centered on M87, the integrated magnitude is $V_p(1''.5) = 14.71 \pm 0.03$. Allowing for projection effects through the galaxy, the magnitude of a 1".5 sphere is $V_s(1''.5) = 15.73 \pm 0.07$ (see Table 2). Allowing for galactic absorption $A_V = 0.14$, the total luminosity is

$$\mathscr{L}(1''.5) = (11.2 \pm 0.8) \times 10^7 \delta_{15}{}^2\, L_\odot ,$$

and the mean mass-luminosity ratio enclosed with radius $r$, taking all material into account, is

$$\langle M/\mathscr{L} \rangle (1''.5) = (58 \pm 16) \delta_{15}{}^{-1} .$$

This is a factor of 10 higher than for the stellar population in the rest of the core and demonstrates the existence of a large, invisible mass in the nucleus of M87.

According to the black hole model shown in Figure 6, the mass of stars enclosed within a 1".5 sphere is

$$M_*(1''.5) = (4.2 \pm 0.3) \times 10^8 \delta_{15}\, M_\odot ,$$

and their luminosity is

$$\mathscr{L}_*(1''.5) = (6.5 \pm 0.3) \times 10^7 \delta_{15}{}^2\, L_\odot .$$

If the residual "anomalous" mass and luminosity of

$$M_s(1''.5) = (6.1 \pm 1.5) \times 10^9 \delta_{15}\, M_\odot$$

$$\mathscr{L}_s(1''.5) = (4.7 \pm 0.2) \times 10^7 \delta_{15}{}^2\, L_\odot$$

are associated, then the mystery object has a mass-luminosity ratio of

$$(M/\mathscr{L})_s = (130 \pm 38) \delta_{15}{}^{-1}$$

in solar units employing the $V$ band.

### *d) Nature of the Central Luminosity Source*

The present data do not define the nature of the central luminous source required to fit the black hole model of § IV*b* above, although there are additional pertinent observations.

i) Spectroscopic data (Sargent *et al.* 1978) show the central regions of M87 to have a late-type stellar spectrum. The change in line strength observed across the nucleus is a barely significant 4%. This places a limit of $V = 16.4$ on the luminosity of a nonthermal continuum source in the center of M87.

ii) The nucleus of M87 is unpolarized, whereas the "jet" is linearly polarized at a level of 20% (Angel 1977, private communication).

On morphological grounds, one might expect blue nonthermal emission akin to that observed in a Seyfert galaxy, and we note that the luminosity of the central point source is $V = 16.7$, which does not violate the constraint given above. However, the colors and slight decrease in line strength would also be consistent with a population of G5 stars.

## V. SUMMARY AND DISCUSSION

We have demonstrated the following points.

i) The core radius of M87 is $r_c = 9''.6 = 700$ pc and the core surface brightness is $\mu_V = 17.20$ mag arcsec$^{-2} = 5.5 \times 10^3\, L_\odot\, \mathrm{pc}^{-2}$. The core luminosity is then $L_0 = 4.0\, L_\odot\, \mathrm{pc}^{-3}$.

ii) The colors of M87 are constant at $(B - V) = +1.02$ and $(V - R) = +0.86$ for $1''.7 < r < 80''$. The central regions are slightly bluer than the rest of the galaxy with $(B - V) = +0.87$ and $(V - R) = +0.74$ for a centered 1" diameter aperture.

iii) The luminosity profile cannot be fitted by isothermal or King models (with constant mass-luminosity ratio) because the central regions ($r < 10''$) contain a bright luminosity cusp. This cusp is not seen in other nearby, normal elliptical galaxies and so adds to the peculiarities exhibited by M87.

iv) In the radial range $1''.7 < r < 80''$ the luminosity profile of M87 can be fitted by a King model containing a central black hole of mass $M_H = 3 \times 10^9\, M_\odot$. An additional point luminosity source with $V = 16.69$, $(B - V) = +0.73$ and $(V - R) = +0.59$ is successful in fitting the profile and colors for $r < 1''.7$.

v) Using the core velocity dispersion $\sigma_v = 278$ km s$^{-1}$ found by Sargent *et al.* (1978), we find for M87 a core mass density of $\rho_0 = 26\, M_\odot\, \mathrm{pc}^{-3}$ and a mass-luminosity ratio $M/\mathscr{L} = 6.5$ (in solar units) for the stellar population. The velocity dispersion increases to 350 km s$^{-1}$ as $r \to 0$ in accord with the black hole model.

vi) A model-independent dynamical analysis of the central regions finds the total mass enclosed by a 1".5 sphere centered in M87 to be $M(1''.5) = 6.5 \times 10^9\, M_\odot$. Since the luminosity is $L(1''.5) = 11.2 \times 10^7\, L_\odot$, the mean mass-luminosity ratio is $M/\mathscr{L}(1''.5) = 58$, a factor of 10 higher than for the stellar population for $r > 1''.7$.

In summary, the data show that the nucleus of M87 contains a supermassive object of mass $M_H \sim 5 \times 10^9\, M_\odot$, radius $r \leq 100$ pc, and $M/\mathscr{L} \geq 60$. Various suggestions may be made as to the possible nature of this object.

1. A small, dense star cluster with a high $M/\mathscr{L}$ may be bound in the core of M87. Suitable objects in the cluster include white dwarfs, neutron stars, black holes, or perhaps even extreme M dwarfs. Such a cluster, as a dynamically bound entity, would have to have a very high velocity dispersion ($\sigma_v > 1000$ km s$^{-1}$) and could therefore mimic a continuum source by virtue of broadening the stellar spectral lines to invisibility (although one could still detect the metallicity break at 3900 Å). This central cluster cannot be akin to the small nucleus seen in M31 (Kinman 1965),

since the M87 "cluster" would contain $\sim 100$ times as much mass and is associated with changes in $M/\mathscr{L}$ and increases in the stellar velocity dispersion (which the M31 cluster is not; Morton, Andereck, and Bernard 1977).

It is unlikely that such a cluster would have been formed by the spiraling in of companion galaxies or globular clusters as suggested for M31 by Tremaine, Ostriker, and Spitzer (1975). The objections are: (i) galaxies could not form an object less than or only 100 pc across; (ii) the total mass in the globular clusters of M87 is $\sim 10^9\ M_\odot$; thus 5 times this amount would already have had to spiral in; and (iii) neither galaxy or globular cluster material could yield $M/\mathscr{L} \geq 60$.

2. Since the relaxation time scale in the core of M87 is $t_R \sim 10^{14}$ yr, it is unlikely that the central cusp is incipient gravothermal collapse (Lynden-Bell and Wood 1968) or runaway mass segregation (Spitzer 1969). In any case, since the stellar population remains close to dynamical equilibrium during such events, the arguments of § IV*c* still apply.

3. It may be possible to explain the photometric and dynamical data if the stellar population is out of dynamical equilibrium. To throw the stars out of equilibrium, however, one must contrive to remove or add a mass $\sim 5 \times 10^9\ M_\odot$ in a dynamical time scale of $\sim 10^5$ yr; furthermore, the disturbance will die away in this dynamical time scale of $10^5$ yr. It is possible to imagine a slingshot mechanism (Saslaw, Valtonen, and Aarseth 1974) removing $\sim 5 \times 10^9\ M_\odot$ from the nucleus of M87, with the resulting ejecta forming the optical jets.

4. Another possibility is that the nucleus of M87 contains a single compact object such as a spinar or massive black hole. It should be emphasized that we are not forced to such a model on either observational or theoretical grounds, but it is consistent with all the data, and is in many ways the most attractive of the models considered. A central black hole could easily fuel itself by consuming mass lost from stars in the cusp to explain the $\sim 10^{42}$ ergs $s^{-1}$ energy output of Virgo A. A mass flux of $\sim 10^{-2}\ M_\odot\ yr^{-1}$ is possible and so an efficiency of conversion to radiation of only 0.002 would be necessary.

M87 is at present probably the most plausible case for a massive black hole in a galaxy nucleus. The existing data are pressing upon the current limits for ground-based observations, and are not likely to be improved upon in the near future. Probably the best hope for a dramatic improvement in the data lies with the Space Telescope, which will offer an order of magnitude increase in resolution for more detailed studies of M87 and a search for similar phenomena in more distant supergiant elliptical radio galaxies.

We thank John Bahcall, Roger Blandford, Peter Goldreich, Jim Gunn, Vincent Icke, John Kormendy, Russell Redman, Martin Rees, Scott Tremaine, and Gerard de Vaucouleurs for discussions and valuable assistance. We also thank Wallace Sargent, Alec Boksenberg, Keith Shortridge, Roger Lynds, and Fred Hartwick for the close cooperation involved in analyzing the M87 data presented in this and the accompanying paper. This work was supported in part by the National Science Foundation, under grant MPS 75-16327 to the Carnegie Institution of Washington.

REFERENCES

Arp, H. C., and Lorre, J. 1976, *Ap. J.*, **210**, 58.
Brandt, J. C., and Roosen, R. G. 1969, *Ap. J. (Letters)*, **156**, L59.
Cohen, M. H., Moffet, A. T., Shaffer, D., Clark, B. G., Kellermann, K. I., Jauncey, D. L., and Gulkis, S. 1969, *Ap. J. (Letters)*, **158**, L83.
de Vaucouleurs, G. 1975, in *Galaxies and the Universe*, ed. A. Sandage, M. Sandage, and J. Kristian (Chicago: University of Chicago Press), p. 557.
de Vaucouleurs, G., Angione, R., and Fraser, C. W. 1968, *Ap. Letters*, **2**, 141.
de Vaucouleurs, G., de Vaucouleurs, A., and Corwin, H. G., Jr. 1976, *Second Reference Catalogue of Bright Galaxies* (Austin: University of Texas Press).
de Vaucouleurs, G., and Nieto, J. L. 1977, preprint.
Felten, J. E. 1968, *Ap. J.*, **151**, 861.
Felten, J. E., Arp, H. C., and Lynds, C. R. 1970, *Ap. J.*, **159**, 415.
Kellermann, K. I., Clark, B. G., Cohen, M. H., Shaffer, D. B., Broderick, J. J., and Jauncey, D. L. 1973, *Ap. J. (Letters)*, **179**, L141.
King, I. R. 1966, *A.J.*, **71**, 64.
———. 1975, in *Dynamics of Stellar Systems, IAU Symposium No. 69*, ed. A. Hayli (Dordrecht: Reidel), p. 99.
Kinman, T. D. 1965, *Ap. J.*, **142**, 1376.
Kormendy, J. 1977, *Ap. J.*, **214**, 359.
Lynden-Bell, D. 1967, *M.N.R.A.S.*, **136**, 101.
Lynden-Bell, D. 1969, *Nature*, **223**, 690.
Lynden-Bell, D., and Wood, R. 1968, *M.N.R.A.S.*, **138**, 495.
Minkowski, R. 1962, in *Problems of Extragalactic Research, IAU Symposium No. 15*, ed. G. C. McVittie (New York: Macmillan), p. 112.
Moffet, A. T. 1975, in *Galaxies and the Universe*, ed. A. Sandage, M. Sandage, and J. Kristian (Chicago: University of Chicago Press), p. 211.
Morton, D. C., Andereck, C. D., and Bernard, D. A. 1977, *Ap. J.*, **212**, 13.
Oemler, A., Jr. 1976, *Ap. J.*, **209**, 693.
Sandage, A. 1973, *Ap. J.*, **183**, 711.
Sandage, A., and Tammann, G. A. 1974, *Ap. J.*, **194**, 559.
Sargent, W. L. W., Young, P. J., Boksenberg, A., Shortridge, K., Lynds, C. R., and Hartwick, F. D. A. 1978, *Ap. J.*, **221**, in press.
Saslaw, W. C., Valtonen, M. J., and Aarseth, S. J. 1974, *Ap. J.*, **190**, 253.
Spitzer, L. 1969, *Ap. J. (Letters)*, **158**, L139.
Tremaine, S. D., Ostriker, J. P., and Spitzer, L., Jr. 1975, *Ap. J.*, **196**, 407.
Westphal, J. A., Kristian, J., and Sandage, A. 1975, *Ap. J. (Letters)*, **197**, L95.
Young, P. J. 1977, "Massive Black Holes in Galactic Nuclei," presented at NATO Conference "Energy Sources and Emission Mechanisms in QSO's," Cambridge.

*Note added in proof.*—G. de Vaucouleurs has kindly sent us his new photographic results, obtained with J. L. Nieto, for the $\mu_B$ profile of M87 at small radii. These were compared with $\mu_B = \mu_V + (B - V)$ measured by the SIT/CCD. After subtracting a zero-point difference of 0.1 mag, the difference in the profiles is less than 0.03 mag

for $1'' < r < 80''$. For $r < 1''$, deviations of 0.1 mag occur due to the higher resolution of the SIT/CCD data (seeing $\sigma_* = 0''.46$ against $\sigma_* = 0''.7$ for the McDonald photographic data). In particular, the McDonald data also demonstrate the shape of the M87 profile as shown in Figure 2, with the steepness of the slope even in the core regions of the galaxy and the reversal in sign of the second derivative of $\mu(\log r)$ between $r = 1''$ and $r = 2\frac{1}{2}''$.

J. A. KRISTIAN: Hale Observatories, 813 Santa Barbara Street, Pasadena, CA 91101

F. P. LANDAUER: Jet Propulsion Laboratory, 4800 Oak Grove Drive, Pasadena, CA 91103

J. A. WESTPHAL: Division of Geological and Planetary Sciences, California Institute of Technology, Pasadena, CA 91125

C. P. WILSON: 5235 James Road, Santa Barbara, CA 93111

P. J YOUNG: Robinson Laboratory of Astrophysics, California Institute of Technology, Pasadena, CA 91125

THE ASTROPHYSICAL JOURNAL, 221:731–744, 1978 May 1


# DYNAMICAL EVIDENCE FOR A CENTRAL MASS CONCENTRATION IN THE GALAXY M87

W. L. W. SARGENT* AND PETER J YOUNG
Hale Observatories, California Institute of Technology, Carnegie Institution of Washington
A. BOKSENBERG*† AND KEITH SHORTRIDGE*
Department of Physics and Astronomy, University College London
C. R. LYNDS
Kitt Peak National Observatory
AND
F. D. A. HARTWICK*
Department of Astronomy, University of Victoria
*Received 1977 September 26; accepted 1977 November 1*

## ABSTRACT

The elliptical galaxies NGC 3379 (E1) and M87 (E0) have been observed spectroscopically with the University College London Image Photon Counting System. Analysis of the redshifts and velocity dispersions as a function of radius by a Fourier method has yielded the following results: (*a*) NGC 3379 exhibits slight rotation ($v_\theta = 15$ km s$^{-1}$ at $r = 14''$) along the N-S direction (22° from the minor axis). The velocity dispersion is 195 km s$^{-1}$ for $r < 14''$; this shows a small decrease with increasing radius. The data, including the photometric profile, is adequately fitted by a King model with log $r_T/r_c = 2.20$ and constant $M/\mathscr{L} = 6$ for $0'' < r < 14''$ (with $r_c = 2''.8$). (*b*) M87 shows no rotation ($v_\theta < 10$ km s$^{-1}$) for $r < 72''$ in the E-W direction. The velocity dispersion at the edge of the core ($r_c = 9''.6$) is 278 km s$^{-1}$, but decreases to 230 km s$^{-1}$ when $r = 72''$. Inside the core a sharp increase is observed, up to 350 km s$^{-1}$ at $r = 1''.5$. The photometric profile and velocity dispersion data outside the core are explained by a King model with $M/\mathscr{L} = 6.5$ and log $r_T/r_c = 2.10$. The data inside the core radius can be explained by a central mass concentration $M = 5 \times 10^9\ M_\odot$ contained within $r = 1''.5$ (=110 pc). For $r < 1''.5$ we find $M/\mathscr{L} = 60$, a factor of 10 higher than that in the outer regions. The observed width (1500 km s$^{-1}$ full width at zero intensity) of the [O II] λ3727 doublet also suggests a central mass of $\sim 5 \times 10^9\ M_\odot$.

We conclude that the observations of M87 are entirely consistent with the presence of a central black hole of $\sim 5 \times 10^9\ M_\odot$.

*Subject headings:* black holes — galaxies: individual — galaxies: internal motions — galaxies: nuclei — galaxies: redshifts

## I. INTRODUCTION

The introduction of linear, two-dimensional detectors has at last made it possible to measure accurate velocity dispersions and redshifts in the outer parts of elliptical galaxies, even in regions where the surface brightness is appreciably below that of the sky. As a result, several topics of current theoretical interest have become amenable to observational study. Perhaps the most important among these are (*a*) the search for evidence for supermassive black holes in the centers of elliptical galaxies, particularly in giant ellipticals in which the presence of such objects has been invoked in order to explain explosive or other nonthermal phenomena, (*b*) studies of the rotation curves and radial variation of velocity dispersion in flattened ellipticals in order to check the hypothesis that such systems are supported by rotation, and (*c*) studies of the radial variation of mass and mass-to-light ratio to investigate whether or not galaxies have massive halos.

In a previous paper (Young *et al.* 1978*a*) the first results of our observational program on elliptical galaxies with the two-dimensional version of the University College London image photon counting system (IPCS) were discussed. The rotation curve and velocity dispersion of the E5 galaxy NGC 4473 were measured out to a radius of 45″ (3.3 kpc) from the center. Here we describe similar measurements for the E1 galaxy NGC 3379 and the E0 galaxy M87 (NGC 4486).

As we shall show in later sections, our results for

* Visiting Astronomers, Kitt Peak National Observatory, which is operated by Associated Universities for Research in Astronomy, Inc., under contract from the National Science Foundation.

† Guest Investigator, Hale Observatories.

NGC 3379 and M87 are strikingly different. Consequently, we shall employ NGC 3379 as an example of a normal elliptical galaxy and a standard of comparison for the remarkable behavior of M87. In § II we describe the observations of the two galaxies. The data reduction procedures are described in § III. The spectra were analyzed by a Fourier method due to Sargent *et al.* (1977, henceforth SSBS) which is outlined in § IV. This section also contains the results of the Fourier analysis. Extensive tests of the Fourier method are contained in § V. In § VI we compare the measurements made in the galaxies with models. A model-independent analysis is described in § VII. In § VIII we describe a procedure (also model independent) by which to obtain the mass-to-light ratio as a function of radius. The results are summarized and briefly discussed in § IX.

## II. OBSERVATIONS

### *a) M87*

The IPCS was attached to the White spectrograph at the Cassegrain focus of the Kitt Peak 4 m telescope in 1976 April. The slit size was 1″ by 102″; the scale at the Cassegrain focus is 6″.56 $mm^{-1}$. The IPCS was used in a mode in which 20 spectra (hereafter referred to as "scans") were accumulated simultaneously, equally spaced along the slit. (A complete set of scans will later be referred to as a frame.) Each spectrum was observed with 1000 channels covering 1060 Å along the direction of dispersion. The spatial resolution along the slit was 5″.4. The 1″ slit projected onto two channels on the detector. In order to mount the IPCS on the spectrograph, it was necessary to remove part of the mu-metal shield around the focusing coil of the electromagnetically focused image tube. As a result the spectra obtained with this arrangement suffered from severe S-distortion. Consequently, as mentioned in § II, it was sometimes necessary to reject data at either end of the spectrum. Also, the focus was inferior to that normally obtained with the device. Careful attention was paid to make observations of the object, the sky, and standard comparison stars under identical operating conditions.

A complete journal of observations made in connection with M87 is given in the first part of Table 1. Observations on the galaxy were made with the slit E-W and placed at various positions relative to the nucleus of the galaxy. Particular care was taken to avoid the region of the optical "jet." The furthest extent of the slit from the center of M87 was 150″. As indicated in Table 1, extensive exposures to measure the sky background were made on an area free of visible stars 1° S of M87. An inert gas wavelength comparison source (containing He, Ne, Ar, and Kr) was recorded frequently. Three bright comparison stars were observed for use in conjunction with the Fourier method used to measure radial velocities, line strengths, and velocity dispersions. These were HR 5709 (K0 III), HR 5741 (K4 III), and HR 5888 (G8 III). Five magn. neutral density filters were inserted during the observations of the stars in order to obtain acceptable counting rates with the IPCS. Further details pertinent to the M87 observations are given in Table 1.

### *b) NGC 3379*

Observations of NGC 3379 were made with the IPCS at the coudé focus of the 5 m Hale telescope in 1977 April. The device was attached to the 36 inch (91 cm) camera in the manner described by Boksenberg and Sargent (1975). As at Kitt Peak the IPCS was operated in a two-dimensional mode in which 17 spectra (scans) were recorded simultaneously, each

TABLE 1

JOURNAL OF OBSERVATIONS FOR M87 AND NGC 3379

| Raw Data Set No. | Object | Night | Slit p.a. | Slit* Position | Spectral Coverage (Å) | Bin Size (Å) | Resolution FWHM (Å) | Time on Object (sec) | Time on Sky (sec) |
|---|---|---|---|---|---|---|---|---|---|
| 1 | M87 | 1 Apr 1976 | 90° | 0" | 3799-4863 | 1.06 | 4.6 | 2600 | 0 |
| 2 | M87 | 1 Apr 1976 | 90° | 102"E | 3799-4863 | 1.06 | 4.6 | 5000 | 0 |
| 3 | HR 5709 | 1 Apr 1976 | 90° | 0" | 3799-4863 | 1.06 | 4.6 | 617 | ... |
| 4 | HR 5741 | 1 Apr 1976 | 90° | 0" | 3799-4863 | 1.06 | 4.6 | 1000 | ... |
| 5 | M87 | 3 Apr 1976 | 90° | 51"W | 3631-4696 | 1.07 | 4.6 | 3000 | 1800 |
| 6 | M87 | 3 Apr 1976 | 90° | 102"W | 3631-4696 | 1.07 | 4.6 | 9600 | 4800 |
| 7 | HR 5709 | 3 Apr 1976 | 90° | 0" | 3631-4696 | 1.07 | 4.6 | 600 | ... |
| 8 | HR 5741 | 3 Apr 1976 | 90° | 0" | 3631-4696 | 1.07 | 4.6 | 513 | ... |
| 9 | HR 5888 | 3 Apr 1976 | 90° | 0" | 3631-4696 | 1.07 | 4.6 | 513 | ... |
| 10 | NGC 3379 | 12 Apr 1977 | 0° | 0" | 3985-4296 | 0.31 | 0.74 | 10500 | 1500 |
| 11 | HD 92706 | 12 Apr 1977 | 0° | 0" | 3985-4296 | 0.31 | 0.74 | 910 | ... |
| 12 | HR 4207 | 12 Apr 1977 | 0° | 0" | 3985-4296 | 0.31 | 0.74 | 400 | ... |

*This column gives the position of the center of the slit relative to the nucleus of the object.

containing 1000 channels spread over 310 Å in wavelength. The scale at the coudé focus is 1".2 $mm^{-1}$, and the observations were made with a slit 1" wide and 40" long. The slit width projected to 2 channels on the detector. The spatial resolution along the slit was 2".4. All observations of NGC 3379 were made with the nucleus of the galaxy at the center of the slit. A complete journal of observations made in connection with NGC 3379 is given in the bottom part of Table 1. Sky exposures were made on an area 5' N of the nucleus. Frequent observations were also made of a hollow cathode Ar-Fe comparison arc. Two bright K giant stars were observed for use in conjunction with the Fourier analysis of the galaxy data. These were HD 92706 (gK2) and HR 4027 (gK1). Neutral density filters were used to cut down the counting rate to an acceptable level during the stellar observations. Further pertinent details of the NGC 3379 observations are given in Table 1.

### c) *Flat Fields*

In order to correct for small-scale variations in sensitivity of the IPCS, observations were made at both Kitt Peak and Palomar of flat fields. For this purpose, at both observatories a diffuse incandescent lamp was observed through the spectrograph slit. At Kitt Peak observations were also made of the comparison arc with a diffuse Mylar screen in place of the grating in the spectrograph. The flat fields were used in the reductions described in the following section.

## III. DATA REDUCTION

The reduction procedure was standardized for all sets of data and consisted of the following steps:

1. All frames (including arcs) were divided by an appropriate flat-field frame:

$$N'(i,j) = N(i,j)/F(i,j) \qquad (1 \le i \le 1000; 1 \le i \le j_{\max}),$$
$$\langle F(i,j)\rangle_{ij} = 1, \qquad (1)$$

where $i$ is the channel number, $j$ is the scan number, and $j_{\max}$ is the total number of scans in a frame (20 for M87 and 17 for NGC 3379).

2. The drifts in the arc lines from frame to frame were scrutinized, and the data broken into sets within which the drifts were less than 0.25 channels. The arcs in each of the resulting sets were summed; and 24 strong, unblended lines were chosen by trial and error to establish a wavelength scale for each scan within a frame by the following least squares procedure. Arc lines of tabulated wavelength $\lambda_k$ were established to be at positions $N_k(j)$ $(1 \le j \le j_{\max})$ in each scan and at a mean position $N_k = \langle N_k(k)\rangle_j$. A least squares procedure on $\epsilon_k$ determined the coefficients $\alpha_i$ in the following relations:

$$N_k + \epsilon_k = \sum_{i=0}^{3} \alpha_i \lambda_k{}^i . \qquad (2)$$

Then a least squares minimization of $\zeta_k(j)$ determined the $b_{mn}$ in the subsequent approximation,

$$N_k(j) - \sum_{i=0}^{3} \alpha_i \lambda_k{}^i + \zeta_k(j) = \sum_{m=0}^{2}\sum_{n=0}^{2} b_{mn}\lambda_k{}^m j^n . \qquad (3)$$

Wavelength $\lambda$ was then considered to be at a position

$$N(\lambda, j) = \sum_{l=0}^{3} \alpha_l \lambda^l + \sum_{m=0}^{2}\sum_{n=0}^{2} b_{mn}\lambda^m j^n . \qquad (4)$$

The deviation of a single arc line was typically 0.3 channels, and so the wavelength scale may be expected to have an internal accuracy of $\sim$0.05 channels.

3. The data were rebinned into 1024 channels on a logarithmic scale by linear interpolation among the original channels. If the new channel overlaps with fraction $f_i$ of the old channel $i$ (containing $N_i$ counts), then

$$N_{\text{new}} = \sum_{i=1}^{1000} f_i N_i ; \qquad \sum_{i=1}^{1000} f_i = 1 . \qquad (5)$$

4. When sky frames $S_k$ were observed, the sky subtraction was performed by linear subtraction of the sum of the sky frames from the sum of the galaxy frames $G_k$:

$$G'(i,j) = \sum_{k=1}^{n_G} G_k(i,j) - (T_G/T_s) \sum_{k=1}^{n_s} S_k(i,j) , \qquad (6)$$

where $T_G$ is the total integration time on the galaxy and $T_s$ is the time on the sky. For the standard stars, sky was subtracted by an equivalent procedure using the scans not containing the star. For the M87 data sets 1 and 2 in Table 1, the sky was not observed. In these cases the scans covering the outer part of the galaxy were used as "sky" for the scans covering the inner part. In particular, for data set 2 taken 102" E of the center of M87, "object" scans were deemed to be $j = 1$ to 8, and "sky" scans $j = 9$ to 16. For reasons to be discussed in § V, such data are to be given low weight when the sky is comparable in brightness to the galaxy.

5. As already mentioned, the M87 data were affected by severe S-distortion. Where the extent of the distortion was less than 0.2 scans, a two-dimensional linear rebinning procedure was used to straighten the scans. Data with distortions in excess of this at the ends of the spectra were not included in the analysis. Table 2 lists the actual wavelength range used.

6. The standard star frames for a particular star were added together when observations on more than one night existed, so as to give the highest possible quality spectra for the Fourier analysis.

Experience has shown that galaxy spectra require at least a total of $10^5$ counts, and preferably $3 \times 10^5$ counts, for the Fourier analysis. To achieve this, adjacent scans were added where necessary. The position of such a summation of scans from $j_1$ to $j_2$

TABLE 2

M87 AND NGC 3379: REBINNED DATA PARAMETERS

| Rebinned Set No. | Raw Data Set No. | Object | Slit p.a. | Slit Position | Spectral Coverage (Å) | Bin Size (km s$^{-1}$) | Resolution FWHM (km s$^{-1}$) | Total No. of Counts on Orbit (N/10$^5$) |
|---|---|---|---|---|---|---|---|---|
| 1 | 1 | M87 | 90° | 0" | 3805-4670 | 60 | 330 | 35.0 |
| 2 | 2 | M87 | 90° | 102"E | 3805-4670 | 60 | 330 | 2.7 |
| 3 | 5 | M87 | 90° | 51"W | 3805-4670 | 60 | 330 | 17.3 |
| 4 | 6 | M87 | 90° | 102"W | 3805-4670 | 60 | 330 | 4.1 |
| 5 | 3,7 | HR 5709 | 90° | 0" | 3805-4670 | 60 | 330 | 11.5 |
| 6 | 4,8 | HR 5741 | 90° | 0" | 3805-4670 | 60 | 330 | 14.6 |
| 7 | 9 | HR 5888 | 90° | 0" | 3805-4670 | 60 | 330 | 7.7 |
| 8 | 10 | NGC 3379 | 0° | 0" | 4000-4283 | 20 | 53 | 21.0 |
| 9 | 11 | HD 92706 | 0° | 0" | 4000-4283 | 20 | 53 | 14.6 |
| 10 | 12 | HR 4207 | 0° | 0" | 4000-4283 | 20 | 53 | 6.6 |

was deemed to be at a luminosity-weighted average position:

$$\langle j \rangle = \sum_{j=j_1}^{j_2} jN_G(j) \Big/ \sum_{j=j_1}^{j_2} N_G(j)\,, \qquad (7)$$

where $N_G(j)$ is the total number of counts in scan $j$.

Table 2 gives the relevant parameters and details of the various sets of rebinned data for M87 and NGC 3579.

## IV. FOURIER ANALYSIS AND RESULTS

In Figure 1 we display spectra of a comparison star, of the outer region ($r = 70''$) of M87, and also of the nucleus of M87. The differences in the line widths are striking, particularly when comparing the two M87 spectra. A detailed examination suggests that the velocity dispersion in the outer regions of M87 is much lower than in the nucleus. Differences in structure around the G band, and the Ca II H and K lines, are also evident. A rough measurement of the line widths gives values $\sigma(r = 70'') \sim 200$ km s$^{-1}$ and $\sigma$(nucleus) $\sim 300$ km s$^{-1}$ for M87. We note, however, that visual techniques for determining velocity dispersions are less reliable than Fourier methods. As SSBS have shown in detail, direct analyses of the data in wavelength space have difficulties in differentiating between line strengths and line widths.

In the Fourier method described by SSBS, the

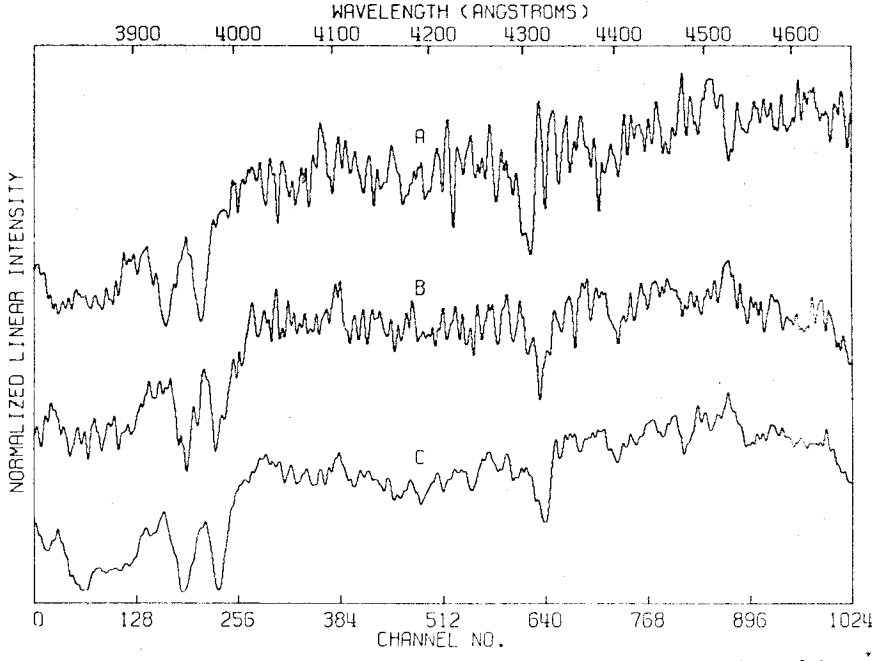


FIG. 1.—IPCS spectra of (*A*) comparison star HR 5709 (K0 III), (*B*) M87 at a distance of 70" W of the center, (*C*) M87 4" E of center. Note the broad, shallow lines of spectrum *C* as compared with *B*. The Fourier velocity dispersions were $\sigma_v = 220$ km s$^{-1}$ for *B* and 300 km s$^{-1}$ for *C*.

discrete Fourier transforms of the galaxy and star spectra $\tilde{G}(k)$ and $\tilde{S}(k)$, respectively, are evaluated. The quotient $Q(k) = \tilde{G}(k)/\tilde{S}(k)$ is then compared by a least squares fit to the broadening function

$$B(k) = \gamma \exp\left[-\frac{1}{2}\left(\frac{2\pi k\sigma_v}{nc\Delta \ln \lambda}\right)^2 + \frac{2\pi i k \ln (1+z)}{n\Delta \ln \lambda}\right], \quad (8)$$

to determine simultaneously the redshift $z$, the velocity dispersion $\sigma_v$, and the relative line strength $\gamma$. Here $n$ is the number of real space channels, and $\Delta \ln \lambda$ the channel width. A weighting function for the least squares analysis is obtained by estimating the standard deviation $\Delta Q(k)$ in the quotient $Q(k)$ and then minimizing

$$\chi^2 = \sum_{k=k_L}^{k_H} \left|\frac{Q(k) - B(k)}{\Delta Q(k)}\right|^2,$$

where $k_H$ and $k_L$ are the upper and lower limits of the domain in Fourier space to be fitted. In previous versions of this analysis an evaluation of the noise level in the data was used to choose a value of $k_H$ ($k_L$ was fixed). To ensure uniformity we have kept $k_H$ fixed for each galaxy. Thus, for M87 we used $k_L = 5$ and $k_H = 80$, while for NGC 3379 we used $k_L = 10$ and $k_H = 40$. As was demonstrated by SSBS, the results do not depend on $k_H$ to any significant degree.

The Fourier analysis procedure described above was carried out for the data on both galaxies. First we discuss the results obtained for NGC 3379. These are given in Figure 2 and Table 3, and are the mean of the values obtained with the two comparison stars listed in Table 1. The spectrograph slit was oriented N-S on this E1 galaxy, at an angle of 22° to the minor axis (the position angle of the major axis is 68° [Dennison 1954, as quoted by de Vaucouleurs 1959]). The core radius of the galaxy is $r_c = 2''.8 \pm 0''.3$ from photometry by Kormendy (1977) and by Young *et al.* (1978*c*). The distance to NGC 3379 is $\Delta = 8$ Mpc (de Vaucouleurs 1975), but we shall include a distance factor $\delta_8 = \Delta/8$ Mpc in all relevant quantities without including possible errors in $\delta_8$ when estimating errors.

Our values for the mean redshift and velocity dispersion of NGC 3379 are $cz = 905 \pm 16$ km s$^{-1}$ and $\sigma_v = 195 \pm 17$ km s$^{-1}$, respectively. These may be compared with previously published values of $cz = 885 \pm 27$ km s$^{-1}$ (de Vaucouleurs, de Vaucouleurs, and Corwin 1976) and $\sigma_v = 240 \pm 40$ km s$^{-1}$ (Faber and Jackson 1976), $187 \pm 6$ km s$^{-1}$ (Burbidge, Burbidge, and Fish 1961), 125 km s$^{-1}$ (de Vaucouleurs 1974), $133 \pm 20$ km s$^{-1}$ (Williams 1977), and 187 km s$^{-1}$ (Minkowski 1962). As usual, the results for $\sigma_v$ range over nearly a factor of 2; these reflect systematic differences between the various methods of analysis. The Fourier method described here has been subject to extensive tests (see SSBS); further tests will be described in § V. We thus are confident that the results are free from systematic errors of more than 10%.

Reference to Figure 2 shows a slight rotational tilt

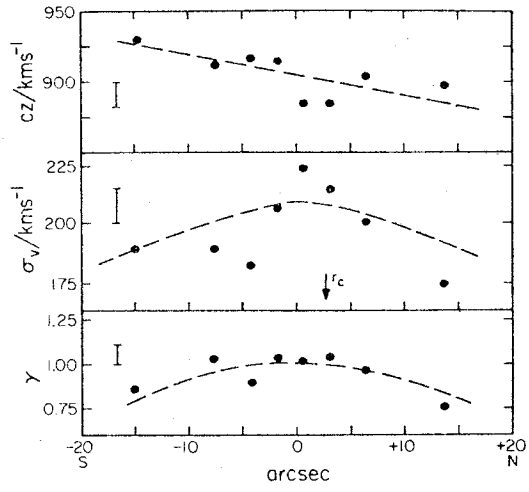


FIG. 2.—Results for NGC 3379. The redshift ($cz$), velocity dispersion ($\sigma_v$) and relative line strength ($\gamma$) of galaxy and comparison star were found simultaneously by Fourier methods. The core radius of the galaxy, $r_c = 2''.8$, is marked. Error bars of length 2 $\sigma$ are given.

in the plot of redshift as a function of radius, even at an angle of 22° to the minor axis. We find a rotation speed of $1.5 \pm 0.5$ km s$^{-1}$ arcsec$^{-1}$ with the N side of the galaxy approaching. Correction to the major axis would give $4.0 \pm 1.3$ km s$^{-1}$ arcsec$^{-1}$.

The velocity dispersion shows a slight decrease away from the center; this was also found by Faber and Jackson (1976), who found $\sigma_v = 210 \pm 20$ km s$^{-1}$ at a distance of $r = 10''$. The line strength parameter $\gamma$ also seems to show a slight decrease away from the center.

We next consider the results for M87. These are given in Table 3 and displayed in Figures 3 and 4. M87 is classified as an E0 galaxy, and the isophotes in the central regions are accurately circular (Young *et al.* 1978*b*). The core radius is $r_c = 9''.6 \pm 0''.5$, and the distance is $\Delta = 13.6$ Mpc (de Vaucouleurs 1975) or $\Delta = 19.5$ Mpc (Sandage and Tammann 1974). We shall adopt $\Delta = 15$ Mpc and include a quantity $\delta_{15} = \Delta/15$ Mpc in later computations.

The mean values for the redshift and velocity dispersion of M87 are $cz = 1287 \pm 21$ km s$^{-1}$ and

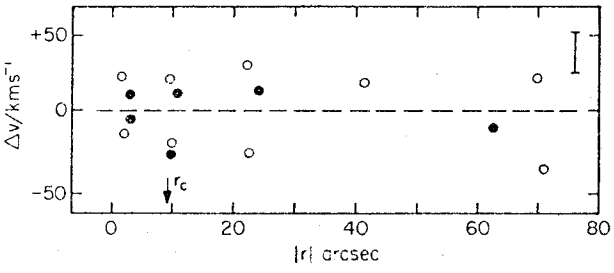


FIG. 3.—Rotational velocities of M87. The open circles (○) are points to the W of the nucleus for which $\Delta v = cz - \langle cz \rangle$ has been plotted; the filled circles (●) are to the E for which $-\Delta v$ has been plotted. The core radius of the galaxy, $r_c = 9''.6$, is marked. A 2 $\sigma$ error bar is given.

TABLE 3

M87 AND NGC 3379: REDSHIFTS, LINE STRENGTHS, AND VELOCITY DISPERSIONS

| Object | Data Set From Table 2 | Scan Block | $N_G/10^5$ | $\langle r'' \rangle$* | $\langle cz \rangle$† (km s$^{-1}$) | $\langle \gamma \rangle^{\neq}$ | $\langle \sigma_v \rangle$ (km s$^{-1}$) |
|---|---|---|---|---|---|---|---|
| M87 | 1 | 5-7 | 3.2 | -22.1 | 1314±16 | 0.96±0.03 | 260±17 |
| | 1 | 8-9 | 6.2 | - 9.2 | 1305±15 | 1.00±0.03 | 295±16 |
| | 1 | 10 | 7.3 | - 1.6 | 1306±20 | 0.95±0.03 | 329±21 |
| | 1 | 11 | 6.7 | + 3.8 | 1293±20 | 0.95±0.03 | 333±21 |
| | 1 | 12-13 | 5.3 | +11.3 | 1277±16 | 1.03±0.03 | 275±16 |
| | 1 | 14-16 | 3.1 | +24.3 | 1276±17 | 0.99±0.03 | 287±18 |
| | 2# | 1-8 | 2.7 | +62.2 | 1297±50 | 0.81±0.08 | 258±64 |
| | 3 | 1-7 | 0.9 | -69.7 | 1306±39 | 0.75±0.07 | 189±48 |
| | 3 | 8-11 | 1.2 | -41.6 | 1304±25 | 0.97±0.05 | 268±29 |
| | 3 | 12-14 | 2.0 | -22.7 | 1259±20 | 0.99±0.04 | 280±21 |
| | 3 | 15-16 | 3.5 | - 9.7 | 1267±16 | 1.09±0.03 | 301±17 |
| | 3 | 17 | 3.9 | - 2.2 | 1273±23 | 1.05±0.04 | 362±26 |
| | 3 | 18 | 3.6 | + 3.2 | 1275±20 | 1.01±0.04 | 321±22 |
| | 3 | 19-20 | 2.2 | + 9.7 | 1314±18 | 1.02±0.04 | 286±19 |
| | 4 | 1-20 | 4.1 | -71.8 | 1250±21 | 0.86±0.04 | 232±23 |
| Mean Value | | | | | 1287±21 | | 278±11§ |
| NGC 3379 | 8 | 1-4 | 1.7 | -14.2 | 930±25 | 0.86±0.18 | 189±33 |
| | 8 | 5-6 | 1.9 | - 7.4 | 911±13 | 1.03±0.11 | 188±18 |
| | 8 | 7 | 2.0 | - 4.1 | 916±16 | 0.90±0.11 | 181±21 |
| | 8 | 8 | 3.9 | - 1.7 | 913±13 | 1.04±0.11 | 206±16 |
| | 8 | 9 | 4.7 | + 0.7 | 883±18 | 1.02±0.12 | 223±21 |
| | 8 | 10 | 2.5 | + 3.1 | 883±16 | 1.04±0.10 | 214±16 |
| | 8 | 11-12 | 2.2 | + 6.5 | 903±18 | 0.97±0.13 | 200±22 |
| | 8 | 13-17 | 2.1 | +13.9 | 899±18 | 0.76±0.11 | 174±25 |
| Mean Value | | | | | 905±16 | | 195±17 |

*Positive values to the E for M87, to the N for NGC 3379

#Questionable data point (sky not observed, see § V).

†Heliocentric

≠ Reduced such that mean value of $\gamma$ in the region $r < 4r_c$ is unity.

§ Mean value for $10'' < |r| < 42''$ intended to represent the dispersion outside the central spike but not including the gradual drop in the outer regions.

$\sigma_v = 278 \pm 11$ km s$^{-1}$, where the value for $\sigma_v$ refers to the region $10'' < r < 42''$. These may be compared with the values of $cz = 1257 \pm 16$ km s$^{-1}$ (de Vaucouleurs, de Vaucouleurs, and Corwin 1976), $\sigma_v = 490 \pm 55$ km s$^{-1}$ (Minkowski 1962), $550 \pm 70$ km s$^{-1}$ (Brandt and Roosen 1969), and $315 \pm 20$ km s$^{-1}$ (Faber and Jackson 1976). The older values of $\sigma_v$ are undoubtedly too high, being measured by visual methods, but our value is consistent with that of Faber and Jackson (1976) when one allows for the fact that their measurements are systematically 22% higher than those of SSBS.

We see from Figure 3 that there is no evidence for rotation along the E-W direction in M87; the velocity amplitude is less than 10 km s$^{-1}$ for $r < 72''$. This is not surprising considering the circularity of the central isophotes and the low rotation velocities found in flattened elliptical systems (Bertola and Capaccioli 1975; Young *et al.* 1978*a*).

The velocity dispersion varies with radius, as was suspected from a crude examination of the spectra in Figure 1 of the sharpness of the spectral lines. It falls from $\sigma_v = 350$ km s$^{-1}$ at $r = 1''.5$, to $\sigma_v = 220$ km s$^{-1}$ at $r = 72''$. Outside the core radius the variations of $\sigma_v$ are gradual, but inside the core radius the value of $\sigma_v$ rises rapidly, as may be seen from Figure 4. The data have not been corrected to allow for seeing or resolution effects; were this to be done, the central

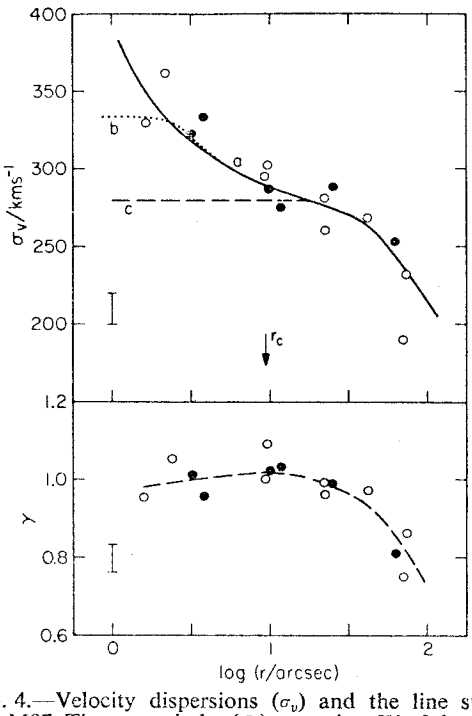


FIG. 4.—Velocity dispersions ($\sigma_v$) and the line strengths ($\gamma$) for M87. The open circles (○) are points W of the nucleus, and the filled circles (●) are E. The core radius, $r_c = 9''.6$, of the galaxy is marked. Error bars of length $2\sigma$ are given. Curve (*a*) is the velocity dispersion predicted by the black hole model fitted to the photometric data, (*b*) is the same model convolved with the seeing disk and slit size for the spectroscopic observations, and (*c*) is the King model that would prevail if the black hole were absent.

increase would be even more pronounced. (In § VI we shall allow for such effects when fitting models to the data.) The decrease in the line strength $\gamma$ away from the nucleus is also notable. Such an effect was found in NGC 3379 and also in NGC 4473 (Young *et al.* 1978*a*). However, the line strength $\gamma$ shows only a very slight drop as $r \to 0$, in the nuclear regions themselves; for $r < r_c$ we find $\Delta\gamma/\gamma \leq 0.04$. This observation places a limit on the amount of non-thermal blue radiation emitted by the central bright nucleus, this limit being 20% of the light emitted inside the central 1".5 radius (see Young *et al.* 1978*b*).

Figure 5 shows spectra of the nucleus and of the immediately adjacent regions of M87. The slightly greater velocity dispersion of the nucleus (350 km s$^{-1}$ as opposed to 320 km s$^{-1}$ in the other spectra) manifests itself as slightly broader lines. There are slight differences in structure (for example, in the Fe lines around 4700 Å) in the central spectrum, but there is certainly no filling in of the Ca II H and K lines as is observed in the region of the jet.

## V. FURTHER TESTS OF THE FOURIER METHOD

The Fourier method as described and used here was exhaustively tested by SSBS. Their conclusions may be summarized as follows:

1. The Fourier method gave results in agreement with visual techniques involving artificial broadening of the stellar lines.

2. Artificial "galaxy" spectra were obtained by convolving a template star with a Gaussian broadening function. These yielded the correct values for the

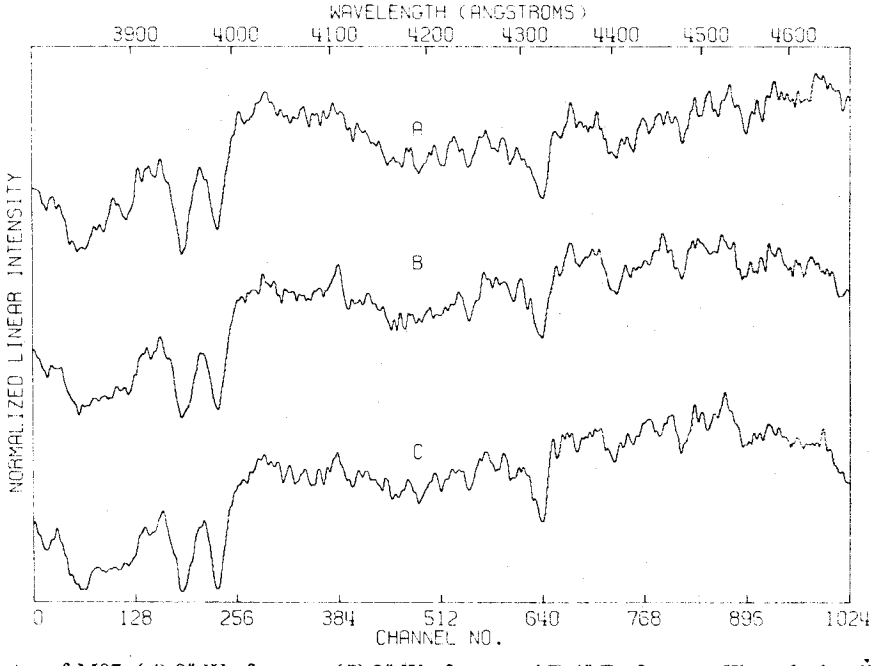


FIG. 5.—IPCS spectra of M87. (*A*) 9″ W of center, (*B*) 2″ W of center, (*C*) 4″ E of center. The velocity dispersions found from Fourier analysis were $\sigma_v = 300$ km s$^{-1}$, 350 km s$^{-1}$, and 325 km s$^{-1}$, respectively; this is in accord with the line widths by visual inspection. The line strengths vary by less than 4% in these three spectra.

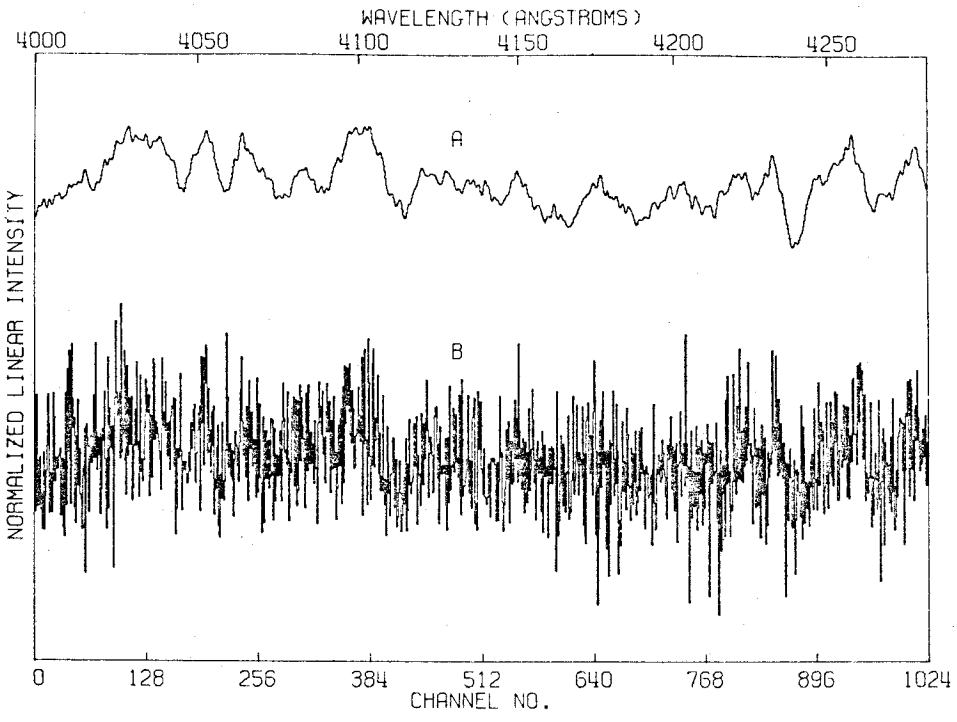


FIG. 6.—(*A*) IPCS spectrum of NGC 3379, (*B*) the same spectrum with the noise level artificially enhanced. The Fourier analysis found velocity dispersions for these two spectra differing by only 2 km s$^{-1}$.

broadening parameters when tested against a second star.

3. Different spectral regions gave the same results for $\sigma_v$.

4. Using composite template spectra (or using M32) did not change the results.

5. Differing regions of Fourier space gave identical results.

In the present work we have extended the use of the Fourier method to the faint, outer parts of galaxies. Accordingly, we have made further tests:

1. The spectra for M87 contain the Ca II H and K lines. Since these are the strongest features and are on the square root part of the curve of growth, changes in metallicity will affect these lines differently from the weaker ones. That this effect is small and does not bias the $\sigma_v$ results has been tested by performing reductions on the spectra excluding the H and K lines. No significant difference was apparent.

2. The effect of differing signal-to-noise ratios in the various spectra was tested by artificially adding noise with a random number generator. Figure 6 shows a (smoothed) test spectrum of NGC 3379 together with a severely degraded version. A succession of such degraded spectra with progressively greater noise was analyzed by the SSBS Fourier method to obtain a series of $cz$, $\gamma$, $\sigma_v$ values. In Figure 7 these are plotted against the effective numbers of photon counts in the galaxy spectrum, $N_G$, required to produce the various noise levels, assuming photon statistics. The results in Figure 7 show that there is no systematic deviation with varying $N_G$, and that the two spectra in Figure 6 yield values of $\sigma_v$ differing by only 2 km s$^{-1}$! All the results in this paper were based on $N_G > 10^5$, and most have $N_G > 3 \times 10^5$.

3. Similar tests were made by adding random noise to template star spectra. Here results are different. The method failed when $N_S$ became $\lesssim 5 \times 10^5$, particularly if the galaxy spectrum was itself rather noisy. This is to be expected since we divide by $\tilde{S}(k)$, the Fourier transform of the star spectrum, and so fluctuations of $\tilde{S}(k)$ toward zero will have a large effect on the ratio $\tilde{G}(k)/\tilde{S}(k)$.

4. The results obtained in tests (2) and (3) lead us to recommend that: (*a*) Template stars should have at least $N_s = 10^6$ counts in the whole spectrum. (*b*) Given high-quality template star spectra, acceptable results for the galaxies can be obtained with $N_G = 10^5$ photons; however, $N_G \gtrsim 3 \times 10^5$ counts is preferable.

5. A central blue "continuum" source may be present in the nucleus of M87 (Young *et al.* 1978*b*). This may be nonthermal synchrotron emission, or merely a cluster of early-type stars. To test whether this would bias the velocity dispersion results, a noisy continuum level was added to selected spectra. The Fourier method successfully extracted the correct $cz$, $\gamma$, and $\sigma_v$ values even when this added continuum was 10 times as big as the galaxy continuum. We are therefore confident that such a blue continuum cannot bias the results for the velocity dispersion near the center of M87.

6. The effects of a contaminating sky spectrum were tested by adding sky and its derivative (to

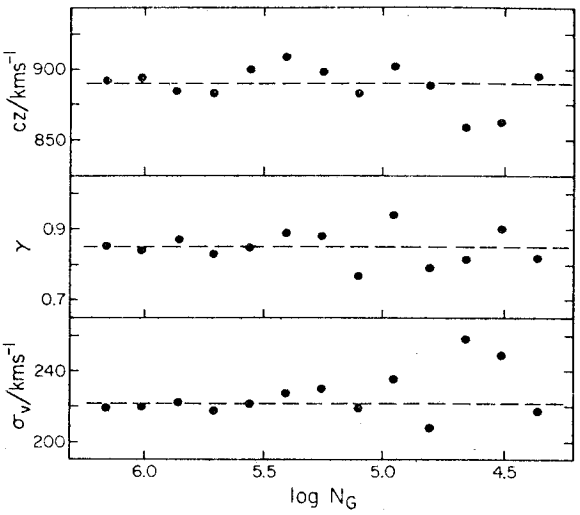


FIG. 7.—Results of tests on an artificially degraded spectrum of NGC 3379. The noise level was enhanced to simulate real data with a total of $N_G$ photons counted in the whole spectrum. The Fourier method was used to find redshifts ($cz$), line strengths ($\gamma$), and velocity dispersions ($\sigma_v$) for this series of spectra. No systematic trend in the results is evident, demonstrating the insensitivity of the method to signal-to-noise ratio.

simulate slightly misbinned sky subtraction) to one of the M87 spectra. Since the sky contains a solar spectrum from zodiacal light at zero redshift and velocity dispersion, it may be expected to affect the Fourier results. As might be guessed, the addition of "sky derivative" had little effect, but the addition of sky had a very serious effect. This was empirically determined to be:

$$\frac{\Delta\sigma_v}{\sigma_v} \sim \frac{3}{2}\left(\frac{\Delta N_s}{N_s}\right)\left(\frac{N_s}{N_G}\right), \qquad (9)$$

where $\Delta\sigma_v$ is the error induced in $\sigma_v$, $(\Delta N_s/N_s)$ is the fractional mis-subtraction of the sky (measured relative to the sky itself, positive for sky, negative for anti-sky) and $(N_s/N_G)$ is the ratio of strength of the sky to that of the galaxy. From equation (9) we see that an error in the sky level of only 20% will perturb $\sigma_v$ by 70 km s$^{-1}$. The effect can go either way, depending on the sign of the error.

Accordingly, we have made considerable efforts to ensure that the sky subtraction is correct; we can guarantee it to $\sim$2% ($\Delta\sigma_v \sim 7$ km s$^{-1}$), having made the following checks: (*a*) The plots of the sky-subtracted galaxy spectra were inspected to ensure that the night-sky emission lines have been correctly removed. (*b*) The various sky frames were subtracted from one another. The photometric stability of the IPCS was checked by scrutiny of the total counts in series of object and sky frames. (*c*) Galaxy and sky frames were cross-correlated to check that no peak was present at the origin.

The check using the night-sky emission lines is not good to better than $\sim$10% but was used to ensure that a gross error had not been made. Inspection of the photometric stability of the counting rates on sky and galaxy suggests expected subtraction errors of $\lesssim$2%. This was the accuracy of the sky intersubtraction tests, further checked using method (*c*). Fortunately the sky subtraction affects only the outermost data points where the sky brightness is comparable with that of the galaxy. Here we have multiple sets of data which are in reasonable agreement with each other. However, the problem with the sky subtraction is the reason for our suspicion of the result obtained from data set 2 (see Table 3).

It is clear from these considerations that velocity dispersion measurements in the outer regions of galaxies must be carried out on dark, photometric nights, and that sky monitoring should be conducted frequently and preferably with a total integration time equal to that spent on the galaxy.

7. The correlation coefficient between the parameters $cz$, $\gamma$, and $\sigma_v$ were typically found to be $r(cz, \gamma) = 10^{-8}$, $r(cz, \sigma_v) = 10^{-8}$, and $r(\gamma, \sigma_v) = 0.4$. As might be expected, there is a positive correlation between the values of $\gamma$ and $\sigma_v$; this is visible in Figure 7. A fall in the determined value of $\sigma_v$ is usually accompanied by a fall in $\gamma$. On these grounds one might suspect the data for the outer regions of NGC 3379 and M87 where $\sigma_v$ and $\gamma$ both decrease. However, the effect would have to be of the order $|\Delta\sigma_v/\sigma_v| \sim 0.25$ in both of the data points for M87 at $r \sim 70''$. We consider this unlikely in view of the evidence of Figure 1 and the stability of the Fourier method which we have demonstrated in the previous sections.

## VI. COMPARISON WITH MODELS

We have used the data in Table 3 on the radial variation of $\sigma_v$ in order to calculate the mass distributions in the two galaxies. We find that in the case of NGC 3379 a theoretical model from the family calculated by King (1966) fits both the photometric data and the dynamical observations reasonably well. However, in the case of M87 a simple theoretical model does not give a satisfactory fit to the data. Consequently, for M87 we have devised a procedure to obtain the mass distribution which is model independent. This will be described in § VII. We first consider the model fits to the two galaxies.

### *a) NGC 3379*

The photometric profile of NGC 3379 is adequately fitted by a King model with $\log r_T/r_c = 2.20$, although there may be a central spike detectable only by deconvolution of the seeing effects (de Vaucouleurs and Capaccioli 1978). The core radius is $r_c = 2''.8 = 109\delta_8$ pc. In Figure 2 we have plotted the predicted variation of $\sigma_v$ with radius according to this model; it would seem adequate to explain the slight fall in $\sigma_v$ out to $r = 14''$. This fit suggests that $M/\mathscr{L}$ will be constant for $r \leq 14''$, a question to be examined in more detail in § VIII.

Using the photometric data of Kormendy (1977) and Young *et al.* (1978*c*), we find a central surface

brightness of $\mu_V = 15.85 \pm 0.02$ mag arcsec$^{-2}$ and a core radius $r_c = 2''.8 \pm 0''.3 = (109 \pm 12)\,\delta_8$ pc. Correcting for a galactic absorption of $A_V = 0.14$, we find a projected central luminosity $L_c = (1.9 \pm 0.1) \times 10^4\,L_\odot$ pc$^{-2}$, and a central luminosity $L_\odot = (186 \pm 10)\,\delta_8^{-1}\,L_\odot$ pc$^{-3}$. Taking $\sigma_v = 195 \pm 17$ km s$^{-1}$, the central density $\rho_0 = 9\sigma_v^2/4\pi G r_c^2 = (515 \pm 105)\,\delta_8^{-2}\,M_\odot$ pc$^{-3}$. The central mass-to-light ratio is then $M/\mathscr{L} = (6 \pm 1)\,\delta_8^{-1}$.

### b) *M87*

The photometric profile of the outer regions ($20'' < r < 5'$) of M87 may be fitted by a King model with $\log r_T/r_c = 2.10$; however, the center is grossly deviant, with a steep starlike "cusp" (Young *et al.* 1978*b*). An additional blue source exists for $r < 1''.5$. Figure 4 shows that the velocity dispersion data are also inconsistent with any sort of King or isothermal model since there is a sharp central spike inside the core radius. The CCD photometric data of Young *et al.* (1978*b*) has been fitted with a King model containing a central black hole. Parameters of the fit are found to be:

Galaxy core radius:

$$r_c = 9''.6 \pm 0''.5 = (698 \pm 36)\delta_{15}\ \text{pc},$$

Core surface brightness:

$$\mu_V = 17.20 \pm 0.02\ \text{mag arcsec}^{-2}.$$

On correcting for a galactic absorption of $A_V = 0.14$ mag, we find

Core surface luminosity:

$$L_c = (5.5 \pm 0.1) \times 10^3\,L_\odot\,\text{pc}^{-2}$$

Core space luminosity:

$$L_0 = (4.0 \pm 0.2)\delta_{15}^{-1}\,L_\odot\,\text{pc}^{-3},$$

Core space density: $\rho_0 = (26 \pm 3)\delta_{15}^{-2}\,M_\odot\,\text{pc}^{-3}$,

Mass-luminosity ratio of central stellar population:

$$M/\mathscr{L} = (6.5 \pm 0.6)\delta_{15}^{-1}.$$

The "core" parameters given above are not those for an isothermal sphere fit since, as we mentioned above, this model does not agree with the observed profile. Rather they are parameters representing the fit of the black hole model and are the values pertinent to the isothermal model that results if the black hole is not present. The value of $M/\mathscr{L}$ is surprisingly small; this is due mainly to the fact that our value of $\sigma_v$ is down by a factor of 2 on older values. The black hole mass fitted by Young *et al.* (1978*b*) is $M_H = (2.6 \pm 0.5) \times 10^9\,M_\odot$. We have fitted the expected velocity dispersion from this model to the data points in Figure 4, where we see that the agreement is satisfactory. We discuss the presence of a central mass further in § VIII.

## VII. THE MASS DISTRIBUTION IN THE CENTER OF M87

### a) *Further Analysis of* $\sigma_v(r)$

It is possible to deduce the mass distribution in M87 on quite general principles which do not depend on fitting specific models. By taking the first moment of the spherical, collisionless Boltzmann equation it is easy to show that:

$$\frac{d}{dr}\left[\rho_*(r)\sigma_v^2(r)\right] = -\frac{GM(r)}{r^2}\,\rho_*(r), \qquad (10)$$

where $\rho_*(r)$ is the density of the stars which give rise to the observed luminosity and $\sigma_v(r)$, as before, is the radial component of the velocity dispersion of these same stars. In deriving equation (10) it is assumed that $\sigma_v$ is isotropic. $M(r)$ refers to the *total* mass inside radius $r$, not just the mass of the stellar population which radiates the observed light. Equation (10) can easily be transformed into the following expression for $M(r)$:

$$M(r) = \frac{r\sigma_v^2(r)}{G} \times \left[-\frac{d\ln L_*}{d\ln r} - \frac{d\ln (M/\mathscr{L})_*}{d\ln r} - \frac{d\ln \sigma_v^2}{d\ln r}\right], \qquad (11)$$

where $L_*(r)$ and $(M/\mathscr{L})_*(r)$ are respectively the luminosity density and the mass-to-light ratio of the visible stars at radius $r$. The innermost measurement of $\sigma_v$ is 350 km s$^{-1}$ at a radius $r = 1''.5 \equiv 110\delta_{15}$ pc from the center of M87. In fact, this value for the central $\sigma_v$ is too low; it has to be corrected for the contribution from stars in the line of sight in the outer parts of the galaxy. This correction was made by fitting a polynomial function to the observed radial distribution of $\sigma_v$ and then inverting the appropriate Abel integral. The resulting corrected $\sigma_v = 400$ km s$^{-1}$ was found to be insensitive to the precise polynomial fit. Consequently, we find for the total mass inside $r = 1''.5$:

$$M(1''.5) = 4 \times 10^9\left[-\frac{d\ln L_*}{d\ln r} - \frac{d\ln (M/L)_*}{d\ln r} - \frac{d\ln \sigma_v^2}{d\ln r}\right] M_\odot. \qquad (12)$$

In the centers of normal galaxies, which may be represented by isothermal spheres, the logarithmic derivative terms are small or vanish altogether. [Note that near the origin in an isothermal sphere the main term is $(d\ln L_*/d\ln r) \sim -3(r/r_c)^2$; this has the correct behavior at the origin.] In M87, however, the behavior is quite different: by fitting smooth curves through the data we find $(-d\ln \sigma_v^2/d\ln r) = 0.6 \pm 0.3$ and $(-d\ln L_*/d\ln r) = 1.0 \pm 0.1$. The logarithmic derivative of $\sigma_v^2$ is rather uncertain because of observational scatter, but in any case it is clear that

$(-d \ln \sigma_v^2/d \ln r) > 0$. The value of $(d \ln L_*/d \ln r)$, obtained by correcting the photometric data of Young *et al.* (1978*b*) for projection effects inside the galaxy, is well determined. We recall that there is little evidence, either from broad-band colors or from the behavior of the line strength index $\gamma$, for changes in the stellar population in the central regions of M87. For this reason we can neglect the term $[d \ln (M/L)_*/d \ln r]$ in equation (12). We then find $M(r < 1''.5) = (6.5 \pm 1.5) \times 10^9 \delta_{15}\, M_\odot$. Most of the uncertainty in this value lies in the term $(d \ln \sigma_v^2/d \ln r)$ in equation (12). From the photometry we find the total luminosity emitted by the central 1".5 radius to be $V = 14.71 \pm 0.03$ mag. After correction for Galactic absorption $A_v = 0.14$ mag, the total luminosity $\mathscr{L}_P(1''.5) = (2.8 \pm 0.1) \times 10^8 \delta_{15}^2\, L_\odot$. Allowing for projection effects through M87, we find the total brightness inside a sphere of radius 1".5 to be $V = 15.73 \pm 0.07$ mag. Consequently, the luminosity density in the $V$ band is $\mathscr{L}_S(1''.5) = (11.2 \pm 0.8) \times 10^7 \delta_{15}^2\, L_\odot$. Combining this with our earlier mass estimate, we find that the average mass-to-light ratio inside 1".5 is $\langle M/\mathscr{L} \rangle (r < 1''.5) = 58 \pm 16 \delta_{15}^{-1}$ solar units.

We recall that the analysis in § VI led to a value $M/\mathscr{L} \sim 6$ for the stellar population near the center ($r \sim 10''$) of M87. The central value of $M/\mathscr{L}$ is a factor of 10 higher than this and strongly suggests that the nucleus of M87 contains a large, dark central mass. In § VIII we shall return to this point when we calculate the integrated mass-to-light ratio inside $r$, $\langle M/\mathscr{L} \rangle (r)$, as a function of radius.

### *b) λ3727 Emission as a Probe of the Central Mass*

In Figure 8 we display the [O II] λ3727 emission doublet observed in data set 5 of Table 1. The profile agrees with that observed by Walker and Hayes (1967), and we find widths (after correcting for the instrumental resolution) FWHM [O II] = 600 km s$^{-1}$, FWZI [O II] = 1500 km s$^{-1}$. Furthermore, we have determined the emission redshift to be $cz_{em} = 1144 \pm 20$ km s$^{-1}$, which gives a discrepancy $cz_{ab} - cz_{em} = 143 \pm 30$ km s$^{-1}$. A similar discrepancy was noted by Humason (quoted in Baade and Minkowski 1954), by Minkowski (1959), and by Walker and Hayes (1967). The latter authors found $cz_{ab} - cz_{em} = 210$ km s$^{-1}$; however, they took the wavelength of the emission peak which, with their line profile, is ~80 km s$^{-1}$ shortward of the center of luminosity (which we have used).

Walker and Hayes described the structure of the [O II] clouds to consist of (*a*) a broad component contained within the seeing disk ($r \sim 1''$), and (*b*) narrower features protruding out to $r \sim 4''$. Because of their asymmetric profiles, it is likely that the broadening mechanism is simply mass motions of the gas clouds.

We appreciate the dangers of associating the broad lines with gas clouds swirling around a massive object, especially in view of the possibility of ejection or infall. We note, however, that the narrow component has FWHM = 600 km s$^{-1}$, corresponding to $\sigma = 260$ km s$^{-1}$ at $r \sim 3''$. This is roughly equal to the velocity dispersion found for the stellar population ($\sigma_v = 300$ km s$^{-1}$) at the same radius. Moreover, the broad component inside $r = 1''$ indicates a central mass $M_N = v^2 r/G = 9.2 \times 10^9 (r_c/1'') \delta_{15}\, M_\odot$, where we have adopted a Keplerian velocity equal to half the FWZI velocity, and $r_c$ is the (unknown) distance of the cloud structures from the center of M87.

In summary, the widths of both components of the λ3727 emission line are entirely consistent with the

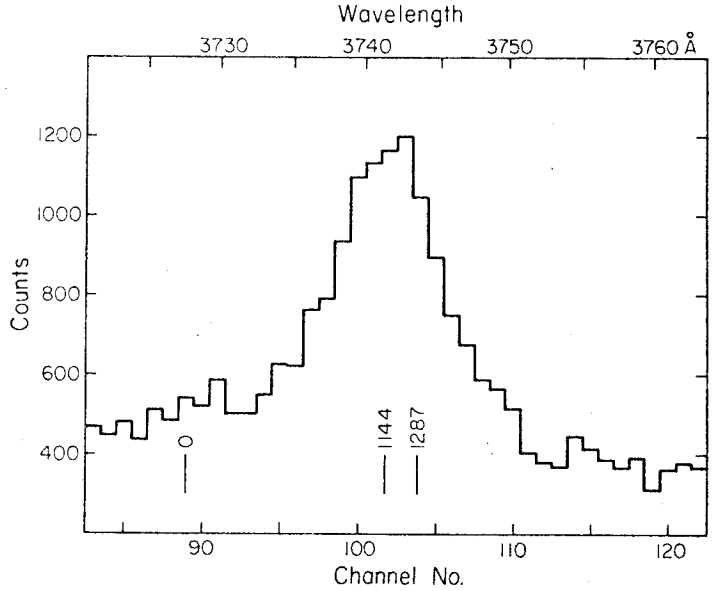


FIG. 8.—The [O II] λ3727 doublet in the nucleus of M87. The vertical markers give the rest wavelength ($v = 0$ km s$^{-1}$), the redshift of the center of luminosity of the [O II] lines ($v = 1144$ km s$^{-1}$), and the stellar absorption redshift of M87 ($v = 1287$ km s$^{-1}$).

hypothesis that the emitting gas is contained by a central mass of the order of that found from our earlier considerations.

### VIII. DETERMINATION OF $\langle M/\mathscr{L}\rangle$ AS A FUNCTION OF RADIUS

To solve the problem of the determination of $(M/\mathscr{L})(r)$, we consider the equation of stellar hydrodynamics,

$$\frac{d}{dr}[\rho(r)\sigma_v^2(r)] = \frac{4\pi G\rho(r)}{r^2}\int_0^r s^2\rho(s)ds\,, \qquad (13)$$

where $\sigma_v^2(r)$ is a given, observed function of $r$. (Note that we have again assumed isotropy of $\sigma_v$ and spherical symmetry for the galaxy.) This equation can be solved in principle to give $\rho(r)$, given $\sigma_v(r)$. The luminosity profile $L(r)$ can be determined from the surface photometry; the ratio $\rho(r)/L(r)$ then gives $(M/\mathscr{L})(r)$. In practice, the data for $\sigma_v(r)$ are subject to a scatter of about 10%. The solution of equation (13) ultimately involves differentiating an empirical function and is therefore impracticable. Instead, we shall adopt an integral approach which determines the mean $M/\mathscr{L}$ contained within a given radius, denoted $\langle M/\mathscr{L}\rangle(r)$. This method is less sensitive to the errors but is adequate to detect changes by a factor of 2 in $M/\mathscr{L}$. We compute:

$$M(r) = \frac{r\sigma_v^2(r)}{G}\left[-\frac{d\ln L}{d\ln r} - \frac{d\ln\sigma_v^2}{d\ln r}\right], \qquad (14)$$

which again neglects the (probably small) logarithmic derivative $[d\ln(M/\mathscr{L})/d\ln r]$. Even if this derivative is of order unity, it will still be outweighed by the term $(d\ln L/d\ln r)$ which is typically $-2.3$. The derivative $(d\ln\sigma_v^2/d\ln r)$ is found by fitting a smooth curve through the $\sigma_v$ data points. This will not lead to particularly reliable values because of scatter in the data points, but again we note that this is not critical because $(d\ln L/d\ln r)$ dominates equation (14). This last derivative may be obtained accurately by correcting the surface photometry for projection effects through the galaxy. Our equation for $M(r)$ has the merit that all quantities are locally determined, so that errors at one point $r$ do not propagate catastrophically as they would in solving equation (13) directly. Having obtained $M(r)$, we compute from the photometry

$$\mathscr{L}(r) = 4\pi\int_0^r L(s)s^2ds\,, \qquad (15)$$

and so obtain the ratio $\langle M/\mathscr{L}\rangle(r) = M(r)/\mathscr{L}(r)$.

We first apply this procedure to NGC 3379. The relevant quantities are listed in Table 4 and the results illustrated in Figure 9. As might be expected from the fact that a King model with constant $M/\mathscr{L}$ fits the data, there are no significant radial variations in $\langle M/\mathscr{L}\rangle$.

A similar procedure applied to M87 yields dramatically different results, as may be seen by inspection of Table 5 and Figure 10. The large nuclear mass discussed in §§ VI and VII produces an increase in $\langle M/\mathscr{L}\rangle(r)$ for $r < 10''$ up to a central value of $\langle M/\mathscr{L}\rangle \sim 60$. Outside $r = 10''$, the $\langle M/\mathscr{L}\rangle$ values

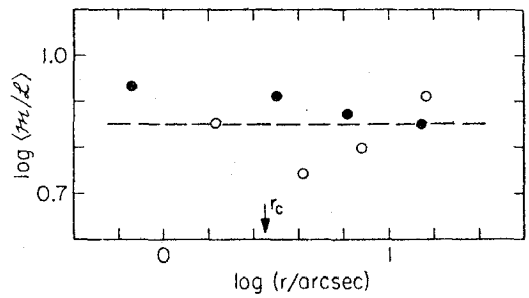


FIG. 9.—Mean mass-luminosity ratio enclosed within radius $r$ [$\langle M/\mathscr{L}\rangle(r)$] as a function of $r$ in NGC 3379. Open circles (○) are to the S, and filled circles (●) are to the N of the center. The core radius of the galaxy, $r_c = 2''.8$, is marked.

TABLE 4

RADIAL DEPENDENCE OF $(M/\mathscr{L})$ FOR NGC 3379

| Radius (arcsec) | $\sigma_v$ (observed) (km s$^{-1}$) | $\sigma_v$† (deprojected) (km s$^{-1}$) | $\frac{d\ln\sigma_v^2}{d\ln r}$† | $\frac{d\ln L(r)}{d\ln r}$* | $\frac{M(r)}{10^8\,M_\odot}$ | $\frac{\mathscr{L}(r)}{10^8\,L_\odot}$* | $\langle M/\mathscr{L}\rangle(r)$ |
|---|---|---|---|---|---|---|---|
| 0.7 | 223 | 225 | -0.00 | -0.18 | 0.49 | 0.057 | 8.6 |
| 1.7 | 206 | 209 | -0.01 | -0.80 | 4.5 | 0.65 | 6.9 |
| 3.1 | 214 | 218 | -0.03 | -1.75 | 20 | 2.5 | 7.9 |
| 4.1 | 181 | 186 | -0.05 | -2.18 | 22 | 4.1 | 5.3 |
| 6.5 | 200 | 207 | -0.09 | -2.47 | 54 | 7.4 | 7.3 |
| 7.4 | 188 | 196 | -0.12 | -2.56 | 53 | 8.7 | 6.1 |
| 13.9 | 174 | 186 | -0.26 | -2.56 | 103 | 15.0 | 6.9 |
| 14.2 | 189 | 202 | -0.26 | -2.56 | 124 | 15.5 | 8.0 |

*Obtained from photometry by Kormendy (1977), and Young et al. (1978c).

†Obtained by fitting a smooth curve through the data points in Table 3.

TABLE 5

RADIAL DEPENDENCE OF $(M/\mathscr{L})$ FOR M87

| Radius (arcsec) | $\sigma_v$ (observed) (km s$^{-1}$) | $\sigma_v$† (deprojected) (km s$^{-1}$) | $\frac{d \ln \sigma_v^2}{d \ln r}$† | $\frac{d \ln L(r)}{d \ln r}$* | $\frac{M(r)}{10^{10}\ M_\odot}$ | $\frac{\mathscr{L}(r)}{10^{10}\ L_\odot}$* | $\langle M/\mathscr{L} \rangle(r)$ |
|---|---|---|---|---|---|---|---|
| 1.6 | 329 | 395 | -0.62 | -1.01 | 0.66 | 0.011 | 60 |
| 2.2 | 362 | 423 | -0.50 | -0.94 | 0.94 | 0.015 | 63 |
| 3.2 | 321 | 360 | -0.40 | -0.87 | 0.86 | 0.029 | 30 |
| 3.8 | 333 | 367 | -0.36 | -0.88 | 1.04 | 0.040 | 26 |
| 9.2 | 295 | 310 | -0.26 | -1.43 | 2.45 | 0.22 | 11.1 |
| 9.7 | 301 | 317 | -0.25 | -1.45 | 2.72 | 0.24 | 11.3 |
| 9.7 | 286 | 301 | -0.25 | -1.45 | 2.45 | 0.24 | 10.2 |
| 11.3 | 275 | 287 | -0.25 | -1.66 | 2.92 | 0.32 | 9.1 |
| 22.1 | 260 | 269 | -0.09 | -2.27 | 6.20 | 0.92 | 6.7 |
| 22.7 | 280 | 290 | -0.09 | -2.27 | 7.40 | 0.93 | 7.9 |
| 24.3 | 287 | 297 | -0.10 | -2.28 | 8.37 | 1.0 | 8.1 |
| 41.6 | 268 | 283 | -0.18 | -2.29 | 13.5 | 1.9 | 7.2 |
| 62.6 | 258 | 276 | -0.29 | -2.30 | 20.3 | 2.7 | 7.4 |
| 69.7 | 189 | 203 | -0.33 | -2.30 | 12.4 | 3.0 | 4.2 |
| 71.8 | 232 | 250 | -0.35 | -2.30 | 19.5 | 3.1 | 6.4 |

*Obtained from CCD photometry by Young et al. (1978b).

†Obtained by fitting a smooth curve to the data points of Table 3 and Figure 4.

are roughly those found earlier for the stellar population in M87 (with $M/\mathscr{L} = 6$). Since a King model with $M/\mathscr{L}$ = constant fits the data for the outer regions of M87, we do not expect any significant rise in $M/\mathscr{L}$ at large radii; this expectation is confirmed in Figure 10.

We have found no evidence for an increase in $M/\mathscr{L}$ at large radii, and thus no evidence for massive halos, in NGC 3379 and M87. However, we note that the observations for NGC 3379 and M87 only extend to 5 and 7 core radii, respectively. We were successful in detecting an increase in $M/\mathscr{L}$ at large radii in the elliptical galaxy NGC 4473 (Young *et al.* 1978*a*) where observations extended to 14 core radii. Now the equation of hydrostatic equilibrium has the power law solution:

$$\rho = \rho_0 \left(\frac{r_0}{r}\right)^{k+2};$$

$$\sigma_v^2(r) = \frac{2\pi}{1-k^2} G\rho_0 r_0^2 \left(\frac{r_0}{r}\right)^k \quad (|k| < 1). \qquad (16)$$

Since the luminosity profile $L(r)$ has a typical gradient $(d \ln L/d \ln r) = -2.30$ in the outer regions of a galaxy, an observation that $k = -(d \ln \sigma_v^2/d \ln r) < 0.3$ would suggest that $M/\mathscr{L}$ ultimately increases with radius.

## IX. CONCLUSIONS

### *a) Summary of the Measurements*

We have used the IPCS detector working in a fully two-dimensional mode in order to determine the radial variation of radial velocity $cz$, line strength $\gamma$, and velocity dispersion $\sigma_v$ in the elliptical galaxies M87 and NGC 3379. Values of these parameters were derived from the observed spectra by an application of the Fourier method described by SSBS. The main conclusions are as follows:

1. NGC 3379 exhibits a slight rotation from observations made in P.A. 0° (the major axis is at P.A. 68°). The semiamplitude is $4.0 \pm 1.3$ km s$^{-1}$ arcsec$^{-1}$ when corrected to the major axis. The line strength and $\sigma_v$ decrease slightly with increasing radius.

2. The mean photometric profile of NGC 3379 and the measurements of $\sigma_v$ (observed out to $r = 14''$) are both adequately fitted by a King (1966) model with $\log r_T/r_c = 2.20$ and $M/\mathscr{L} = (6 \pm 1)(\Delta_{\rm Mpc}/8)^{-1}$, where $\Delta_{\rm Mpc}$ is the distance in Mpc. Overall, there is no evidence in NGC 3379 for an increase in $M/\mathscr{L}$ with radius. However, the observations extend out to only 5 core radii.

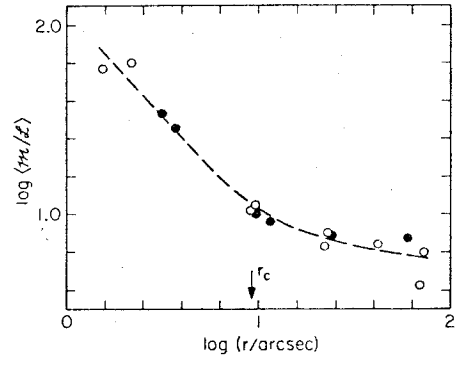


FIG. 10.—Mean mass-luminosity ratio enclosed within radius $r$ [$\langle M/\mathscr{L} \rangle(r)$] as a function of $r$ in M87. Open circles (○) are to the W of the nucleus, and filled circles (●) are to the E. The core radius of the galaxy, $r_c = 9''.6$, is marked.

3. In M87 the amplitude of any rotation is less than 10 km s$^{-1}$ along an E-W axis for $r \leq 72''$. The line strength index is sensibly constant inside the core radius $r_c = 9''.6$, but then falls off with increasing radius. The velocity dispersion shows a complex behavior; $\sigma_v$ rises slowly from about 220 km s$^{-1}$ at $r = 72''$ to $\sigma_v = 280$ km s$^{-1}$ at $r = r_c$. It then rises rapidly with decreasing $r$, reaching a maximum measured value of $\sigma_v = 350$ km s$^{-1}$ at $r = 1''.5$.

4. The photometric profile and the radial run of $\sigma_v$ in M87 are adequately fitted by a King model with $\log r_T/r_c = 2.10$ for $20'' < r < 72''$. The value of $M/\mathscr{L}$ in these outer regions is $6.5 \pm 0.6\,(\Delta_{\rm Mpc}/15)^{-1}$ solar units, where $\Delta_{\rm Mpc}$ is the distance in Mpc. As in the case of NGC 3379, there is no evidence from our data for an increase in $M/\mathscr{L}$ with increasing radius in M87.

5. The sharp increase in $\sigma_v$ inside the core radius in M87, combined with the photometric data of Young *et al.* (1978*b*), leads to the conclusion that $\langle M/\mathscr{L}\rangle$ increases rapidly as $r \to 0$. We showed quantitatively in §§ VI, VII, and VIII, by different approaches, that the value of $M/\mathscr{L}$ in the central $1''.5$ radius is about 60 solar units, despite the fact that the quality of the stellar population (as indicated by the line strength index $\gamma$) remains sensibly constant with radius. The data imply that M87 contains a central, dark mass of about $5 \times 10^9\ M_\odot$ inside $r = 110\delta_{15}$ pc.

### *b) Discussion*

In their outer regions the two galaxies M87 and NGC 3379 behave quite similarly. The photometric and dynamical measurements are consistent with King models and there is no sign of a massive halo in the form of a gradual outward increase in $M/\mathscr{L}$. In both galaxies our elaborate measurements and methods of analysis have led to a lower value for the mass-to-light ratio ($M/\mathscr{L} \sim 6$) than has been obtained in less complete studies of elliptical galaxies.

In their central regions M87 and NGC 3379 exhibit quite different properties. In the case of NGC 3379 the data are fitted tolerably by the same King model which fits the outer regions. In M87 an additional dark central mass must be added to the King model. We estimated that $5 \times 10^9\ M_\odot$ must be concentrated in a volume less than $110\delta_{15}$ pc in radius. It is not possible to prove from our data that this object is a black hole. However, the fact that as we approach the center of M87 the stellar population, as adduced from the spectral lines, does not change its gross character whereas the value of $\langle M/\mathscr{L}\rangle$ rises markedly implies to us that the presence of a central, supermassive black hole must be a serious possibility. It is easy to imagine high-resolution spectroscopic and photometric observations which could be carried out with the Space Telescope to further test this hypothesis.

We are extremely grateful to the many members of the Kitt Peak staff who made the special arrangements required for these observations. We also thank J. Fordham for his assistance with the IPCS. We especially thank Jim Westphal, Jerry Kristian, Chris Wilson, and Fred Landauer for the close cooperation involved in analyzing the M87 data presented in this and the accompanying paper. W. S. thanks the National Science Foundation for support under grant AST 75-00555. The work at University College London was supported by grants from the UK Science Research Council. We also thank Peter Goldreich, Scott Tremaine, and Paul Schechter for invaluable discussions.

## REFERENCES

Baade, W., and Minkowski, R. 1954, *Ap. J.*, **119**, 215.
Bertola, F., and Capaccioli, M. 1975, *Ap. J.*, **200**, 439.
Boksenberg, A., and Sargent, W. L. W. 1975, *Ap. J.*, **198**, 31.
Brandt, J. C., and Roosen, R. G. 1969, *Ap. J. (Letters)*, **156**, L59.
Burbidge, E. M., Burbidge, G. R., and Fish, R. A. 1961, *Ap. J.*, **134**, 251.
Dennison, E. W. 1954, thesis, University of Michigan (unpublished).
de Vaucouleurs, G. 1959, in *Handbuch der Physik*, ed. S. Flügge (Berlin-Götingen-Heidelberg: Springer-Verlag), **53**, 311.
———. 1974, in *IAU Symposium No. 58, The Formation and Dynamics of Galaxies*, ed. J. R. Shakeshaft (Dordrecht: Reidel), p. 1.
———. 1975, in *Stars and Stellar Systems*, Vol. **9**, ed. A. Sandage, M. Sandage, and J. Kristian (Chicago: University of Chicago Press), p. 557.
de Vaucouleurs, G., and Capaccioli, M. 1978, in preparation.
de Vaucouleurs, G., de Vaucouleurs, A., and Corwin, H. G., Jr. 1976, *Second Reference Catalogue of Bright Galaxies* (Austin: University of Texas Press).
Faber, S. M., and Jackson, R. E. 1976, *Ap. J.*, **204**, 668.
King, I. R. 1966, *A.J.*, **71**, 64.
Kormendy, J. 1977, *Ap. J.*, **214**, 359.
Minkowski, R. 1959, in *IAU Symposium No. 9, Paris Symposium on Radio Astronomy*, ed. R. N. Bracewell (Stanford: Stanford University Press), p. 335.
———. 1962, in *IAU Symposium No. 15, Problems of Extragalactic Research*, ed. G. C. McVittie (New York: Macmillan), p. 112.
Sandage, A. R., and Tammann, G. A. 1974, *Ap. J.*, **194**, 559.
Sargent, W. L. W., Schechter, P. L., Boksenberg, A., and Shortridge, K. 1977, *Ap. J.*, **212**, 326 (SSBS).
Walker, M. F., and Hayes, S. 1967, *Ap. J.*, **149**, 481.
Williams, T. B. 1977, *Ap. J.*, **214**, 685.
Young, P. J, Sargent, W. L. W., Boksenberg, A., Lynds, C. R., and Hartwick, F. D. A. 1978*a*, preprint.
Young, P. J, Westphal, J. A., Kristian, J. A., Wilson, C. P., and Landauer, F. 1978*b*, *Ap. J.*, **221**, in press.
———. 1978*c*, in preparation.

A. BOKSENBERG and KEITH SHORTRIDGE: Department of Physics and Astronomy, University College London, Gower Street, London WC1E 6BT, England

F. D. A. HARTWICK: Department of Astronomy, University of Victoria, Victoria V8W 2Y2, B.C., Canada

C. R. LYNDS: Kitt Peak National Observatory, P.O. Box 26732, Tucson, AZ 85726

W. L. W. SARGENT and PETER YOUNG: Department of Astronomy 105-24, California Institute of Technology, Pasadena, CA 91125

THE ASTROPHYSICAL JOURNAL, 222:450–455, 1978 June 1


# DYNAMICS OF THE FLATTENED ELLIPTICAL GALAXY NGC 4473

PETER YOUNG AND W. L. W. SARGENT*
Hale Observatories, California Institute of Technology, Carnegie Institution of Washington
A. BOKSENBERG*
Department of Physics and Astronomy, University College London
C. R. LYNDS
Kitt Peak National Observatory
AND
F. D. A. HARTWICK*
Department of Astronomy, University of Victoria
*Received 1977 September 12; accepted 1977 December 8*

## ABSTRACT

Spectroscopic observations of the E5 galaxy NGC 4473 to a distance of 45″ (=3300 pc) from the center along the major axis are used to make the first estimates of the radial variation of rotation and velocity dispersion in a galaxy away from the regions of the core. Analysis with Fourier techniques shows the rotation curve to have an observed semiamplitude of 60 km s$^{-1}$ (or 86 km s$^{-1}$ when corrected for projection). The velocity dispersion $\sigma_v$ = 180 km s$^{-1}$ is constant along the major axis of the galaxy to a distance of 45″, and the line strengths fall by 35%. The kinetic energy ratio $T_{\rm rot}/T_{\rm ran}$ = 0.08 demonstrates that the galaxy is pressure supported.

The mass interior to 3.3 kpc radius is determined to be 4.6 × 10$^{10}$ $M_\odot$, with a density that follows the law $\rho(r) \propto r^{-2}$. The mass to light ratio of the system is $M/L$ = 6; we show that $M/L$ increases slowly with radius; $d \ln (M/L)/d \ln r$ = 0.3.

*Subject headings:* galaxies: internal motions — galaxies: redshifts — stars: stellar dynamics

## I. INTRODUCTION

Most current theoretical models of their formation and structure demand rapid rotation in flattened elliptical galaxies (Larson 1974, 1975; Gott 1973, 1975, 1977; Gott and Thuan 1976; Thuan and Gott 1977; Lynden-Bell 1967; Jones 1976; Prendergast and Tomer 1970; Wilson 1975; Hunter 1977). However, the rotation curve observed in NGC 4697 by Bertola and Capaccioli (1975) showed a velocity semiamplitude of only 60 km s$^{-1}$, with a central velocity dispersion of $\sigma_v$ = 310 km s$^{-1}$ (King and Minkowski 1966). On the assumption that $\sigma_v$ was independent of radius, Bertola and Capaccioli estimated a ratio of energy in rotation to that in random motions $T_{\rm rot}/T_{\rm ran}$ = 0.02, far below the value of 0.30 predicted by the theories.[1] Subsequently, Binney (1976) derived models of elliptical galaxies in which the flattening is not due to rotation.

We have obtained spectra of NGC 4473 (an E5 system in Virgo) with the University College London image photon counting system (IPCS) used in its two-dimensional mode. This type of digital data is particularly suited to the determination of accurate redshifts, velocity dispersions, and line strengths by the Fourier method (Sargent *et al.* 1977, henceforth SSBS). The simultaneous solution for velocity dispersion as well as the rotation curve represents considerable improvement over previous work.

In § II we discuss the data and their reduction; in § III we present the results; in § IV the mass and $M/L$ are derived. The conclusions are summarized in § V.

## II. OBSERVATIONS AND REDUCTIONS

The IPCS (Boksenberg 1972; Boksenberg and Burgess 1973) was used to observe NGC 4473 at the Cassegrain focus of the Kitt Peak 4 m telescope in 1976 April with the "gold" spectrograph. The spectra covered 600 Å spread over 1024 channels and were centered at λ4200. The IPCS was used in a two-dimensional mode to collect 20 scans simultaneously along the slit, which was 1″ wide and 102″ long.

Observations were made with the slit oriented along the major axis (P.A. = 90°) of the galaxy. Two comparison stars were also observed: HR 5709 (K0 III) and an anonymous, faint, K-giant star at 12$^h$28$^m$0, +12°46′ (1950.0). A 5 mag neutral density filter was used to reduce the counting rate for HR 5709. A journal of observations is given in Table 1. Exposures on the galaxy were interlaced with observations of the sky (1° N and 1° S of NGC 4473) and an inert gas comparison arc containing He, Ne, Ar, and Kr. The

* Guest Investigator, Kitt Peak National Observatory, which is operated by the Association of Universities for Research in Astronomy, Inc., under contract with the National Science Foundation.

[1] Illingworth (1977) has recently found that Bertola and Capaccioli's result applies quite generally to flattened elliptical galaxies; Illingworth also used only the central velocity dispersion in reaching his conclusion.

TABLE 1

NGC 4473 DATA PARAMETERS*

| Data Set | Object | Slit† Position | Time on Object (s) | Time on Sky (s) | Total Counts ($N/10^5$) |
|---|---|---|---|---|---|
| 1..... | NGC 4473 | 0 | 10000 | 3600 | 82.2 |
| 1*a*‡..... | NGC 4473 | 0 | 4000 | 1200 | 32.4 |
| 1*b*‡..... | NGC 4473 | 0 | 6000 | 2400 | 49.8 |
| 2..... | NGC 4473 | 41″ W | 3300 | 1650 | 22.8 |
| 3..... | HR 5709 | 0 | 1300 | ... | 19.6 |
| 4..... | Star 1228+12 | 0 | 1427 | ... | 2.8 |

* After rebinning to log $\lambda$ scale.

† Position of center of slit relative to star or galaxy nucleus.

‡ For the purpose of determining the rotation curve, data set 1 was broken down into 1*a* and 1*b*.

slit width was chosen to subtend two channels, or 1.2 Å, on the detector. However, the actual resolution, determined from the arc lines, was 2.3 Å full width at half-maximum, which corresponds to 170 km s$^{-1}$.

Two-dimensional cubic polynomial fits to the arc frames were used to establish the wavelength scale and to rebin the sky-subtracted data to a logarithmic scale at intervals of $\Delta \ln \lambda = -1.33 \times 10^{-4}$ ($=40$ km s$^{-1}$). The data reduction procedures are discussed at greater length in a paper on similar observations of NGC 3379 and M87 (Sargent *et al.* 1978). The Fourier method (SSBS) was employed to determine the redshift $cz$, the velocity dispersion $\sigma_v$, and the line strength parameter $\gamma$ as a function of radius. Since the determination of a velocity dispersion requires higher-quality data (i.e., more photons) than does the determination of a redshift, the observations were divided up in two different ways. Tables 1 and 2 illustrate the data blocks used to determine $\sigma_v$ and $\gamma$, and Tables 1 and 3 show the data blocks used to find $cz$. Exhaustive tests on the Fourier method have been conducted and are detailed in the paper on NGC 3379 and M87.

## III. THE RESULTS

The results—given in Tables 2 and 3, and depicted in Figures 1, 2, and 3—are the mean of the parameters obtained from the two comparison stars, with double weight given to HR 5709 (since the quality of the spectrum was superior). Errors shown in the diagrams and tables are $\pm 2\,\sigma$.

In Figure 1 we have plotted the $\sigma_v$ and $\gamma$ values in logarithmic radius coordinates. It is clear that $\sigma_v(r)$ is a constant ($\Delta\sigma_v < 6$ km s$^{-1}$) for $r < 45''$. The line strength parameter contrasts with this by a sharp decrease for $r > 8''$, possibly indicative of a fall in metallicity away from the center of NGC 4473.

TABLE 2

LINE STRENGTHS AND VELOCITY DISPERSION FOR NGC 4473

| Data Set from Table 1 | Scan Blocks | $N_G/10^5$ | $\langle r'' \rangle$* | $\gamma$†‡ | $\sigma_v$‡ (km s$^{-1}$) |
|---|---|---|---|---|---|
| 1..... | 1–5 | 3.2 | −39.5 | 0.81 ± 0.05 | 196 ± 19 |
| 1..... | 6–7 | 3.8 | −21.2 | 0.92 ± 0.04 | 209 ± 16 |
| 1..... | 8 | 4.4 | −13.0 | 0.97 ± 0.04 | 193 ± 12 |
| 1..... | 9 | 11.8 | −7.1 | 1.09 ± 0.04 | 185 ± 9 |
| 1..... | 10 | 25.5 | −1.2 | 1.16 ± 0.04 | 195 ± 8 |
| 1..... | 11 | 18.3 | +4.7 | 1.07 ± 0.04 | 188 ± 9 |
| 1..... | 12 | 6.3 | +10.6 | 0.88 ± 0.04 | 181 ± 13 |
| 1..... | 13–14 | 4.4 | +18.9 | 0.77 ± 0.04 | 171 ± 14 |
| 1..... | 15–20 | 3.8 | +38.9 | 0.80 ± 0.05 | 193 ± 19 |
| 2..... | 1–13 | 1.2 | −44.8 | 0.71 ± 0.06 | 180 ± 33 |
| 2..... | 14–15 | 2.4 | −14.8 | 1.02 ± 0.05 | 192 ± 16 |
| 2..... | 16 | 4.8 | −4.8 | 1.05 ± 0.04 | 174 ± 13 |
| 2..... | 17 | 8.3 | +1.2 | 1.13 ± 0.04 | 169 ± 10 |
| 2..... | 18 | 4.0 | +7.2 | 1.08 ± 0.04 | 188 ± 13 |
| 2..... | 19–20 | 2.1 | +15.0 | 0.87 ± 0.05 | 177 ± 17 |
| Mean value..... | | | | | 186 ± 10 |

* Along major axis (E-W direction). Positive values are E.

† Normalized such that $\langle\gamma\rangle = 1$ for $r < 30''$.

‡ Errors quoted are $\pm 2\,\sigma$.

TABLE 3

ROTATION CURVE FOR NGC 4473

| Data Set from Table 1 | Scan Blocks | $\frac{N_G}{10^5}$ | ⟨r"⟩* | cz# (km s$^{-1}$) | Δv†# (km s$^{-1}$) |
|---|---|---|---|---|---|
| 1(a) | 1-7 | 2.8 | -29.6 | 2200 ± 17 | -64 ± 17 |
| 1(a) | 8 | 2.0 | -13.0 | 2200 ± 20 | -64 ± 20 |
| 1(a) | 9 | 5.7 | - 7.1 | 2199 ± 16 | -65 ± 16 |
| 1(a) | 10 | 10.3 | - 1.2 | 2246 ± 15 | -18 ± 15 |
| 1(a) | 11 | 6.1 | + 4.7 | 2294 ± 17 | +30 ± 17 |
| 1(a) | 12 | 2.1 | +10.6 | 2334 ± 23 | +70 ± 23 |
| 1(a) | 13 | 1.0 | +16.8 | 2307 ± 27 | +43 ± 27 |
| 1(a) | 14-20 | 2.1 | +40.8 | 2331 ± 18 | +67 ± 18 |
| 1(b) | 1-7 | 4.8 | -30.2 | 2208 ± 28 | -56 ± 28 |
| 1(b) | 8 | 2.4 | -13.6 | 2220 ± 20 | -44 ± 20 |
| 1(b) | 9 | 6.1 | - 7.7 | 2200 ± 15 | -64 ± 15 |
| 1(b) | 10 | 15.2 | - 1.8 | 2252 ± 13 | -12 ± 13 |
| 1(b) | 11 | 12.2 | + 4.1 | 2298 ± 16 | +34 ± 16 |
| 1(b) | 12 | 4.2 | +10.0 | 2316 ± 22 | +52 ± 22 |
| 1(b) | 13 | 1.7 | +16.2 | 2303 ± 23 | +39 ± 23 |
| 1(b) | 14-20 | 3.3 | +40.2 | 2318 ± 21 | +54 ± 21 |
| 2 | 1-13 | 1.2 | -44.8 | 2204 ± 20 | -60 ± 20 |
| 2 | 14 | 0.8 | -16.8 | 2205 ± 31 | -59 ± 31 |
| 2 | 15 | 1.5 | -10.8 | 2219 ± 22 | -45 ± 22 |
| 2 | 16 | 4.8 | - 4.8 | 2210 ± 18 | -54 ± 18 |
| 2 | 17 | 8.3 | + 1.2 | 2301 ± 16 | +37 ± 16 |
| 2 | 18 | 4.0 | + 7.2 | 2307 ± 18 | +43 ± 18 |
| 2 | 19 | 1.4 | +13.2 | 2336 ± 22 | +72 ± 22 |
| 2 | 20 | 0.6 | +19.2 | 2329 ± 25 | +65 ± 25 |
| MEAN VALUE | | | | 2264 ± 15 | |

*Along major axis (EW direction). Positive values are to the E.

†Difference from mean heliocentric redshift cz = 2264 km s$^{-1}$.

#Errors quoted are ± 2σ.

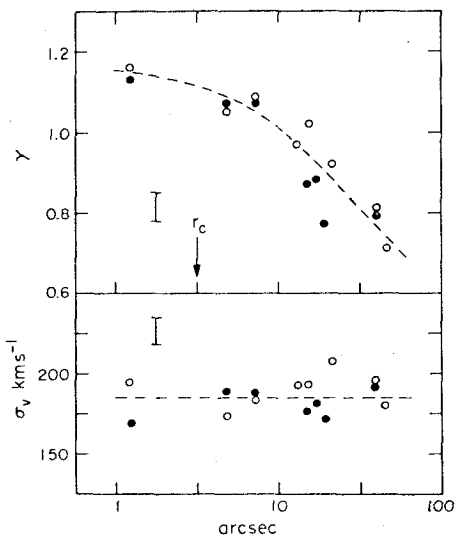


FIG. 1.—The line strength parameter $\gamma$ and velocity dispersion $\sigma_v$ as a function of radius in NGC 4473. Open circles are the W side of the galaxy, and filled circles are the E side. An error bar of length 2 $\sigma$ pertinent to all the points is given. The core radius of the galaxy $r_c$ = 3".3 is marked.

Figure 2 shows spectra taken on each side of the center of NGC 4473 (along the major axis), together with the central spectrum. It is apparent that rotation in this galaxy is small. A progressive increase in redshift going from west to east along the major axis indicates that the west side is approaching and the east side is receding at only 60 km s$^{-1}$ with respect to the center. This result is confirmed in Figure 3 where we show the folded rotation curve, which rises sharply from the origin and is flat from $r$ = 10" to $r$ = 45". The amplitude is only 60 km s$^{-1}$, surprisingly small for an E5 system but similar to that found in NGC 4697 (also E5) by Bertola and Capaccioli (1975).

A summary of the quantitative results is as follows:

i) The central velocity dispersion $\sigma_v = 186 \pm 10$ km s$^{-1}$. There is no detectable change with radius out to 45"; in this interval, $\Delta\sigma_v < 6$ km s$^{-1}$. This is to be compared with the values found for the center of NGC 4473 $\sigma_v = 160 \pm 30$ km s$^{-1}$ by Morton and Chevalier (1973) and $\sigma_v = 110 \pm 20$ km s$^{-1}$ found by Williams (1977). These two results are based on visual methods and thus are probably subject to systematic errors. Our value has been determined by a method which has been exhaustively tested, which has high

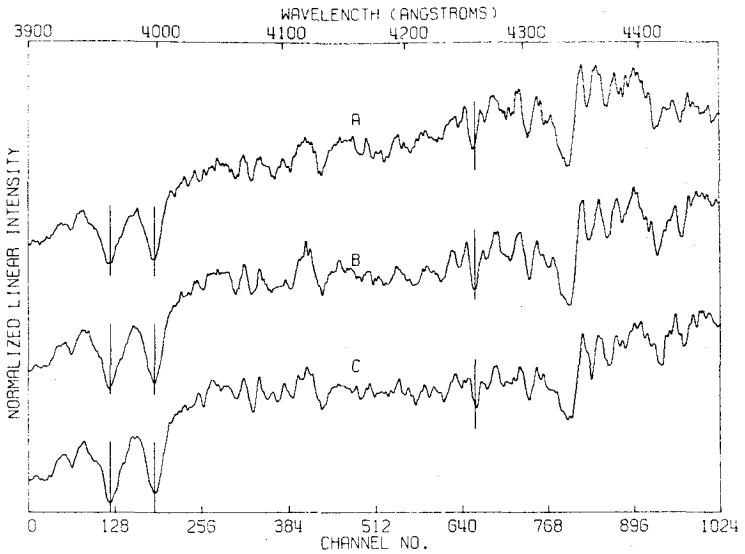


FIG. 2.—IPCS data for NGC 4473. All spectra have been normalized to a maximum of unity. Spectrum A is the data 10″ W of the center of NGC 4473, B is the center, and C is for 10″ E. The vertical markers are at the mean redshift position $cz = 2264$ km s$^{-1}$ of the H and K, and Ca I λ4227 lines.

discrimination, and whose systematic errors are less than ~10%.

ii) The mean heliocentric redshift $cz = 2264 \pm 15$ km s$^{-1}$. Previous values are $2241 \pm 75$ km s$^{-1}$ (de Vaucouleurs and de Vaucouleurs 1964; Humason, Mayall, and Sandage 1956) and $2281 \pm 30$ km s$^{-1}$ (Morton and Chevalier 1973).

iii) The amplitude of the rotation curve $v_\theta = 60 \pm 3$ km s$^{-1}$. This does not agree with the results of Morton and Chevalier (1973), who found $v_\theta = 100$ km s$^{-1}$ at $r = 10''$. We have checked our data and scrutinized the plots; a velocity amplitude as large as 100 km s$^{-1}$ can be ruled out. The rotation velocity in the inner regions was found to be 32 km s$^{-1}$ arcsec$^{-1}$ (Morton and Chevalier 1973). We cannot measure this parameter owing to our spatial resolution along the slit of only 5″.9.

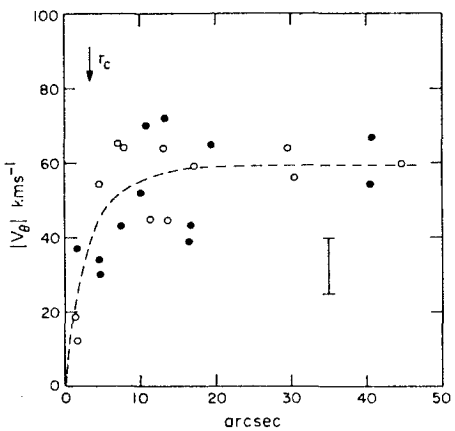


FIG. 3.—Folded rotation curve for NGC 4473. Open circles are the W side of the galaxy, and filled circles are the E side. An error bar of length 2 σ is given which applies to all the points. The core radius of the galaxy $r_c = 3''.3$ is marked.

The amplitude of the rotation curve must be corrected for projection effects. Since the curve is flat, this is a simple operation and yields

$$u_\theta = v_\theta\left(\frac{k-1}{2}\right)\left[\Gamma\left(\frac{k-1}{2}\right)\Big/\Gamma\left(\frac{k}{2}\right)\right]^2,$$

when the luminosity profile $L(r) \propto r^{-k}$ (Γ is the gamma function). In the present region, NGC 4473 follows the $r^{1/4}$ law (de Vaucouleurs 1959; Young *et al.* 1978), so $k = 2.3$ (this is simply the value of the logarithmic derivative $-d \ln L/d \ln r$ in the region of interest). Thus the corrected rotational velocity on the flat part of the rotation curve is $u_\theta = 1.44\, v_\theta = 86 \pm 4$ km s$^{-1}$. Since the rotation is not dynamically important for NGC 4473 (as will be demonstrated in § IV) and since the observed rotation curve is not particularly well-defined, we are not justified in using a full deprojection procedure employing more accurate photometry.

The velocity dispersion values must also be corrected for rotation effects. In the outer regions ($r > 5''$) this is fairly simple, since the rotation curve is flat. For this case, and when the luminosity $L(r) \propto r^{-k}$, we find that the contribution to the observed $\sigma_v{}^{*2}$ due to differential rotation is given by

$$\sigma_R{}^2 = u_\theta{}^2\left\{\left(\frac{k-1}{k}\right) - \left(\frac{2}{k-1}\right)^2\left[\Gamma\left(\frac{k}{2}\right)\Big/\Gamma\left(\frac{k-1}{2}\right)\right]^4\right\},$$

$$\sigma_v{}^{*2} = \sigma_v{}^2 + \sigma_R{}^2,$$

where $\sigma_v$ is the stellar velocity dispersion. The formula for $\sigma_R{}^2$ is derived by taking a luminosity-weighted value of $\langle v^2 \rangle$ due to rotation along a line of sight in the

galaxy and then setting $\sigma_R^2 = \langle v^2 \rangle - \langle v \rangle^2 = \langle v^2 \rangle - v_\theta^2$. With our values of $k = 2.3$ and $u_\theta = 86$ km s$^{-1}$, we find $\sigma_R = 0.28\, u_\theta = 24$ km s$^{-1}$. The velocity dispersion in the outer regions is then corrected to $\sigma_v = 184 \pm 10$ km s$^{-1}$. For the central value we use the Morton and Chevalier (1973) rotation curve for the inner regions, together with a luminosity profile by Young *et al.* (1978). We find $\sigma_R = 55$ km s$^{-1}$, and thus the central velocity dispersion becomes $\sigma_v(0) = 178 \pm 10$ km s$^{-1}$. In summary, these corrections are small; subsequently, we shall take $\sigma_v = 180 \pm 10$ km s$^{-1}$, independent of $r$.

## IV. DERIVATION OF MASS AND MASS TO LIGHT RATIO

Estimates of the distance to NGC 4473 (in the Virgo cluster) range from $\Delta = 13.6$ Mpc (de Vaucouleurs 1975) to $\Delta = 19.5$ Mpc (Sandage and Tammann 1974). We shall adopt $\Delta = 15$ Mpc and shall give explicitly in the results the dependence on distance through the parameter $\delta_{15} = \Delta/15$, without including this uncertainty in the formal errors. We shall assume, to simplify the analysis, that NGC 4473 (E5) is seen edge-on (the results do not depend critically on the inclination angle).

If we suppose NGC 4473 to be a series of self-similar oblate spheroids with eccentricity $e$ and a density distribution $\rho(a)$ along the major axis $a$, then the equation of hydrostatic equilibrium is

$$\frac{1}{\rho(r)} \frac{d}{dr} [\rho(r)\sigma_v^2(r)] - \frac{u_\theta^2(r)}{r} = -\frac{4\pi G(1 - e^2)^{1/2}}{r} \int_0^r \frac{\rho(a)a^2 da}{(r^2 - a^2e^2)^{1/2}} \tag{1}$$

for points on the major axis, where $u_\theta(r)$ is the rotational velocity and $\sigma_v(r)$ is the velocity dispersion (we have assumed equality of the two dispersions in the equatorial plane while permitting these dispersions to differ from the dispersion perpendicular to the plane). Since $u_\theta$ and $\sigma_v$ are constant (for $r > 5''$), equation (1) may be written

$$\sigma_v^2 \frac{d \ln \rho}{d \ln r} - u_\theta^2 = -4\pi G(1 - e^2)^{1/2} \int_0^r \frac{\rho(a)a^2 da}{(r^2 - a^2e^2)^{1/2}}. \tag{2}$$

Now the radial luminosity distribution in an elliptical galaxy approximates to a power law. If we assume that the radial density distribution is also a power law, $\rho \propto r^{-l}$, then it is easy to show from equation (2) that $l = 2$. Thus, if we let $\rho(a) = \rho_0(a_0/a)^2$, we find

$$u_\theta^2 + 2\sigma_v^2 = 4\pi G(1 - e^2)^{1/2} \rho_0 a_0^2 (\sin^{-1} e)/e. \tag{3}$$

The mass within a spheroid of major axis $a$ is

$$M(a) = 4\pi(1 - e^2)^{1/2} \rho_0 a_0^2 a, \tag{4}$$

and thus the mass distribution is

$$\frac{M(a)}{a} = \frac{u_\theta^2 + 2\sigma_v^2}{G} \left( \frac{e}{\sin^{-1} e} \right). \tag{5}$$

NGC 4473 has an ellipticity $\epsilon = 0.5$, which corresponds to an eccentricity $e = 0.87$. Inserting the appropriate quantities into equation (5), we find $M(a)/a = (1.4 \pm 0.1) \times 10^7\, M_\odot$ pc$^{-1}$, independent of the distance scale. From the relative magnitudes of the force terms it is clear that the galaxy is supported by pressure rather than by rotation. The total mass interior to $r = 45'' = 3270\, \delta_{15}$ pc is

$$M(45'') = (4.6 \pm 0.3) \times 10^{10}\, \delta_{15}\, M_\odot.$$

From de Vaucouleurs, de Vaucouleurs, and Corwin (1976) we find that NGC 4473 has a total magnitude $B_T = 11.03 \pm 0.06$, an effective radius $A_e/2 = 36''.0 \pm 2''.6$, a color index $(B - V)_e = 0.94 \pm 0.02$, and a galactic absorption value $A_B = 0.19$ (or $A_v = 0.14$). The total luminosity enclosed within an ellipsoid with dimensions $45'' \times 45'' \times 22''.5$ may be estimated using the tables of Young (1976). We find $B(45'') = 11.99 \pm 0.08$ or $V(45'') = 11.05 \pm 0.08$. Allowing for the absorption $A_v = 0.14$, we find $L(45'') = (8.3 \pm 0.7) \times 10^9\, \delta_{15}^2\, L_\odot$ and $\langle M/L \rangle (r < 45'') = (5.5 \pm 0.7)\, \delta_{15}^{-1}$ in solar units employing the $V$ band.

To further emphasize the unimportance of rotation in the dynamics of NGC 4473, we may calculate the kinetic energy ratio

$$T_{\rm rot}/T_{\rm ran} = \tfrac{1}{3}(u_\theta/\sigma_v)^2 = 0.08 \pm 0.02.$$

A Maclaurin (fluid) spheroid with the same ellipticity as NGC 4473 (i.e., $\epsilon = 0.5$) would have $\langle u_\theta \rangle = 227$ km s$^{-1}$ and $T_{\rm rot}/T_{\rm ran} = 0.53$. If the galaxy is, in fact, a simple pressure-supported oblate spheroid, then we may expect the velocity dispersion along the minor axis to be somewhat lower than that along the major axis. This would modify slightly the calculated ratio $T_{\rm rot}/T_{\rm ran}$.

From dynamical considerations it was found necessary to postulate $\rho(a) = \rho_0(a_0/a)^2$, external to the core regions. The luminosity profile $L(r)$ follows the $r^{1/4}$ law in the region of interest, and thus $d \ln L/d \ln r = -2.31$. Since $d \ln \rho/d \ln r = -2.0$, we find $d \ln (M/L)/d \ln r \approx +0.3$. Thus $M/L$ rises slowly with increasing radius.

We also note that the core radius of NGC 4473 is $r_c = 3''.3 = 240\, \delta_{15}$ pc (Young *et al.* 1978). The rotation curve of Morton and Chevalier (1973) for the inner regions suggests that the maximum rotational amplitude is reached at the edge of the isothermal core. A reasonable model of NGC 4473 consists of a rigidly rotating, constant-density core, external to which $u_\theta = $ const. and $\rho(r) \propto r^{-2}$.

Last, we note that correction for the unknown inclination angle will not change our conclusions, if the galaxy is a spheroid. Since NGC 4473 is an E5 galaxy, "correcting" it to an E7 with an inclination angle $i = 25°$ results in $u_\theta = 95$ km s$^{-1}$, and rotation remains dynamically unimportant.

## V. CONCLUSIONS

We have found that

i) In the E5 system NGC 4473 the velocity dispersion is constant at $\sigma_v = 180$ km s$^{-1}$ for $r \leq 45''$. The rotation curve is flat, with $u_\theta = 86$ km s$^{-1}$ for $5'' < r < 45''$.

ii) Consequently, the galaxy is pressure supported. Along the major axis the ratio of the pressure gradient force to the centrifugal force is $2\sigma_v^2/u_\theta^2 = 9.4$. Furthermore, $T_{\rm rot}/T_{\rm ran} = 0.08$.

iii) The constancy of $\sigma_v$ and $u_\theta$ implies $\rho(r) \propto r^{-2}$ and $M(r) \propto r$. Since $L(r) \propto r^{-2.3}$, we find $(M/L)(r) \propto r^{+0.3}$. Numerically, $M(r)/r = 1.4 \times 10^7\, M_\odot$ pc$^{-1}$, which gives $M(r < 45'' = 3300\ \text{pc}) = 4.6 \times 10^{10}\, \delta_{15}\, M_\odot$. Since $L(r < 45'') = 8.3 \times 10^9\, \delta_{15}\, L_\odot$, we find a mean $M/L(r < 45'') = 5.5\, \delta_{15}^{-1}$ solar units employing the $V$ band.

Binney (1976) has shown that a flattened elliptical galaxy with an anisotropic velocity dispersion and modest rotation can be formed by collapse of initially asymmetric configurations. Clearly, work on these and consanguineous models with third integral dependences will be profitable. More exotic models which may be relevant include tumbling triaxoids, the prolata of Miller (1978), or objects akin to Riemann ellipsoids (Chandrasekhar 1969) in which the stars may partake of a streaming motion at variance with the rotation of the quadratic surface.

We are extremely grateful to the many members of the Kitt Peak staff who made the special arrangements required for these observations. We also thank J. Fordham and K. Shortridge for their assistance with the IPCS. W. L. W. S. thanks the National Science Foundation for support under grant AST 75-00555. The work at University College London was supported by grants from the UK Science Research Council. We also thank Peter Goldreich, Donald Lynden-Bell, and Paul Schechter for invaluable discussions.

## REFERENCES

Bertola, F., and Capaccioli, M. 1975, *Ap. J.*, **200**, 439.
Binney, J. 1976, *M.N.R.A.S.*, **177**, 19.
Boksenberg, A. 1972, in *Auxiliary Instrumentation for Large Telescopes*, Proc. ESO–CERN Conf., ed. S. Lausten and A. Reiz, p. 295.
Boksenberg, A., and Burgess, D. E. 1973, in *Astronomical Observations with Television Type Sensors*, ed. J. W. Glaspey and G. A. H. Walker (Vancouver: University of British Columbia), p. 21.
Chandrasekhar, S. 1969, *Ellipsoidal Figures of Equilibrium* (New Haven: Yale University Press).
de Vaucouleurs, G. 1959, *Handbuch der Physik*, **53**, 311.
———. 1975, in *Galaxies and the Universe*, ed. A. Sandage, M. Sandage, and J. Kristian (Chicago: University of Chicago Press), p. 557.
de Vaucouleurs, G., and de Vaucouleurs, A. 1964, *Reference Catalogue of Bright Galaxies* (Austin: University of Texas Press).
de Vaucouleurs, G., de Vaucouleurs, A., and Corwin, H. G., Jr. 1976, *Second Reference Catalogue of Bright Galaxies* (Austin: University of Texas Press).
Gott, J. R. 1973, *Ap. J.*, **186**, 481.
———. 1975, *Ap. J.*, **201**, 296.
———. 1977, *Ann. Rev. Astr. Ap.*, **15**, 235.
Gott, J. R., and Thuan, T. X. 1976, *Ap. J.*, **204**, 649.
Humason, M. L., Mayall, N. U., and Sandage, A. R. 1956, *A.J.*, **61**, 97.
Hunter, C. 1977, *A.J.*, **82**, 271.
Illingworth, G. 1977, *Ap. J. (Letters)*, **218**, L43.
Jones, B. J. T. 1976, *Rev. Mod. Phys.*, **48**, 107.
King, I. R., and Minkowski, R. 1966, *Ap. J.*, **143**, 1002.
Larson, R. B. 1974, *M.N.R.A.S.*, **166**, 585.
———. 1975, *M.N.R.A.S.*, **173**, 671.
Lynden-Bell, D. 1967, *M.N.R.A.S.*, **136**, 101.
Miller, R. H. 1978, in preparation.
Morton, D. C., and Chevalier, R. A. 1973, *Ap. J.*, **179**, 55.
Prendergast, K. H., and Tomer, E. 1970, *A.J.*, **75**, 674.
Sandage, A. R., and Tammann, G. A. 1974, *Ap. J.*, **194**, 559.
Sargent, W. L. W., Schechter, P. L., Boksenberg, A., and Shortridge, K. 1977, *Ap. J.*, **212**, 326 (SSBS).
Sargent, W. L. W., Young, P. J, Boksenberg, A., Shortridge, K., Lynds, C. R., and Hartwick, F. D. A. 1978, *Ap. J.*, **221**, 731.
Thuan, T. X., and Gott, J. R. 1977, *Ap. J.*, **216**, 194.
Williams, T. B. 1977, *Ap. J.*, **214**, 685.
Wilson, C. P. 1975, *A.J.*, **80**, 175.
Young, P. J. 1976, *A.J.*, **81**, 807.
Young, P. J, Westphal, J. A., Kristian, J. A., and Wilson, C. P. 1978, in preparation.

A. Boksenberg: Department of Physics and Astronomy, University College London, Gower Street, London, WC1E 6BT, England

F. D. A. Hartwick: Department of Astronomy, University of Victoria, Victoria V8W 2Y2, B.C., Canada

C. R. Lynds: Kitt Peak National Observatory, P.O. Box 26732, Tucson, AZ 85726

W. L. W. Sargent and Peter Young: Department of Astronomy 105-24, California Institute of Technology, Pasadena, CA 91125